Copy No. _____

Defence Research and Development Canada
Recherche et développement pour la défense Canada

DEFENCE R&D DÉFENSE

Modeling of Impact Properties of Auxetic Materials

Phase 1

Lei Jiang, Dustin Pearson, Ken MacKay
Martec Limited

Prepared by:
Martec Limited
400-1800 Brunswick Street
Halifax, Nova Scotia B3J 3J8

Contractor's Document Number: TR-13-36
Contract Project Manager: TLei Jiang, 902-425-5101
PWGSC Contract Number: W7707-135609/001/HAL
Contract Scientific Authority: Dr. J.P. Szabo, Defence Scientist, 902-427-3427

Defence R&D Canada – Atlantic

Contract Report
DRDC Atlantic CR 2013-103
August 2013

Canada

Modeling of Impact Properties of Auxetic Materials

Phase 1

Lei Jiang, Dustin Pearson, Ken MacKay
Martec Limited

Prepared By:
Martec Limited
400-1800 Brunswick Street
Halifax, Nova Scotia B3J 3J8 Canada

Contractor's Document Number: TR-13-36
Contract Project Manager: Lei Jiang, 902-425-5101
PWGSC Contract Number: W7707-135609/001/HAL
CSA: Dr. J.P. Szabo, Defence Scientist, 902-427-3427

Defence R&D Canada – Atlantic

Contract Report
DRDC Atlantic CR 2013-103
August 2013

Scientific Authority

Original signed by J.P. Szabo

J.P. Szabo

Contract Scientific Authority

Approved by

Original signed by Leon Cheng

Leon Cheng

Head/ Dockyard Laboratory (Atlantic)

Approved for release by

Original signed by Leon Cheng

Leon Cheng

Chair, Document Review Panel

Abstract

The report describes a recent numerical investigation on the impact properties of auxetic foams, which are special materials with a negative Poisson’s ratio. These materials have been hypothesized to have some unique characteristics and may provide advantages over conventional engineering materials in certain applications. The objective of the present study was to gain a better understanding of the behaviour of the auxetic foams subjected to impact loads and to determine the influence of the various geometric parameters associated with the material on its performance as protective layer of military structures through a parametric study. A simplified model was utilized, which included conventional and re-entrant honeycomb foam structures resting on a rigid surface and impacted by a rigid mass. The time histories of the internal energy absorption, the impact force and the velocity reduction of the impacter were predicted and used to compare the relative performance of the honeycombs with different geometries. The numerical analyses were first carried out based on shell elements in LS-DYNA and the finite element models were verified for linear and nonlinear static analyses. However, the numerical results of impact simulations indicated some issues with the treatment of the internal contacts between the deformed ribs. Further analyses are underway at the present time to use solid elements which can deal with the contact conditions more reliably.

Résumé

Le présent rapport contient la description d’une étude numérique portant sur les propriétés de résistance aux chocs des mousses auxétiques, des matériaux spéciaux qui possèdent un coefficient de Poisson négatif. Selon certaines hypothèses, ces matériaux présenteraient des caractéristiques exceptionnelles et offriraient, pour certaines applications, des avantages marqués comparativement aux matériaux techniques classiques. La présente étude avait pour objectifs de mieux comprendre le comportement des mousses auxétiques soumises à des charges de choc et de réaliser une étude paramétrique afin de déterminer les effets de divers paramètres géométriques du matériau sur son efficacité comme couche de protection de structures militaires. Le modèle simplifié utilisé comprenait des structures de mousses alvéolaires classiques et réentrantes qui reposent sur une surface rigide et subissent l’impact d’un corps solide. Des calculs ont permis de prévoir la variation en fonction du temps de paramètres distincts tels que l’absorption de l’énergie interne, la force de choc et la réduction de la vitesse de la charge de choc, et les résultats ont servi à comparer la performance relative de structures alvéolaires ayant différentes caractéristiques géométriques. Les analyses numériques initiales étaient basées sur des éléments en forme de coques produits grâce au code LS-DYNA et la validité des modèles à éléments finis a été vérifiée au chapitre des analyses statiques linéaire et non linéaire. Toutefois, les résultats de la simulation numérique de l’impact indiquent la présence de certains problèmes liés au traitement des contacts internes entre les nervures déformées. Les analyses supplémentaires qui sont présentement en cours d’exécution visent à employer des éléments solides pouvant modéliser avec une meilleure fiabilité les conditions de contact susmentionnées.

This page intentionally left blank.

Executive summary

Modeling of Impact Properties of Auxetic Materials: Phase 1

Jiang, Lei; Pearson, Dustin; MacKay, Ken; DRDC Atlantic CR 2013-103; Defence R&D Canada – Atlantic; August 2013.

Introduction: One approach to improving the protection of military land vehicles, naval vessels, and personnel from conventional or asymmetric threats (such as Improvised Explosive Devices) is to seek new armour materials with improved performance. Auxetic materials have recently been hypothesized to exhibit some unique characteristics due to their negative Poisson’s ratio and may provide advantages over conventional engineering materials for certain applications. The objective of the present study carried out by Martec Limited was to investigate the impact properties of the auxetic polymer foams and determine the influence of the geometric parameters associated with the auxetic materials on their protective performance against impact loadings.

Results: Finite element models of auxetic and conventional foams were studied using LS-DYNA. Initial work focused on linear and nonlinear static analyses. For the linear static cases, very good agreement was obtained for the equivalent material properties predicted from finite element models and analytical solutions. The nonlinear static results were reasonable and suggested that the Poisson’s ratios of the auxetic materials are sensitive to the level of deformations due to the variation of the auxetic geometry. The dynamic problem of an auxetic polymer foam layer attached to a rigid surface and impacted by a rigid mass was considered next. Parametric studies using shell elements seemed to suggest that the auxetic foams having smaller internal angle θ and lower void fractions are more effective as a protecting layer. However, because some computational issues were discovered in the shell element solutions, the above observations are not definitive and require further investigation.

Significance: This study is part of a Technology Investment Fund project entitled "Development of Multifunctional Auxetic Materials for Lightweight Personal Protection", whose overall goals are to develop and evaluate negative Poisson's ratio materials for military use. The results of this numerical modelling study will shed light on the energy absorption characteristics of auxetic foam materials, and the possible benefits of incorporating auxetic materials into lightweight armour designs. New armour designs incorporating novel auxetic materials may ultimately result in improved soldier protection from blast and impact threats, while reducing the load burden of the dismounted combat soldier.

Future plans: A Phase 2 investigation has been initiated to perform impact simulations using solid elements, and which are expected to provide a more reliable treatment of contact conditions. In addition, the ability of foam materials with conventional or re-entrant void geometry to protect an underlying metal substrate from impact damage will be determined, and compared to the effect of solid polymer coatings (containing no honeycomb shaped air voids) of equivalent mass.

Sommaire

Modeling of Impact Properties of Auxetic Materials: Phase 1

Jiang, Lei; Pearson, Dustin; MacKay, Ken ; DRDC Atlantic CR 2013-103 ; R & D pour la défense Canada – Atlantique; août 2013.

Introduction : Parmi les approches qui visent à accroître la protection des véhicules militaires terrestres, des navires militaires et du personnel contre les menaces classiques et asymétriques (comme les engins explosifs improvisés), on compte la mise au point de nouveaux matériaux de blindage plus efficaces. Selon certaines hypothèses récentes, les matériaux auxétiques présenteraient des caractéristiques exceptionnelles attribuables à leur coefficient de Poisson négatif et ils offriraient, pour certaines applications, des avantages marqués comparativement aux matériaux techniques classiques. La présente étude, qui a été réalisée par la société Martec Limited, avait pour objectifs d'examiner les propriétés de résistance aux chocs des mousses polymères auxétiques et de déterminer les effets de divers paramètres géométriques des matériaux auxétiques sur leur efficacité de protection contre les charges de choc.

Résultats : On a étudié des modèles à éléments finis de mousses classiques et auxétiques en utilisant le code LS-DYNA. Les travaux initiaux comportaient principalement des analyses statiques linéaires et non linéaires. Dans le cas des analyses statiques linéaires, il existe un très bon accord entre les propriétés des matériaux prévues à partir des modèles à éléments finis et celles prévues à l'aide des solutions analytiques. Les résultats des analyses statiques non linéaires sont adéquats et ils laissent croire que les coefficients de Poisson des matériaux auxétiques sont sensibles à l'importance des déformations subies, lesquelles sont attribuables à la variation des structures géométriques auxétiques. On a ensuite étudié le problème dynamique d'une couche de mousse polymère auxétique fixée à une surface rigide et soumise à l'impact d'un corps solide. Les résultats d'études paramétriques basées sur l'emploi d'éléments en forme de coques semblent indiquer que les mousses auxétiques qui présentent un angle interne θ plus petit et de plus faibles fractions poreuses constituent des couches de protection plus efficaces. Il faut toutefois signaler que des problèmes de calcul ont été relevés dans les solutions obtenues avec les éléments en forme de coques et, conséquemment, les observations susmentionnées ne sont pas définitives et exigent l'exécution d'études plus poussées.

Importance : La présente étude fait partie intégrante d'un projet du Fonds d'investissement technologique intitulé « Mise au point de matériaux auxétiques multifonctionnels pour équipement de protection individuelle léger », dont les objectifs généraux visent à mettre au point et évaluer des matériaux qui possèdent un coefficient de Poisson négatif destinés à des utilisations militaires. Les résultats de l'étude de modélisation numérique permettront de clarifier les caractéristiques liées à l'absorption d'énergie des mousses auxétiques et d'établir les avantages que pourrait entraîner l'intégration de matériaux auxétiques à des structures de blindage ou des dispositifs pare-balles légers. Les nouveaux produits de ce type pourraient mieux protéger les soldats contre l'effet de souffle des explosions et les chocs connexes, tout en réduisant le poids de la charge des fantassins débarqués.

Perspectives : Les travaux de la phase 2 ont été lancés afin d'effectuer des simulations d'impact à l'aide d'éléments solides, lesquels devraient permettre de modéliser avec une meilleure fiabilité les conditions de contact. De plus, la capacité de diverses mousses présentant des structures alvéolaires classiques ou réentrantes de protéger un substrat métallique sous-jacent contre les dommages causés par l'impact sera déterminée et comparée à celle de revêtements de polymères solides (ne contenant pas d'alvéoles) de masse équivalente.

This page intentionally left blank.

Table of contents

Abstract …….. i

Résumé …..... i

Executive summary iii

Sommaire iv

Table of contents vii

List of figures viii

List of tables xii

1 Introduction.......... 1

2 Literature Review 2

- 2.1 Basic characteristics of auxetic materials.......... 2
- 2.2 Geometric structures and models 3
- 2.3 Unique properties of auxetic materials.......... 7
- 2.4 Homogenized material properties of auxetic materials 10
- 2.5 Contact and impact problems of auxetic materials.......... 14

3 Formulation and verification of finite element models for impact simulations.......... 16

- 3.1 Formulation of test cases.......... 16
- 3.2 Approximate polymer material properties.......... 19
- 3.3 Calculation of effective material properties 22
- 3.4 Verification of the finite element model.......... 22
  - 3.4.1 Linear and nonlinear static analysis.......... 23
  - 3.4.2 Effect of extent of the finite element model 37
  - 3.4.3 Effect of material properties.......... 37
  - 3.4.4 Effect of impacter mass 41

4 Results of parametric study.......... 44

- 4.1 Test cases for parametric study 44
- 4.2 Representative results of shell element 44
- 4.3 Investigation of solid element 45

5 Conclusions.......... 63

References 65

List of figures

Figure 1: Schematic diagram of positive (a) and negative (b) Poisson's ratio deformations. (Reproduced from Reference [1]) 2

Figure 2: Deformation of conventional (a) and re-entrant (b) honeycomb networks. (Reproduced from Reference [1]) 3

Figure 3: Examples of 2D re-entrant structures (a) Double arrowhead structure (b) Star honeycomb structure (c) Structurally hexagonal re-entrant honeycomb (d) Structure formed from lozenge grids (e) Structure formed from square grids (f) Structure formed from sinusoidal ligaments. (Reproduced from Reference [4]) 4

Figure 4: Conventional (a) and re-entrant (b) of tetrakaidecahedron. (Reproduced from Reference [6]) 5

Figure 5: Chiral honeycombs (a) Formed with the same chiral units (b) Formed with symmetrical chiral (Reproduced from Reference [4]) 5

Figure 6: The newly proposed model: (a) the conventional hexagonal honeycomb model for conventional foams, (b) the 'rotation of rigid units (joints)' model for auxetic foams, and (c) an idealised representation of the 'rotation of rigid joints' model where the joints are represented by perfectly rigid equilateral triangles. (Reproduced from Reference [7]) 6

Figure 7: Structural computational model of a periodic assembly of reinforced units with a ring shaped flexible frame: (a) Assembly with the periodicity cell indicated by a rectangle; (b) the representative (periodicity) cell; (c) the computational cell and the use of symmetry in both directions – loading and boundary conditions. (Reproduced from Reference [8]) 8

Figure 8: Indentation resistance of conventional and auxetic materials. (Reproduced from Reference [1]) 9

Figure 9: Cell geometry and coordinate system used for (a) conventional and (b) re-entrant hexagonal cells. (Reproduced from Reference [15]) 10

Figure 10: Geometry of unit cell of chiral honeycomb. (Reproduced from Reference [20]) 12

Figure 11: Periodic cells of conventional and re-entrant honeycomb structures. 16

Figure 12: Shell element model for a re-entrant honeycomb structure with $\theta=-20^O$. 18

Figure 13: Details of the shell element model shown above. 18

Figure 14: Polymer material properties to be used in the present numerical study. 19

Figure 15: Original and converted stress-strain curve for strain rate 30/s using E=84.7 MPa. 21

Figure 16: Original and converted stress-strain curve for strain rate 30/s using E=166.7 MPa. 21

Figure 17: Original (blue) and deformed (black) configurations of a conventional honeycomb structure ($\theta=20^O$) subjected to horizontal tension. 25

Figure 18: Original (blue) and deformed (black) configurations of a conventional honeycomb structure ($\theta=20^O$) subjected to vertical tension. 25

Figure 19: Original (blue) and deformed (black) configurations of a re-entrant honeycomb structure ($\theta=20^O$) subjected to horizontal compression. 26

Figure 20: Original (blue) and deformed (black) configurations of a re-entrant honeycomb structure ($\theta=20^O$) subjected to vertical compression. 26

Figure 21: Final deformed configuration of an auxetic structure subjected to horizontal tensile stresses. 27

Figure 22: Load-horizontal displacement curve of the marked node on the right edge. 27

Figure 23: Load-vertical displacement curves at the two nodes marked on the top and bottom edges of the auxetic structure. 28

Figure 24: Variation of the effective Poison's ratio of the auxetic structure with the level of deformation. 28

Figure 25: Typical deformed configurations of unit cells in horizontally loaded re-entrant honeycomb that explained deformation-dependent of Poisson's Ratio. 29

Figure 26: Final deformed configuration of an auxetic structure subjected to vertical tensile stresses. 31

Figure 27: Load-vertical displacement curve of the node marked on the top edge. 31

Figure 28: Load-horizontal displacement curves at the two nodes marked at the bottom of the right and left edges of the auxetic structure. 32

Figure 29: Variation of the effective Poison's ratio of the auxetic structure with the level of deformation. 32

Figure 30: Final deformed configuration of an auxetic structure subjected to horizontal compressive stresses. 33

Figure 31: Load-horizontal displacement curve of the node marked on the right edge. 33

Figure 32: Load-vertical displacement curves at the two nodes marked on the top and bottom edges of the auxetic structure. 34

Figure 33: Variation of the effective Poison's ratio of the auxetic structure with the level of deformation. 34

Figure 34: Final deformed configuration of an auxetic structure subjected to vertical compressive stresses. 35

Figure 35: Load-vertical displacement curve of the node marked on the top edge. 35

Figure 36: Load-horizontal displacement curves at the two nodes marked in the middle of the right and left edges. 36

Figure 37: Variation of the effective Poison's ratio of the auxetic structure with the level of deformation. 36

Figure 38: Normalized reaction force histories obtained using FE models of 16 columns of re-entrant unit cells with different angles. 38

Figure 39: Normalized reaction force histories obtained using FE models of 8 columns of re-entrant unit cells with different angles. 38

Figure 40: Normalized internal energy histories obtained using FE models of 16 columns of re-entrant unit cells with different angles. 39

Figure 41: Normalized internal energy histories obtained using FE models of 8 columns of re-entrant unit cells with different angles. 39

Figure 42: Reaction force histories obtained using different elastic-plastic material parameters that approximate the material behavior of polyurea. 40

Figure 43: Internal energy histories obtained using different elastic-plastic material parameters that approximate the material behavior of polyurea. 40

Figure 44: Velocity histories of the impacter obtained using different elastic-plastic material parameters that approximate the material behavior of polyurea. 41

Figure 45: Reaction force histories obtained using different mass ratios of the impacter and the polyurea foam. 42

Figure 46: Internal energy histories obtained using different mass ratios of the impacter and the polyurea foam. 42

Figure 47: Velocity histories of impacter obtained using different mass ratio of the impacter and the polyurea foam. 43

Figure 48: Shell element predicted deformation process for re-entrant honeycomb with $\theta=40^o$ and void fraction of 0.5 under vertical impact. 46

Figure 49: Shell element predicted deformation process for re-entrant honeycomb with $\theta=40^o$ and void fraction of 0.5 under horizontal impact. 47

Figure 50: Normalized internal energy absorption for honeycomb structures with $\theta=10^o$ and various void fractions under vertical impact. 48

Figure 51: Normalized internal energy absorption for honeycomb structures with $\theta=20^o$ and various void fractions under vertical impact. 48

Figure 52: Normalized internal energy absorption for honeycomb structures with $\theta=30^o$ and various void fractions under vertical impact. 49

Figure 53: Normalized internal energy absorption for honeycomb structures with $\theta=40^o$ and various void fractions under vertical impact. 49

Figure 54: Normalized impact force for honeycomb structures with $\theta=10^o$ and various void fractions under vertical impact. 50

Figure 55: Normalized impact force for honeycomb structures with $\theta=20^o$ and various void fractions under vertical impact. 50

Figure 56: Normalized impact force for honeycomb structures with $\theta=30^o$ and various void fractions under vertical impact. 51

Figure 57: Normalized impact force for honeycomb structures with $\theta=40^o$ and various void fractions under vertical impact. 51

Figure 58: Normalized reduction of impacter velocity for honeycomb structures with $\theta=10^o$ and various void fractions under vertical impact. 52

Figure 59: Normalized reduction of impacter velocity for honeycomb structures with θ=20° and various void fractions under vertical impact. 52

Figure 60: Normalized reduction of impacter velocity for honeycomb structures with θ=30° and various void fractions under vertical impact. 53

Figure 61: Normalized reduction of impacter velocity for honeycomb structures with θ=40° and various void fractions under vertical impact. 53

Figure 62: Normalized internal energy absorption for honeycomb structures with θ=10° and various void fractions under horizontal impact. 54

Figure 63: Normalized internal energy absorption for honeycomb structures with θ=20° and various void fractions under horizontal impact. 54

Figure 64: Normalized internal energy absorption for honeycomb structures with θ=30° and various void fractions under horizontal impact. 55

Figure 65: Normalized internal energy absorption for honeycomb structures with θ=40° and various void fractions under horizontal impact. 55

Figure 66: Normalized impact force for honeycomb structures with θ=10° and various void fractions under horizontal impact. 56

Figure 67: Normalized impact force for honeycomb structures with θ=20° and various void fractions under horizontal impact. 56

Figure 68: Normalized impact force for honeycomb structures with θ=30° and various void fractions under horizontal impact. 57

Figure 69: Normalized impact force for honeycomb structures with θ=40° and various void fractions under horizontal impact. 57

Figure 70: Normalized reduction of impacter velocity for honeycomb structures with θ=10° and various void fractions under horizontal impact. 58

Figure 71: Normalized reduction of impacter velocity for honeycomb structures with θ=20° and various void fractions under horizontal impact. 58

Figure 72: Normalized reduction of impacter velocity for honeycomb structures with θ=30° and various void fractions under horizontal impact. 59

Figure 73: Normalized reduction of impacter velocity for honeycomb structures with θ=40° and various void fractions under horizontal impact. 59

Figure 74: Solid element predicted deformation process for re-entrant honeycomb with θ=40° and void fraction of 0.5 under vertical impact. 60

Figure 75: Internal energy absorption for honeycomb structure with θ=40° and void fraction of 0.5 under vertical impact predicted using different elements and contact options. 61

Figure 76: Impact force for honeycomb structure with θ=40° and void fraction of 0.5 under vertical impact predicted using different elements and contact options..................... 61

Figure 77: Reduction of impacter velocity for honeycomb structure with θ=40° and void fraction of 0.5 under vertical impact predicted using different elements and contact options. 62

List of tables

Table 1: Proposed test cases for void fraction VF=0.845 17

Table 2: Converted stress-plastic strain curves for strain rate 30/s using different values of Young's Modulus. 20

Table 3: Analytical solutions of effective properties of auxetic materials defined in Table 1 under small deformations 23

Table 4: Comparison of analytical and numerical solutions of effective properties of auxetic material under small deformations 24

Table 5: Test matrix for parametric study 44

1 Introduction

Auxetic materials are special materials that have a negative Poisson's ratio. This type of material becomes thicker in the direction perpendicular to the applied force when stretched [1-5]. Auxetic materials have generated considerable interest in recent years because of their unique mechanical properties and have been demonstrated to provide a number of advantages over the more conventional engineering materials, such as higher indentation resistance, higher fracture toughness and greater resistance to impact damage. These unique features of the auxetic materials make them potential candidates for a variety of applications.

The objective of the present contract is to investigate the impact properties of auxetic materials through finite element-based numerical simulations, and thus explore the possibility for using them to provide protection to military structures or personnel. A review of the various analytical and numerical models for auxetic materials will first be provided in the next chapter, which will be followed by a discussion on the generation and verification of the finite element models to be utilized in the present numerical study. The results from the parametric study will be presented in Chapter 4 and conclusions and recommendations for further work will be outlined in Chapter 5.

2 Literature Review

2.1 Basic characteristics of auxetic materials

Our everyday experience tells us that when we stretch a piece of material, for example an elastic band, the material not only becomes longer in the direction of stretch but also becomes thinner in cross-section. Similarly, a material under compression usually expands laterally. In both these cases the behaviour of the material under deformation is governed by one of the fundamental mechanical properties of materials, named the Poisson's ratio (ν). The Poisson's ratio of a material is defined as the ratio of the lateral contractile strain to the longitudinal tensile strain for a material undergoing tension in the longitudinal direction, i.e., it tells us how much a material becomes thinner when it is stretched. Consequently, by definition most materials have a positive Poisson’s ratio as indicated in Figure 1a [1].

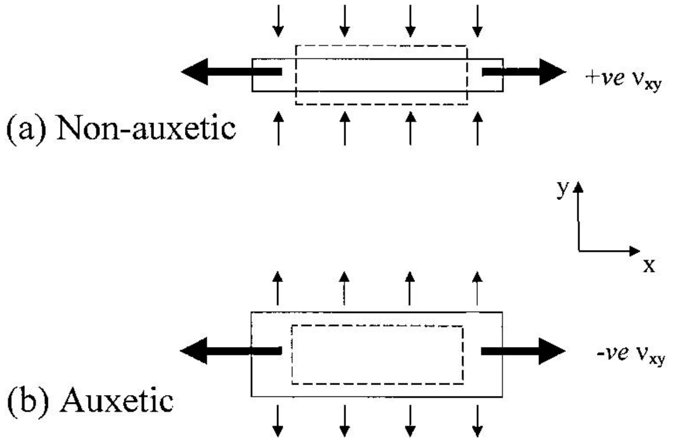

Figure 1: Schematic diagram of positive (a) and negative (b) Poisson’s ratio deformations. (Reproduced from Reference [1])

Poisson's ratio has historically been the least studied of the quartet of elastic constants for isotropic materials. The three other elastic constants are the Young's modulus (*E*), shear modulus (*G*), and bulk modulus (*K*), and they are important from an engineering point of view since they present the stiffness, rigidity, and compressibility of a material, respectively. In most of the undergraduate texts on the mechanics of materials, it was implied or even stated that all materials possess a positive Poisson’s ratio. However, the possibility that ν may be negative has been an accepted consequence of classical elasticity theory, implying that, in this case, the material undergoes lateral expansion when stretched longitudinally (see Fig. 1b), and becomes thinner when compressed. In fact when viewing the Poisson's ratio as a measure of a material's change in volume on being deformed, a negative ν is simply an extension of the increase in volume exhibited by a material with a positive ν of less than +1/2. Materials that exhibit this novel and counter-intuitive behaviour are known as auxetic materials.

2.2 Geometric structures and models

A classic example on how the Poisson's ratio can be tailored by careful design of material architecture is given in Figure 2. Here the structure is a 2D honeycomb network deforming by hinging of the ribs forming the network. For individual cells having the conventional hexagonal geometry (Fig. 2a) we see that the cells elongate along the y-axis and close up along the x-axis in response to stretching the network in the y-direction, giving a positive Poisson's ratio (ν). By maintaining the same deformation mechanism (rib hinging), but modifying the honeycomb cell geometry to adopt the re-entrant "bow-tie" structure shown in Figure 2b, the alignment of the diagonal ribs along the horizontal direction of applied stretch causes them to move apart along the vertical direction, thereby resulting in the auxetic effect.

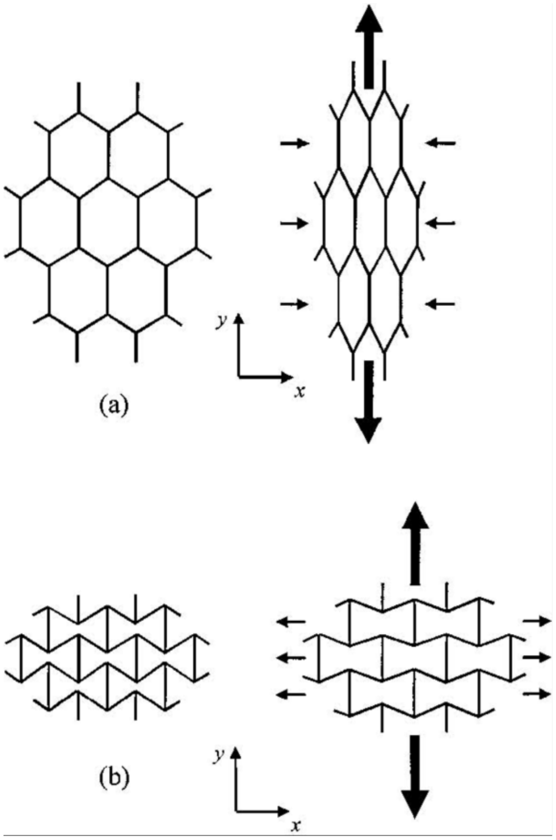

Figure 2: Deformation of conventional (a) and re-entrant (b) honeycomb networks. (Reproduced from Reference [1])

Although hinging of the ribs is considered in the above paragraph to demonstrate the origin of the auxetic behaviour of the re-entrant hexagonal honeycomb network, in reality, most honeycombs of this type of structure deform predominantly by flexure of the diagonal ribs, with hinging and axial stretching of the ribs also occur simultaneously [3-4].

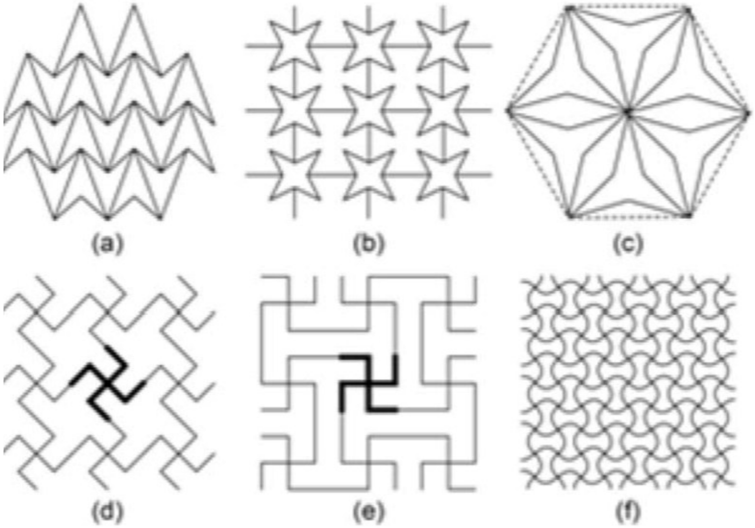

Figure 3: Examples of 2D re-entrant structures (a) Double arrowhead structure (b) Star honeycomb structure (c) Structurally hexagonal re-entrant honeycomb (d) Structure formed from lozenge grids (e) Structure formed from square grids (f) Structure formed from sinusoidal ligaments. (Reproduced from Reference [4])

Auxetic effects can also be obtained from other re-entrant structures, as shown in Figure 3. Opening or closing of the arrowheads or stars in double arrowhead (Figure 3a) and star honeycomb (Figure 3b) structures leads to auxetic behaviour due to rib flexure and/or hinging under uniaxial loading,. A structurally hexagonal re-entrant honeycomb (Figure 3c) has been suggested to obtain better planar isotropic properties than the 2D re-entrant structure shown in Figure 2b due to structural symmetry along radical directions. The re-entrant structures shown in Figure 3d and Figure 3e were formed from lozenge and square grids by eliminating some side lines in each grid. In these figures, the repeating units (unit-cells) are highlighted in thicker lines. The auxetic effects in these structures are obtained due to rotation and extension of each side in the unit-cells. Another example is the structure formed with the sinusoidal ligaments (Figure 3f), where the auxetic effect comes from opening up of re-entrant cells into almost rectangular cells.

Besides 2D re-entrant structures, 3D re-entrant structures may also exist and produce auxetic effects. As shown in Figure 4, a 3D re-entrant cell has been used to explain the auxetic behaviour of auxetic foams. This cell was produced by transformation of the conventional cell structure (Figure 4a) into a re-entrant cell structure (Figure 4b) in which the ribs protrude inward. When the vertically protruding ribs are under tension, the ribs in the lateral directions will tend to move outward, leading to lateral expansion. On the other hand, when compression is applied, the ribs will bend inward further, thus resulting in lateral contraction in response to axial compression. Based on this model, auxetic polymeric foams could be easily understood.

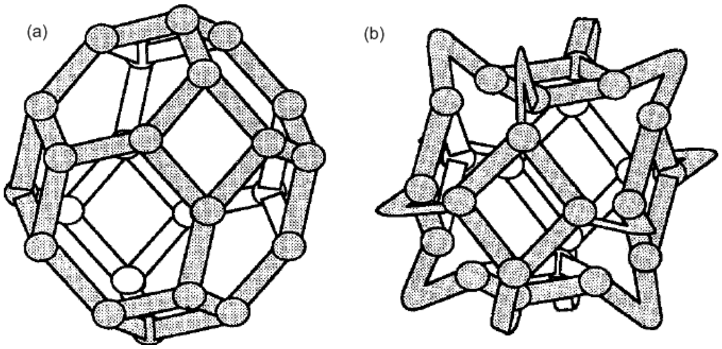

Figure 4: Conventional (a) and re-entrant (b) of tetrakaidecahedron. (Reproduced from Reference [6])

Chiral structures are another class of structures which have been developed for auxetic honeycombs. As shown in Figure 5, in this kind of structure, basic chiral units (highlighted in thick lines) are firstly formed by connecting straight ligaments (ribs) to central nodes which may be circles or rectangles or other geometrical forms. The whole chiral structures are then formed by joining together the chiral units. The auxetic effects are achieved through wrapping or unwrapping of the ligaments around the nodes in response to applied forces. According to the theoretical and experimental investigations, Poisson's ratio of the chiral structure in Figure 5a under in-plane deformations is around -1. In contrast to most of other auxetic structures, this structure can maintain a high auxetic effect over a significant range of strains. Based on this structure, a novel class of structure referred as 'meta-chiral' (Figure 5b) has been recently developed. In this kind of structure, either the same chiral units (also called chiral building blocks) or symmetric units can be connected together to form different chiral structures. For example, the structure in Figure 5b is formed by connecting the symmetric blocks where the node in each chiral building block is a rectangle. Although the building blocks may be polygons with arbitrary number of edges, only those formed with 3, 4, or 6 ligaments can be used to construct space filling periodic structures. In addition, it is evident that the auxetic effects of a given chiral structure depend on the shape of node (building block) and the length of attached ligaments.

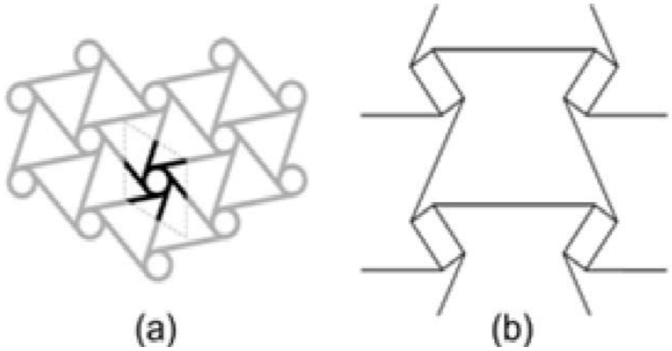

Figure 5: Chiral honeycombs (a) Formed with the same chiral units (b) Formed with symmetrical chiral (Reproduced from Reference [4])

Another popular model for explaining the presence of the negative Poisson's ratios in auxetic foams manufactured through the compression/heat treatment process is the "rotating units" model [7]. This model is based on the hypothesis that the changes in the microstructure during the manufacturing process based on compression and heat treatment will produce the "geometry of the joints" due to large deformations along the length of the ribs which buckle due to the tri-axial compression. The model also assumes that the "additional thickness" in the proximity of the joints will make them behave as "rigid joints". In this way, the model can be described as "rigid units" that rotate relative to each other during the manufacturing process. The macrostructure of the foam then "freezes" in this more compact form which contains the necessary structure feature for the "rotating rigid joints" mechanics to operate and generate the experimentally observed auxetic behaviour. The extent of the auxeticity will depends mainly on the rigidity of the joints (the "rigid joints") when compared to the flexibility of the units connecting them (the ribs).

Figure 6 shows how a conventional idealised two-dimensional hexagonal model for the conventional foam (Fig. 6a) can be converted through the compression/heat treatment process into an auxetic form (Fig. 6b) without the need of inversion of the 'Y-joints' or rib breakage. Here it is assumed that during the heating/compression process, there is extensive buckling in the ribs, which form 'kinks' or 'folds' at their centre. In the meantime, the 'Y-shaped joints' behave like 'rigid triangles', rotate relative to each other. This process produces a more compact microstructure (Fig. 6b) which when uni-axially loaded will exhibit auxetic behaviour as a result of re-rotation of the 'triangular joints' and unfolding of the 'kinks'.

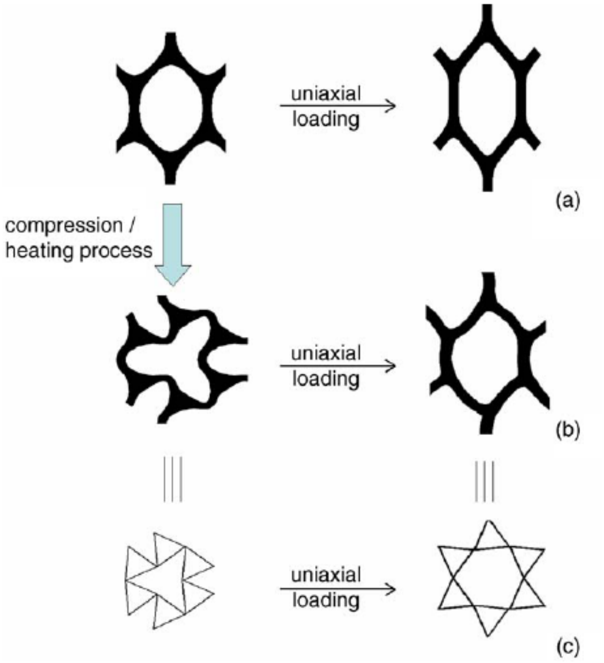

Figure 6: The newly proposed model: (a) the conventional hexagonal honeycomb model for conventional foams, (b) the 'rotation of rigid units (joints)' model for auxetic foams, and (c) an idealised representation of the 'rotation of rigid joints' model where the joints are represented by perfectly rigid equilateral triangles. (Reproduced from Reference [7])

In an idealised scenario where the joints are assumed to be 'equilateral triangles' and 'perfectly rigid', the system would exhibit in-plane Poisson's ratios of −1 (Fig. 6c). However, in reality, the Poisson's ratios would be expected to be less negative as the joints will neither be perfectly rigid, nor regular in shape. This is consistent with the fact that the experimentally measured Poisson's ratios in the heat-treated auxetic polyurethane foam were around −0.60.

New design concepts for constructing auxetic structures still continue to appear in the literature. One example is the "arch frame" model recently proposed in Reference [8] which contained 2D assemblies of identical units made of a flexible frame with a sufficiently rigid reinforcing core at the centre, as indicated in Figure 7. The core increases the frame resistance to the tangential movement thus ensuring high shear stiffness, whereas the normal stiffness is low because it is controlled by the local bending response of the frame. The structures considered have hexagonal symmetry, which lead to macroscopically isotropic elastic properties in the plane perpendicular to the axis of the symmetry. The macroscopic Poisson's ratio was computed using a direct micro-structural approach and the results indicated that the proposed design could produce a macroscopically isotropic system with negative Poisson's ratio close to the lower bound of -1.

Very recently, a class of hybrid materials which showed negative Poisson's ratio at the macroscopic scale were proposed [9]. These materials were formed by embedding micro-structural elements that produced negative Poisson's ratio into a matrix with a positive Poisson's ratio. Analytical solutions of the effective Young's modulus and Poisson's ratio were obtained for the case of spherical inclusions with negative Poisson's ratio randomly situated in the matrix. The inclusions were assumed to be in a finite concentration, but have a multi-scale distribution over radii. The Young's moduli of the matrix and inclusions were set to be identical and the Poisson's ratio of the inclusion was taken to be -0.99. The solution indicated that with the increase of the volume fraction of inclusions, the effective Poisson's ratio of the hybrid material tends to -0.99. This agreed with expectations as it indicated that when the volume fraction approached unity, the behaviour of the hybrid material approached to that of the inclusions. Interestingly, the effective Young's modulus of the hybrid material can increase significantly, up to four times of the Young's moduli of the matrix and inclusions. This maximum value appeared at a certain concentration of the inclusions. Both the value of the maximum effective Young's modulus and the inclusion concentration at which the maximum Young's modulus occurred increased with increasing incompressibility of the matrix.

2.3 Unique properties of auxetic materials

Because of negative Poisson's ratio effect, auxetic materials exhibit a series of fascinating properties compared with the conventional materials [4], such as increased shear modulus, increased indentation resistance, increased fracture toughness and increased energy absorption. These properties will be discussed in the following paragraphs.

The auxetic effect can be used to tailor the mechanical properties of a structure to reach enhanced performance. In elasticity theory, the material's elastic behaviour is expressed by four constants: the Young's modulus (E), the shear modulus (G), the bulk modulus (K) and the Poisson's ratio (ν). For isotropic materials, the four constants are not independent. They are related by the following equations: $G = E/(2(1+\nu))$ and $K = E/(3(1-2\nu))$. Most structural materials are required to have a higher K than G. If we can change the microstructure of a material in a way that E remains constant but ν changes, we can alter the values of K and G. For example, when decreasing ν to -1, a very high shear modulus relative to the bulk modulus can be obtained. In other words, the material becomes difficult to shear but easy to deform volumetrically.

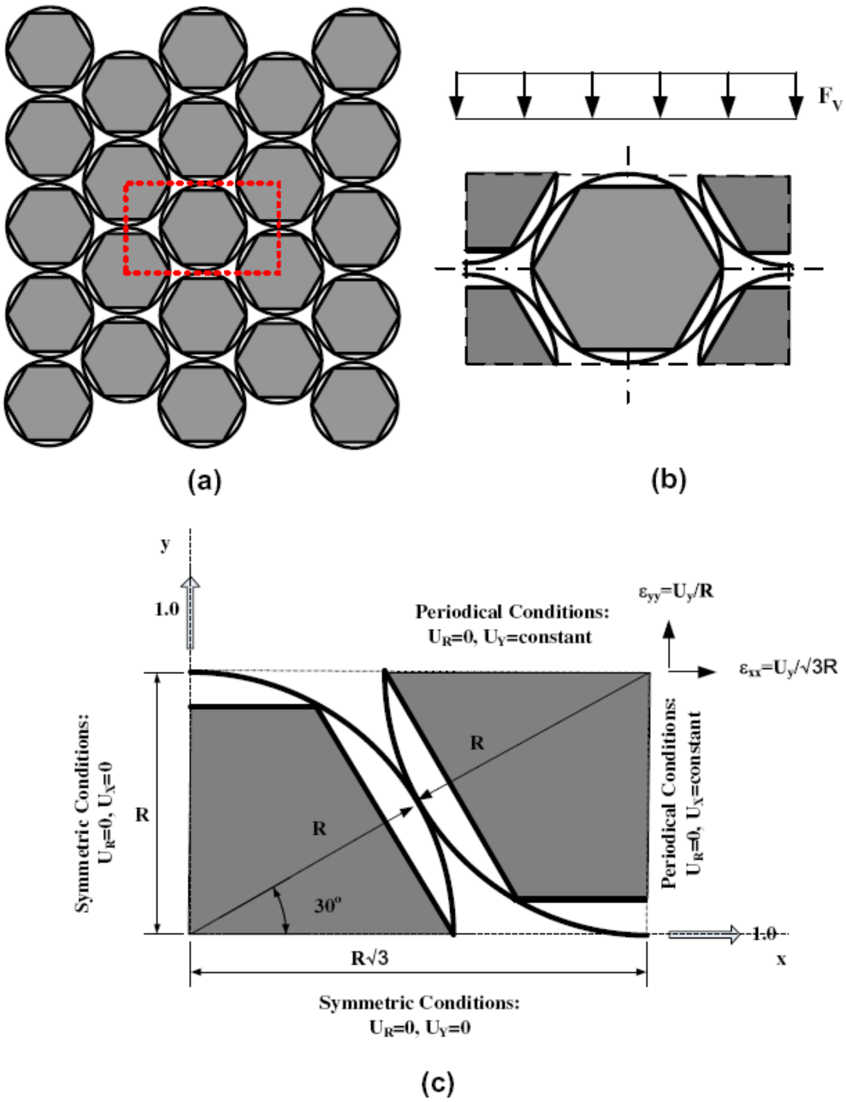

Figure 7: Structural computational model of a periodic assembly of reinforced units with a ring shaped flexible frame: (a) Assembly with the periodicity cell indicated by a rectangle; (b) the representative (periodicity) cell; (c) the computational cell and the use of symmetry in both directions – loading and boundary conditions. (Reproduced from Reference [8])

Hardness can be increased in an auxetic material due to negative Poisson's ratio. When an object hits an auxetic material and compresses it in one direction, the auxetic material also contracts laterally, that is, material 'flows' into the vicinity of the impact as illustrated in Figure 8. This creates an area of denser material, which is resistant to indentation. This phenomenon can be explained theoretically. The indentation resistance or hardness of an isotropic material is proportional to $E/(1-\nu^2)$ when an indenter with a uniform pressure distribution is assumed. The range of ν for 3D isotropic materials is from -1 to 0.5. Thus, the $(1-\nu^2)$ term will approach to 0 when ν approaches to -1. In this way, for an isotropic material with a given value of E, the indentation resistance increases towards infinity with increasingly negative Poisson's ratio.

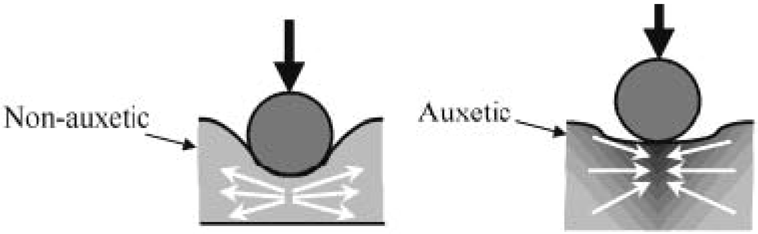

Figure 8: Indentation resistance of conventional and auxetic materials.
(Reproduced from Reference [1])

Compared with non-auxetic materials, auxetic materials have increased fracture toughness. The fracture toughness was explored experimentally as a function of permanent volumetric compression ratio, a processing variable. Compared to that of conventional polyurethane-polyester foam materials, the toughness of auxetic foam is increased by factors of 1.7, 2.1, 2.3, 2.6 and 3.2 with increases of volumetric compression ratio of 2.0, 2.6, 3.2, 3.7 and 4.2, respectively. Auxetic materials also have high crack resistance. If the material has a crack, it expands and closes up the crack when being pulled apart. In other words, this type of material should possess more crack resistance to fracture.

Auxetic materials also show overall superiority on energy absorption compared to the conventional materials. Scarpa et al. [10, 11] investigated the stress-strain behaviours of conventional open-cell rigid grey polyurethane form and the corresponding transformed auxetic material under dynamic crushing. The results indicated that the conventional rigid polyurethane foam did not demonstrate any noticeable resilience under impact, but the auxetic foam showed significantly increased resilience under dynamic loading. The measured stress-strain curves indicated that the dynamic behaviour of the transformed auxetic materials was like a high-density polyurethane cellular solid with low strain-rate sensitivity. For the same strain, the stress in the auxetic material is in general two orders of magnitude higher than that of conventional foam. These results suggest the possibility of using the transformed open-cell forms in impact applications, such as industrial and sensor/equipment packaging.

Enhanced damping properties of the transformed auxetic materials over the original conventional forms were also observed by Scarpa and co-workers [12, 13]. The auxetic foam samples were obtained from off-the-shelf open cell grey polyurethane form by following a manufacturing process based on mechanical deformation on a mould in a temperature-controlled oven. Viscoelastic material properties, including storage modulus and loss factor, were measured for small sinusoidal strain histories using a viscoelastic analysis tensile machine. The same samples were also tested in an acoustic impedance tube to measure acoustic absorption and specific acoustic resistance. The hysteresis of the cycling loading curve was measured to determine the damping loss factors for the various foams. The measurements indicated that the auxetic foams had loss factors 20% higher than those for the conventional foams.

However, it was also noticed that because auxetic materials need substantial porosity in general, they are less stiff than the solid from which they are manufactured. Eventually, this causes limitations on the structural applications of the materials with negative Poisson's ratio. Consequently, for applications that require substantial load-bearing, they are not the best choice [5].

2.4 Homogenized material properties of auxetic materials

A great deal of effort has been made to establish the homogenized material properties, such as the elastic moduli and Poisson's ratios, in the principal directions using analytical and numerical methods. Gibson and co-workers are among the pioneers in this field [14]. By assuming that the deformations in the re-entrant hexagonal honeycomb, shown in Figure 9, were dominated by flexing of the cell walls when an external load is applied, they derived the following equations for the elastic properties of the honeycombs:

$$E_1 = \frac{K_f\left(h/l+\sin\theta\right)}{b\cos^3\theta},\ E_2 = \frac{K_f\cos\theta}{b\left(h/l+\sin\theta\right)\sin^2\theta}$$

$$\nu_{12} = \frac{\sin\theta\left(h/l+\sin\theta\right)}{\cos^2\theta},\ \nu_{21} = \frac{\cos^2\theta}{\left(h/l+\sin\theta\right)\sin\theta} \tag{1}$$

where $K_f = E_s bt^3/l^3$ is the flexure force constant, E_s is the Young's modulus of the base material, b is the depth of the honeycomb structure, and l, h and t are the lengths and thickness of the cell walls, respectively as indicated in Figure 9.

In reality, when the honeycombs are subjected to external loading, they normally undergo combined flexure, stretching and hinging deformations. Considering the contributions from all these deformation modes, Masters and Evans [15] obtained expressions for the effective elastic properties as:

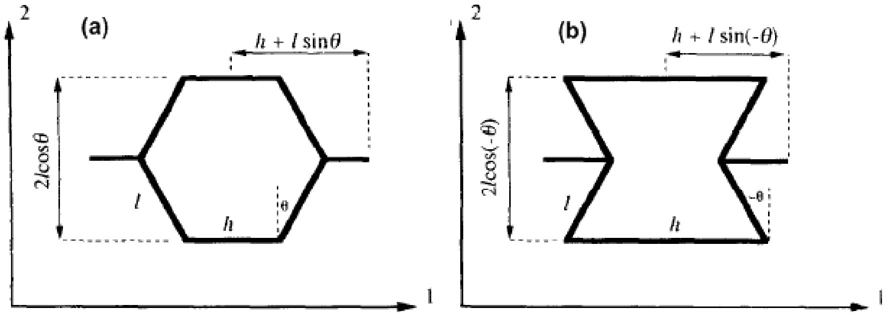

Figure 9: Cell geometry and coordinate system used for (a) conventional and (b) re-entrant hexagonal cells. (Reproduced from Reference [15])

$$E_1 = \frac{h/l + \sin\theta}{b\cos\theta\left(\frac{\cos^2\theta}{K_f} + \frac{\cos^2\theta}{K_h} + \frac{2h/l + \sin^2\theta}{K_s}\right)},\quad E_2 = \frac{\cos\theta}{b\left(h/l + \sin\theta\right)\left(\frac{\sin^2\theta}{K_f} + \frac{\sin^2\theta}{K_h} + \frac{\cos^2\theta}{K_s}\right)},$$

$$\nu_{12} = \frac{\sin\theta\left(h/l + \sin\theta\right)\left(\frac{1}{K_f} + \frac{1}{K_h} - \frac{1}{K_s}\right)}{\left(\frac{\cos^2\theta}{K_f} + \frac{\cos^2\theta}{K_h} + \frac{2h/l + \sin^2\theta}{K_s}\right)},\quad \nu_{21} = \frac{-\sin\theta\cos^2\theta\left(\frac{1}{K_f} + \frac{1}{K_h} - \frac{1}{K_s}\right)}{\left(h/l + \sin\theta\right)\left(\frac{\sin^2\theta}{K_f} + \frac{\sin^2\theta}{K_h} + \frac{\cos^2\theta}{K_s}\right)} \tag{2}$$

where $K_s = E_s bt/l$ and $K_h = G_h bt/l$ indicate the stretching and hinging force constants, respectively and G_h is the shear modulus of the cell wall material. These formulas of elastic material properties were employed by Henderson and co-workers [16, 17] in their investigation on crash performance of cellular foams with reduced relative density.

A systematic and predictive methodology was recently proposed [18] for obtaining equivalent homogenized mechanical properties of auxetic materials of network structures using the discrete asymptotic homogenization method and applied to five different 2D periodic lattices. The equivalent elastic moduli and Poisson's ratios for re-entrant hexagonal are expressed as follows:

$$E_1 = \frac{K_f\left(1 + \sin\theta\right)}{b\cos\theta\left(\cos^2\theta - \eta^2\cos^2\theta + 3\eta^2\right)},\quad E_2 = \frac{K_f\left(1 - \sin\theta\right)}{b\cos\theta\left(\eta^2\cos^2\theta - \cos^2\theta + 1\right)}$$

$$\nu_{12} = \frac{\left(1 - \eta^2\right)\sin\theta\left(1 + \sin\theta\right)}{\left(\cos^2\theta - \eta^2\cos^2\theta + 3\eta^2\right)},\ \nu_{21} = \frac{\left(1 - \eta^2\right)\sin\theta\left(1 - \sin\theta\right)}{\left(\eta^2\cos^2\theta - \cos^2\theta + 1\right)} \tag{3}$$

where $\eta = t/l$ denotes the slenderness ratio of the cell walls. In addition, in the above equations the cell lengths l and h are assumed to be identical. It should be noted that the Gibson's formulas given in Equation (1) contained singularities at θ=0 at which both E_2 and ν_{21} tend to infinity. These singularities are eliminated in Equation (3).

All the analytical solutions discussed so far were based on small deformation theory, so the equivalent elastic modulus and Poisson's ratio give in Equations (1) - (3) are only applicable to small strains from the original reference configurations. However, when the honeycombs are utilized as load-bearing or energy-absorption structures, large deformations are often experienced and in these cases, nonlinear behaviour becomes significant. In order to take into account nonlinear effects on the mechanical behaviour of re-entrant hexagonal honeycombs, a theoretical approach for predicting negative Poisson's ratio under large deformations has been developed [19]. This model is also suitable for small flexure and elastic buckling and provided an extended and refined understanding of the negative Poisson's ratio in auxetic materials. This study indicated that under large deformation, the Poisson's ratio is no longer a constant, but varies significantly with the strain level. At the limit of small strain, the nonlinear solution converged to the linear solution obtained for small flexure deformations. At large deformations, the negative Poisson's ratios are very different in large compressive and tensile stresses. In addition, the

Poisson’s ratios are very sensitive to the geometric parameters, such as the length ratio of the cell walls, *h/l* and the angle θ.

The effective material properties of the chiral honeycombs for small deformation were also presented in the literature [20]. The geometry of this 2D auxetic structure is shown in Figure 5 and the unit cell is detailed in Figure 10 below. Assuming cell wall bending as the primary mechanism for small deformation of the chiral honeycomb, the authors demonstrated that the effective Poisson’s ratio of this material is equal to -1 and the effective Young’s modulus is

$$E = E_s \sqrt{3}\frac{t^3}{L^3}\frac{L^2}{r^2} \tag{4}$$

where all the geometric parameters are given in Figure 10. It should be noted that the equivalent material properties of the chiral honeycomb are identical in the x_1 and x_2 principal directions. In addition, experimental results indicated that the negative Poisson’s ratio of -1 is insensitive to the strain level.

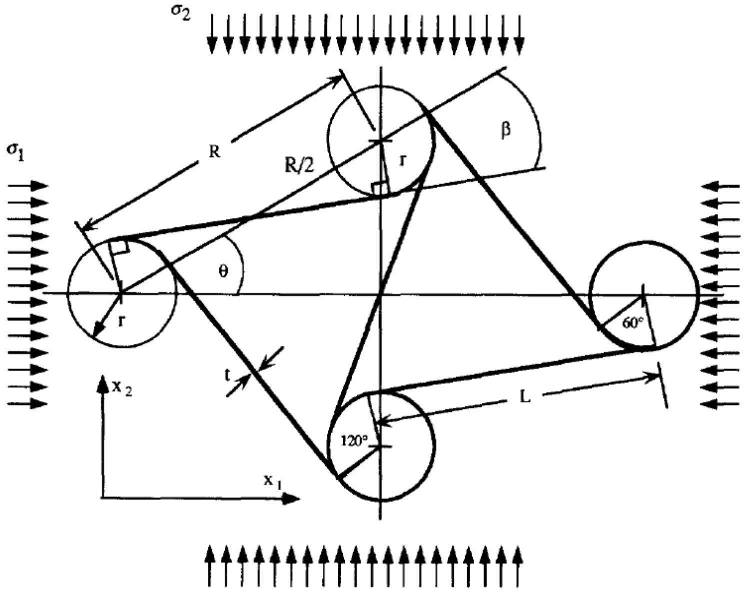

Figure 10: Geometry of unit cell of chiral honeycomb. (Reproduced from Reference [20])

In addition to the 2D auxetic structures discussed above, analytical formulas for equivalent elastic modulus and Poisson’s ratio for 3D conventional and re-entrant foam materials were also developed [6]. In this work, foam materials with negative Poisson’s ratio were made by transforming the cell structure from the convex polyhedral shape of conventional foam cells to a concave or “re-entrant” shape. The equivalent Young’s moduli of both the conventional and re-entrant open cell foams were obtained by modelling the 3D unit cell as an idealized 14-sided unit cell. The analytical solutions were obtained by first calculating deflection of a cell rib under a certain amount of force and then evaluating the Young’s modulus using Hooke’s law. Throughout this study, the deflection of the cell ribs was calculated by the second Castigliano’s theorem [6] and only deflection due to bending was considered as the deflections due to other deformation modes, such as twist and axial compression and tension, were less significant for slender ribs.

The results indicated that the equivalent Young's modulus of the re-entrant foams decreases with permanent volumetric compression ratio and this prediction was supported by experimental results. The results also confirmed that most of the differences between the mechanical properties of the conventional and re-entrant foam materials are associated with the change in cell shapes from convex and concave.

The finite element method has also been used to obtain the equivalent material properties of 2D auxetic materials. In some of the finite element studies, the finite element models involved a single unit cell [7], while in other studies, the patch of the auxetic structures including arrays of unit cells were considered, such as in References [17, 18]. Finite element solutions were compared against the analytical solutions and good agreement between them were often observed. A 3D finite element model for open cell foams was also developed [21]. This model contained a single unit cell in which the ribs were represented by three-dimensional elastic beam elements, thus rib flexing was assumed to be the dominant mode of deformation. The numerical results showed that by altering the cell geometry, both positive and negative Poisson's ratios could be produced with different levels of anisotropy. The 3D results were compared with Gibson's 2D analytical model for re-entrant hexagonal honeycomb. This comparison showed that the 2D approximations failed to model the properties of the three-dimensional network accurately, so a full 3D analysis was required.

Dirrenberger and co-workers applied a finite element-based numerical homogenization technique to determine effective elastic material properties of three periodic auxetic materials, including hexachiral, tetra-antichiral and rotachiral lattices [22]. This homogenization method makes use of finite element models of the unit cell in the periodic structures with periodic boundary conditions. Although this method has been rarely applied to characterizing auxetic materials, it has been widely used by the mechanics of composite materials. In this homogenization method, the macroscopic stress and strain tensors are first calculated through spatial averaging of the finite element produced local stresses and strains, obtained by applying the periodic boundary conditions. These macroscopic stress and strain are subsequently used to generate the fourth-order tensor of effective elastic moduli. The effects of anisotropy and out-of-plane loading were investigated. The results from this study agreed with the previous solutions when comparisons were available and indicated that for the same volumetric fraction, the ligament geometry had a very significant impact on the material properties, as the effective Young's modulus and shear modulus of the rotachiral lattice were found to be one magnitude lower than those of the hexachiral lattice. The same homogenization technique has recently been applied to characterize nonlinear behaviour of hexachiral structures under elastic-plastic deformations [23]. Both isotropic and anisotropic plasticity models were utilized. The results indicated that the auxeticity of the materials was enhanced by plasticity; in particular, the Poisson's ratio became more negative with the increase of plastic deformations.

All the theoretical and numerical models dealt with auxetic materials with perfectly periodic micro-structures. However, the real-world materials normally contain some sort of imperfections from the manufacturing process. As a result, some of measure of heterogeneity is required to account for the deviation from the regular unit cells in the real-work situation. Horrigan and co-workers [24] have attempted to establish the link between heterogeneous networks and its material properties. In this study, the heterogeneous networks were constructed using existing optimization methods, namely genetic algorithm (GA) and differential evolutionary (DE) algorithms, and the material properties of the resulting heterogeneous grids were obtained using the finite element method. This work demonstrated that a honeycomb with negative Poisson's ratio could be created by simply adding disorder to a positive Poisson's ratio one.

A finite element analysis of auxetic plate deformation was performed at the macroscopic level by Strek and co-workers [25]. In this numerical analysis, a thick elastic plate was modelled using the regular solid elements. This plate was loaded on two opposite side walls and constrained along the other two sides. The top and bottom surfaces were left stress free. Simulations were performed for Poisson's ratio between -1 and 0.5 using commercial finite element programs COMSOL and ABAQUS. By comparing the deformation patterns predicted for materials with different values of Poisson's ratios, the auxetic effects were clearly observed. These results confirmed that the macroscopic behaviour of the auxetic materials could be analyzed by the regular finite element programs as long as the effective material properties, such as the elastic moduli and Poisson's ratios, are available.

2.5 Contact and impact problems of auxetic materials

Argatov and co-workers [26] investigated the implications of the negative Poisson's ratio on the quasi-static and dynamic indentation compliances of isotropic homogeneous materials using an analytical approach. The results from this study indicated that the indentation, vibration and impact compliances are all significantly affected when Poisson's ratio of the material assumes a negative value. The friction at the interface of the indenter and the elastic medium was found to enhance the negative Poisson's ratio effect because the fully adhesive contact condition resulted in more negative Poisson's ratio than did the frictionless contact condition. In the Hertz contact problem, it was found that the location of the maximum shear stress changes with decreasing Poisson's ratio. In fact, when the Poisson's ratio became sufficiently negative, the location of the maximum shear stress approached the contact interface. This implied that the contact fracture in auxetic materials should initiate in the surface layer.

An analytical model for contact problems between two isotropic homogeneous soft bodies has been proposed by Wang and Lakes [27] to simulate the contact between human buttocks and seat cushion. The Poisson's ratio of the cushion material was allowed to be negative. The human buttocks were modelled as an ideal sphere of an incompressible material with a low shear modulus. Analyses by both the Hertz contact model and a finite thickness 3D elasticity model showed that using negative Poisson's ratio cushions could reduce the contact pressure. As a result, negative Poisson's ratio cushions might be beneficial in the prevention of pressure sores or ulcers in the sick and in reduction of pressure-induced discomfort in seated people.

Very recently, the structural response of a negative Poisson's ratio structure with regular re-entrant hexagonal unit cells under crush by a rigid wall was investigated by Yang and co-workers [28] through numerical simulations using LS-DYNA. The finite element mesh of the structure was generated using HYPERMESH where all cell walls were discretized into 4-noded shell elements. The bottom of the model was clamped and the top was loaded by a rigid body of known mass and velocity. Two different contact algorithms were utilized, where automatic single surface contact was employed to deal with the contact between the highly deformed cell walls during the loading process and the automatic node-to-surface contact was applied between the negative Poisson's ratio structure and the impacting rigid mass. The mesh geometry and material properties are all well documented in Reference [28]. The numerical results indicated that during the deformation process, the re-entrant structure deformed in a stable and progressive folding patterns. Some local deformations occurred at the early stage, and then the deformations started to propagate through the model until the entire structure was compacted. The analysis resulted in a load-displacement curve from which the energy-absorption of the negative Poisson's ratio structure could be evaluated. This numerical analysis procedure will be utilized in Phase 1 of this proposed contract to quantify the influence of the geometric parameters of the re-entrant hexagonal honeycomb polymer structure on its energy-absorption capability.

3 Formulation and verification of finite element models for impact simulations

3.1 Formulation of test cases

It has been determined that the numerical studies in Phase 1 would be based on the problem configuration utilized in the study of Yang *et al*. [28]. In this configuration, responses of auxetic material samples resting on a rigid surface subjected to impact of a rigid mass were considered. As mentioned earlier, the objective of the present study was to characterize the influence of the various geometric parameters of the auxetic materials, such as the re-entrant angle, rib thickness and void fraction, on the energy absorption behavior of the auxetic material and the force transmitted to the rigid surface.

For the convenience of comparing the numerical results for auxetic material samples with different values of geometric parameters, it is desirable to design the test cases to make them having identical gross dimensions and areal density. Based on this consideration, the test cases are designed using the periodic unit cell shown in Figure 11 below:

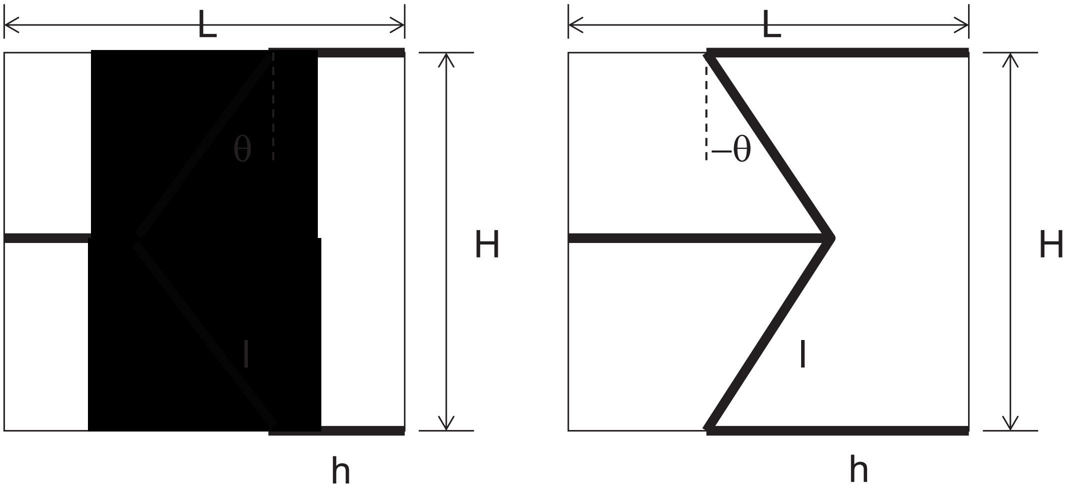

Figure 11: Periodic cells of conventional and re-entrant honeycomb structures.

From this diagram, the rib lengths, l and h, can be determined for any given dimensions of the periodic cell, L and H, and the re-entrant angle θ as

$$l = \frac{H}{2\cos\theta}, \quad h = \frac{L - l\sin\theta}{2} \tag{5}$$

The thicknesses of the ribs can then be determined using the desired void fraction. Denoting the void fraction as V and assuming the thicknesses of all ribs are identical, we have

$$t = \frac{HL(1-V)}{2h+2l} \tag{6}$$

Using the concept described above, the first set of test cases were generated by using H=L=1mm, V=0.846 and different angles as shown in Table 1 below. These angles included the re-entrant cases with θ=-10^o to -40^o degrees, the conventional honeycombs with θ=10^o to 40^o and also a special case in between with θ=0^o. The calculated rib lengths and thicknesses are given in Table 1.

Table 1: Proposed test cases for void fraction VF=0.845.

Model #	Honeycomb Type	Angle θ	*l* (mm)	*h* (mm)	*t* (mm)
1	Re-entrant	-10	0.5077	0.5441	0.0732
2	Re-entrant	-20	0.5321	0.5910	0.0685
3	Re-entrant	-30	0.5774	0.6443	0.0630
4	Re-entrant	-40	0.6527	0.7098	0.0565
5	Re-entrant	-50	0.7779	0.7979	0.0489
6	Conventional	10	0.5077	0.4559	0.0799
7	Conventional	20	0.5321	0.4090	0.0818
8	Conventional	30	0.5774	0.3557	0.0825
9	Conventional	40	0.6527	0.2902	0.0816
10	Conventional	50	0.7779	0.2021	0.0786
11		0	0.5000	0.5000	0.0770

The finite element models for these proposed test cases were generated using the shell element, following the successful impact simulations reported in Reference [28]. At the early stage of the present contract, attempts were made to replicate the analyses reported in the reference using a comparable shell element model and our results were in good agreement with published ones. A typical finite element model for the present analyses is shown in Figures 12 and 13. In the impact simulation, the nodes on the bottom of the auxetic material were constrained against motion in the Z-direction to represent the rigid surface, but permitted to slide in the horizontal direction (One node in the middle of the bottom was constrained against motion in X-direction to eliminate rigid body mode). The top edge was in contact with the impacter, which was described through surface-to-surface contact conditions. The side edges were unconstrained in this model. It should be noted that this treatment of boundary conditions on the sides might result in an underestimation of the overall stiffness of the auxetic structure as the interaction between the model and surrounding materials were ignored. To maintain a reasonable model size for the parametric study, one element was used in the depth (Y) direction as indicated in Figure 13. Displacements in the Y-direction were constrained throughout the model, so its deformation was consistent with the plane strain assumption.

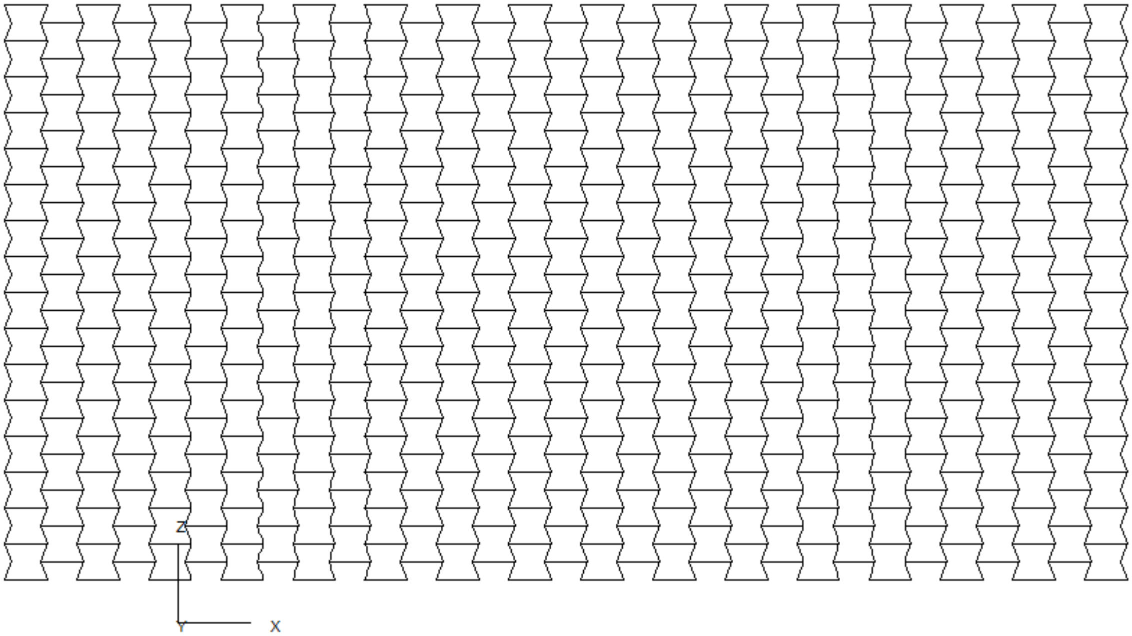

Figure 12: Shell element model for a re-entrant honeycomb structure with θ=-20^{O}.

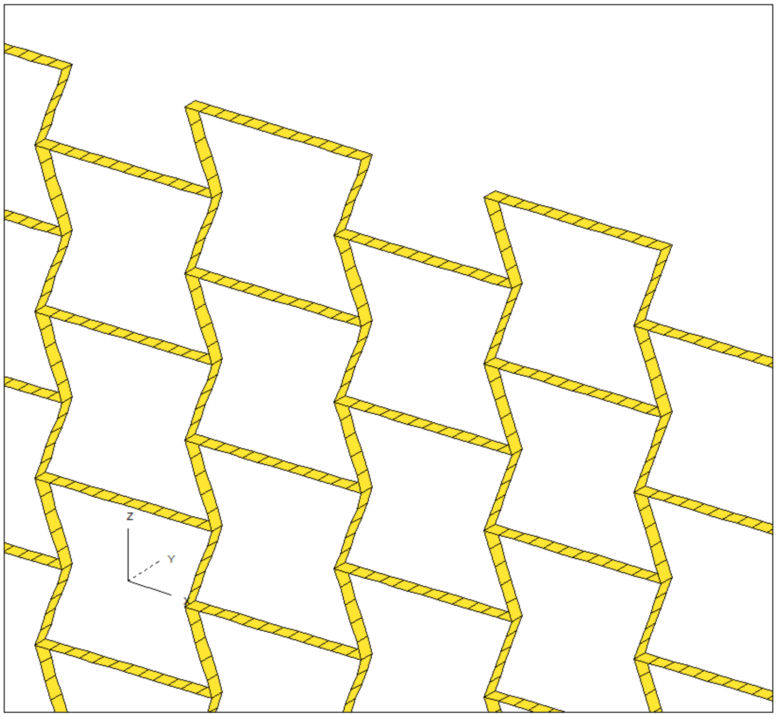

Figure 13: Details of the shell element model shown above.

3.2 Approximate polymer material properties

The polymer material properties provided by the Technical Authority are shown in Figure 14. These generic material properties were generated from a nonlinear viscoelastic material model using typical quasi-static and stress relaxation properties of polyurea.

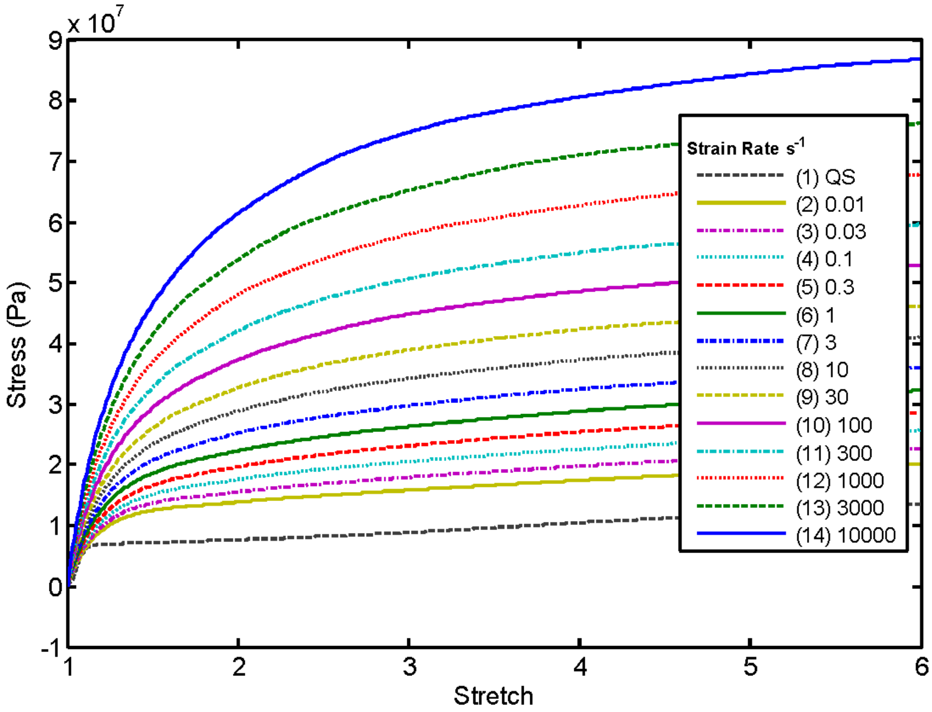

Figure 14: Polymer material properties to be used in the present numerical study.

In the previous numerical studies of polymer coatings, the polymer was always modeled using the nonlinear viscoelastic material model, MAT_77_O, provided in LS-DYNA [29]. In all these previous analyses, the polymer material was represented by using either the 3D solid element or the 2D axisymmetric solid element. In those analyses, the viscoelastic material model, MAT_77, worked reasonably well. However, in the present study of the auxetic materials, use of solid elements would result in excessively large finite element models, making numerical solutions unfeasible. Furthermore, it has been demonstrated by Yang and co-workers [28] that the shell element would be more suitable. Attempts were made to use this viscoelastic material model with the shell element and numerical errors were encountered.

In order to simulate the strain rate dependent behavior of the polymer material shown above, we have decided to use the piecewise linear elastic-plastic material model which allows the users to explicitly specify stress-plastic strain curves at each strain rate value. This material model was successfully applied in Reference [28]. To generate input material parameters for this model, some data processing was required on the original stress-strain curves shown in Figure 14. First of all, a Young's modulus must be defined and secondly, the stress-strain curves need to be converted to stress-plastic strain curves.

The selected Young's modulus supposed to represent the initial slope of the stress-strain curves at all strain rate values. However, due to the wide variation on the initial slope of the different curves, an average value must be used and the selection of this value was not unique. In order to study the sensitivity of the nonlinear dynamic solutions to Young's modulus, two Young's moduli, E=84.7 MPa and E=166.7 MPa, were utilized when generating the approximate material properties. Using these values of Young's modulus, the original stress-strain curves were converted to stress-plastic strain curves as

$$\varepsilon^{p} = \varepsilon - \sigma / E \tag{7}$$

where σ, ε and ε^{p} denote stress, strain and plastic strain respectively. For demonstration purposes, the converted curves for strain rate 30/s using both Young's moduli are shown in Figures 15 and 16 and the stress-plastic strain data are presented in Table 2. It should be noted that before the data conversion, the original stress-strain curves were reduced to a small number of data points that were adequate to represent the stress-strain behavior.

Table 2: Converted stress-plastic strain curves for strain rate 30/s using different values of Young's Modulus.

***E*=84.7 MPa**		***E*=166.7 MPa**	
Stress (Pa)	**Plastic-strain**	**Stress (Pa)**	**Plastic-strain**
17211002.00	0.00	10000000.00	0.00
23273685.00	0.10	17211002.00	0.11
29729010.00	0.37	23273685.00	0.24
33535408.00	0.68	29729010.00	0.55
36285111.00	1.02	33535408.00	0.89
38066392.00	1.34	36285111.00	1.24
39582791.00	1.68	38066392.00	1.57
40874873.00	2.05	39582791.00	1.92
42902901.00	2.72	40874873.00	2.29
46228705.00	4.43	42902901.00	2.98
		46228705.00	4.71

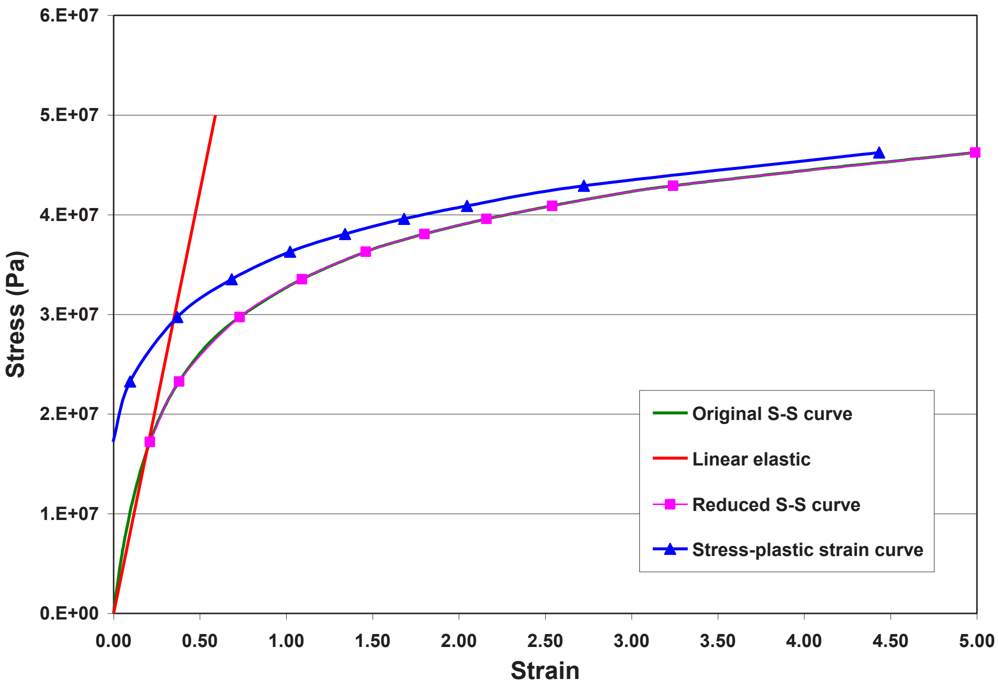

Figure 15: Original and converted stress-strain curve for strain rate 30/s using E=84.7 MPa.

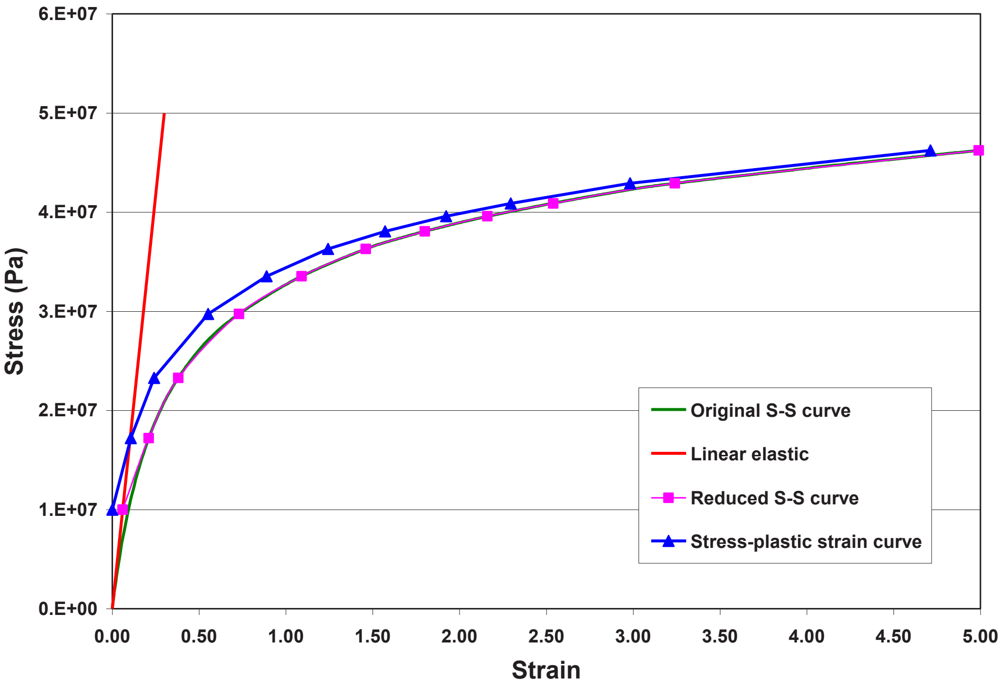

Figure 16: Original and converted stress-strain curve for strain rate 30/s using E=166.7 MPa.

3.3 Calculation of effective material properties

Once the unit cell geometry and the linear elastic properties of the rib material were defined, effective material properties of the auxetic materials could be calculated using the analytical formulas published in the literature, such as Gibson *et al.* [14] and Masters and Evans [15]. In these analytical solutions, Gibson's formula was derived by considering purely flexural (bending) deformations of the ribs, whereas the Masters' formula was more general and also included contributions of hinging and shearing deformations.

In the present work, these analytical solutions were implemented in a MATLAB function for calculating effective material properties from the user supplied geometric parameters, including rib lengths, l and h, thickness t and angle θ, and linear material properties, such as Young's modulus, for the rib material. The calculated effective material properties for the conventional and re-entrant honeycomb structures defined in Table 1 and Young's modulus E=84.7 MPa are summarized in Table 3 below where the global coordinate system was defined in Figure 12. Prior to the above calculations, the MATLAB program was verified by considering the conventional and re-entrant honeycomb geometries previously studied by Henderson and co-worker [16]. The present results are nearly identical to the published analytical solutions.

Examination of the results given in Table 3 led to a number of interesting observations. First of all, the effective material behaviour of auxetic materials is highly orthotropic as the effective elastic moduli and the Poisson's ratios in the two principal directions are very different for all cases considered. In addition, the nature of the orthotropic property is sensitive to the geometry of the unit cell. Secondly, for all cases, the effective elastic moduli are at least one magnitude lower than that of the rib materials. The effective elastic modulus in the vertical direction, E_z, is more sensitive to angle θ than the effective modulus in the horizontal direction E_x. Thirdly, Poisson's ratios in both directions are always of the same sign, for instance, for re-entrant honeycombs, the Poisson's ratios are both negative, but for conventional honeycombs, positive values are always obtained. However, as two competing factors, high Poisson's ratios can never be achieved in both directions at the same time. This observation indicated that in practical applications, the optimum geometric configurations of auxetic materials are problem-orientated and the nature of the loading condition and the deformation pattern of the material must be taken into account. Fourthly, in some cases of the conventional honeycombs, positive values of Poisson's ratio greater than 0.5 are obtained. Please note that this is inadmissible for isotropic, homogeneous materials in continuum mechanics.

3.4 Verification of the finite element model

Once the unit cell geometries were defined and finite element models constructed, great efforts were taken to verify these finite element models before they were utilized in impact simulations. In this verification process, linear and nonlinear static analyses were first performed for different loading orientations. For linear problems, effective material properties were extracted from the finite element solutions and compared with the analytical results. For nonlinear analyses, the results were carefully examined using the engineering judgements. A number of impact simulations were then carried out to investigate the effects of various modelling parameters on the numerical solutions. These modelling parameters included extent of finite element model, the approximate material properties and the approach for modeling the impact mass.

Table 3: Analytical solutions of effective properties of auxetic materials defined in Table 1 under small deformations.

Case	Type	Angle (degrees)	Formula	PR_{zx}	PR_{xz}	E_z (MPa)	E_x (MPa)
6	Conventional	10	Gibson	2.835	0.353	5.476	0.681
			Masters	1.587	0.317	2.935	0.586
7	Conventional	20	Gibson	1.374	0.728	1.316	0.697
			Masters	1.151	0.659	1.057	0.606
8	Conventional	30	Gibson	0.866	1.154	0.495	0.659
			Masters	0.803	1.058	0.442	0.583
9	Conventional	40	Gibson	0.596	1.677	0.200	0.564
			Masters	0.575	1.565	0.188	0.512
10	Conventional	50	Gibson	0.420	2.383	0.074	0.423
			Masters	0.413	2.271	0.072	0.396
1	Re-entrant	-10	Gibson	-2.836	-0.353	4.212	0.524
			Masters	-1.704	-0.318	2.439	0.455
2	Re-entrant	-20	Gibson	-1.374	-0.728	0.773	0.410
			Masters	-1.208	-0.662	0.660	0.362
3	Re-entrant	-30	Gibson	-0.866	-1.155	0.220	0.294
			Masters	-0.827	-1.065	0.206	0.265
4	Re-entrant	-40	Gibson	-0.596	-1.679	0.066	0.187
			Masters	-0.585	-1.573	0.064	0.173
5	Re-entrant	-50	Gibson	-0.420	-2.384	0.018	0.102
			Masters	-0.417	-2.273	0.018	0.097

3.4.1 Linear and nonlinear static analysis

The finite element model verifications for linear and nonlinear static analyses were performed on one conventional with $\theta=20^o$ and one re-entrant honeycomb models with $\theta=-20^o$. The finite element model for the re-entrant case is depicted in Figure 12. This model was constructed using the 4-noded quad shell elements as detailed in Figure 13.

To obtain the effective material properties through finite element analyses, we applied uniform stresses in either the horizontal or vertical directions. The deformed and original configurations of the conventional and re-entrant honeycomb structures from VAST analyses are presented in Figures 17-20. For the horizontal load case, the left edge of the structure was constrained against motion in the X-direction. The Z constraint was only applied at a single node in the middle of the left edge to remove rigid body mode, but allow free contraction and expansion in the Z-direction. For the vertical load case, similar boundary conditions were applied to the bottom of the model. From the deformed configurations in Figures 17-20, it was noticed that although irregular deformations existed near the edges, the deformations in the interior of the model are almost uniform. These areas of uniform deformations allowed computation of average strains from which the effect Poisson's ratios and Young's moduli were evaluated. The effective properties from linear finite element analyses using both VAST and LS-DYNA are compared with the analytical solutions in Table 4. A very good agreement is obtained.

Table 4: Comparison of analytical and numerical solutions of effective properties of auxetic material under small deformations.

Case	Type	Angle	Method	PR_zx	PR_xz	Ez	Ex
7	Conventional	20	Gibson	1.374	0.728	1.316	0.697
			Masters	1.151	0.659	1.057	0.606
			VAST	1.162	0.690	1.149	0.632
			LS-DYNA	1.200	0.690	1.210	0.640
2	Re-entrant	-20	Gibson	-1.374	-0.728	0.773	0.410
			Masters	-1.208	-0.662	0.660	0.362
			VAST	-1.216	-0.657	0.713	0.360
			LS-DYNA	-1.220	-0.687	0.721	0.376

With the success of the linear static analyses, we moved on to nonlinear static analyses to better understand the behavior of the auxetic materials under large deformations. The first nonlinear case considered was the re-entrant honeycomb structure subjected to uniform tension in the horizontal direction, which resulted in a final deformed configuration shown in Figure 21. With the increase of the tensile stress, the horizontal displacement at the loaded edge increased monotonically as shown in Figure 22. However, in the vertical direction, the structure expanded initially, but started to contract once the maximum value was passed (see Figure 23) resulting in a strongly deformation-dependent Poisson's ratio as shown in Figure 24. The Poisson's ratio started with a value consistent with that obtained from linear analysis, but reduced rapidly towards zero when the structure contracted in the vertical direction and returned its original width. This behavior of the re-entrant honeycomb can be explained by the deformed configurations of the unit cells as shown in Figure 25. At the early stage of the deformation process, the honeycomb remained re-entrant, but the angle was gradually reduced (Figure 25 (b)), pushing the horizontal ribs further apart. Over this phase of deformation, the structure expanded in the vertical direction. When the originally angled ribs became vertical (Figure 25 (c)), the vertical expansion reached its maximum value. For further loading, the vertical ribs deformed towards the opposite direction, which pulled the horizontal ribs together causing the structure to contract in the vertical direction (Figure 25(d)). In this case, the originally re-entrant honeycomb behaved just like a conventional honeycomb structure. Through this illustration, it was realized that the deformation-dependency of the Poisson's ratio was caused by the large variations of angle θ.

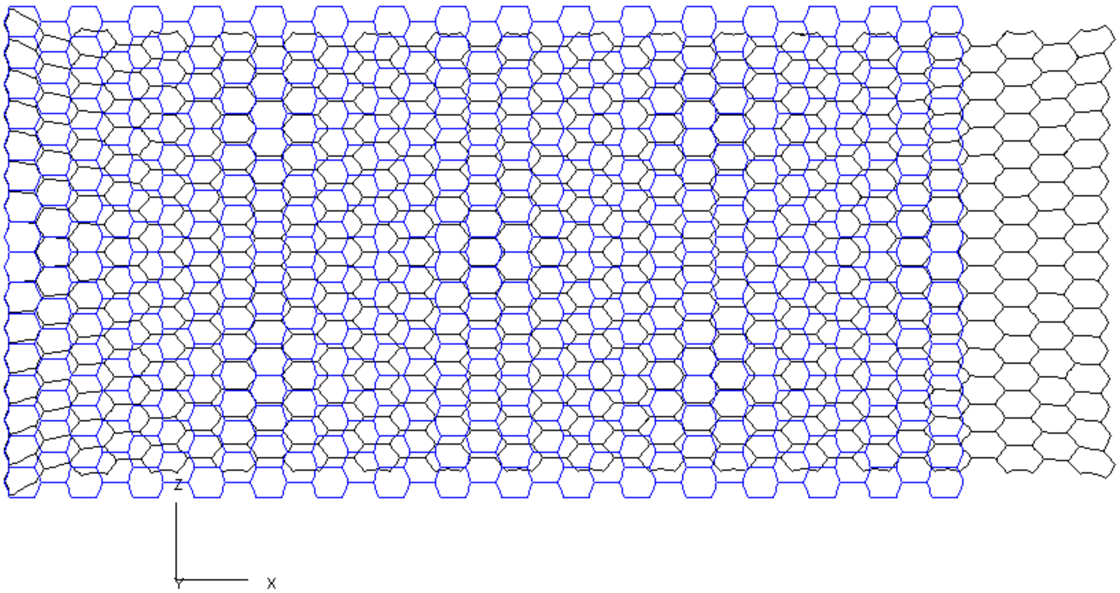

Figure 17: Original (blue) and deformed (black) configurations of a conventional honeycomb structure ($\theta=20^O$) subjected to horizontal tension.

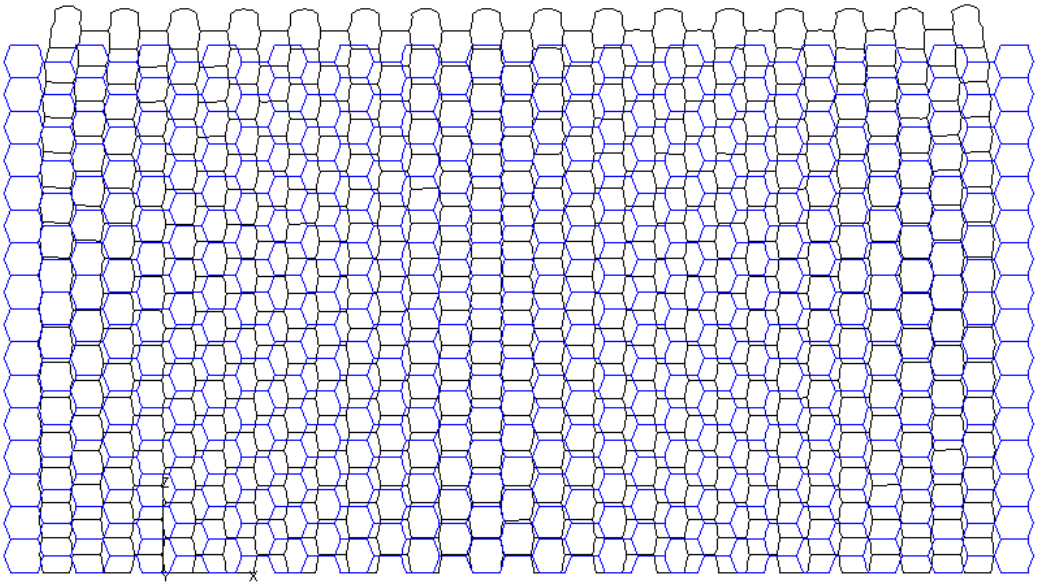

Figure 18: Original (blue) and deformed (black) configurations of a conventional honeycomb structure ($\theta=20^O$) subjected to vertical tension.

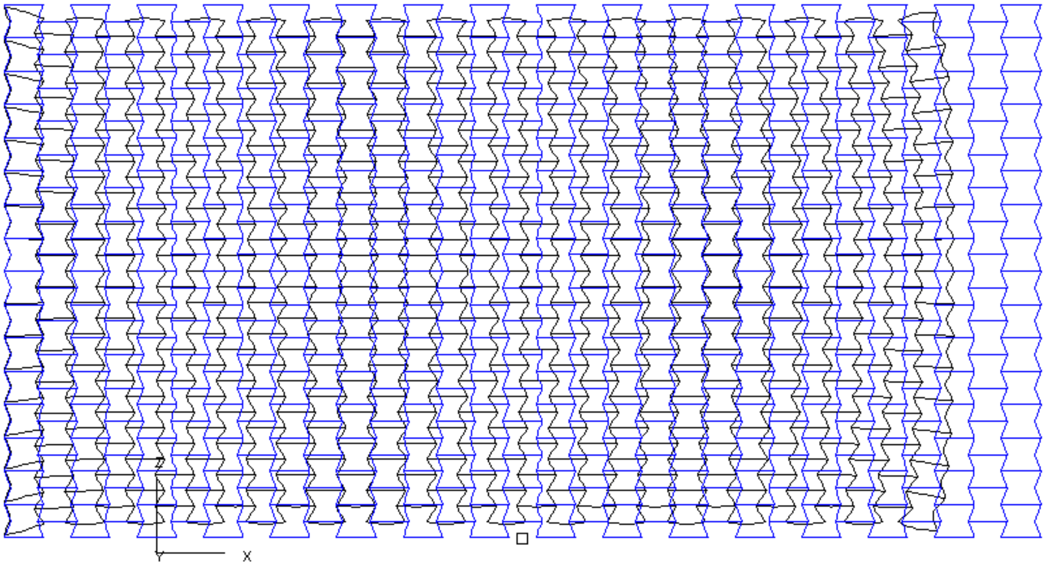

Figure 19: Original (blue) and deformed (black) configurations of a re-entrant honeycomb structure (θ=20^O) subjected to horizontal compression.

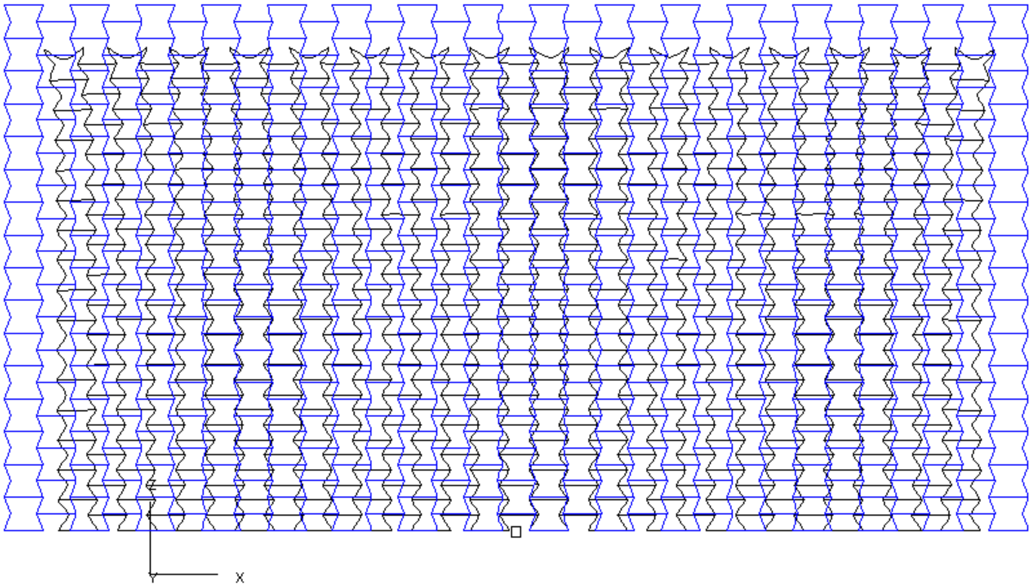

Figure 20: Original (blue) and deformed (black) configurations of a re-entrant honeycomb structure (θ=20^O) subjected to vertical compression.

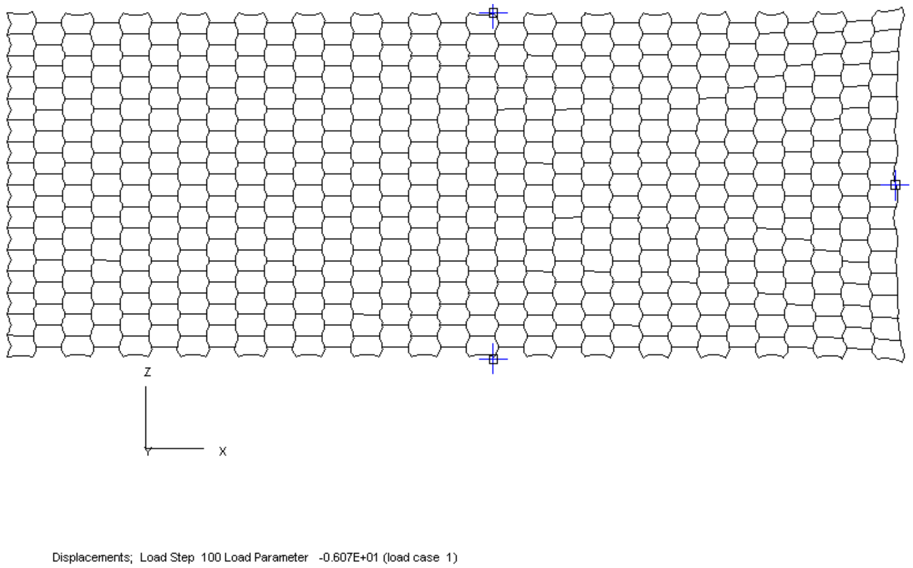

Figure 21: Final deformed configuration of an auxetic structure subjected to horizontal tensile stresses.

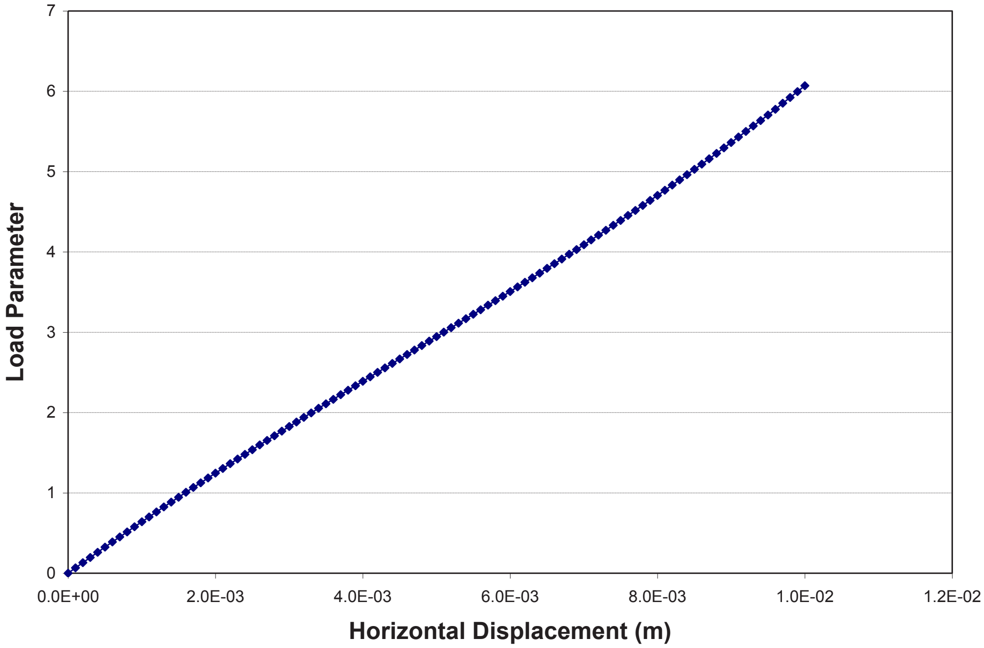

Figure 22: Load-horizontal displacement curve of the marked node on the right edge.

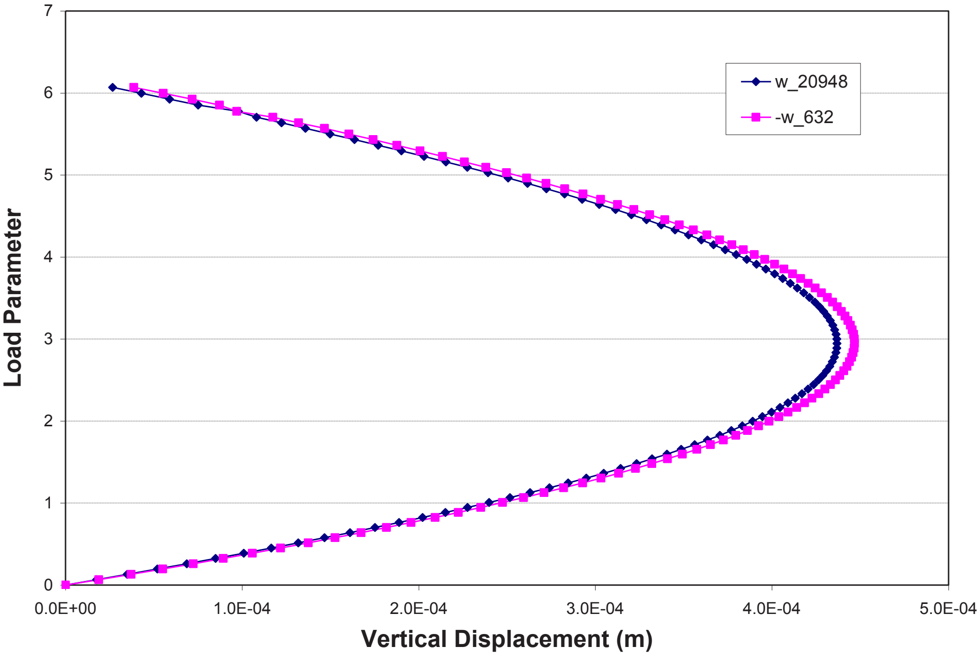

Figure 23: Load-vertical displacement curves at the two nodes marked on the top and bottom edges of the auxetic structure.

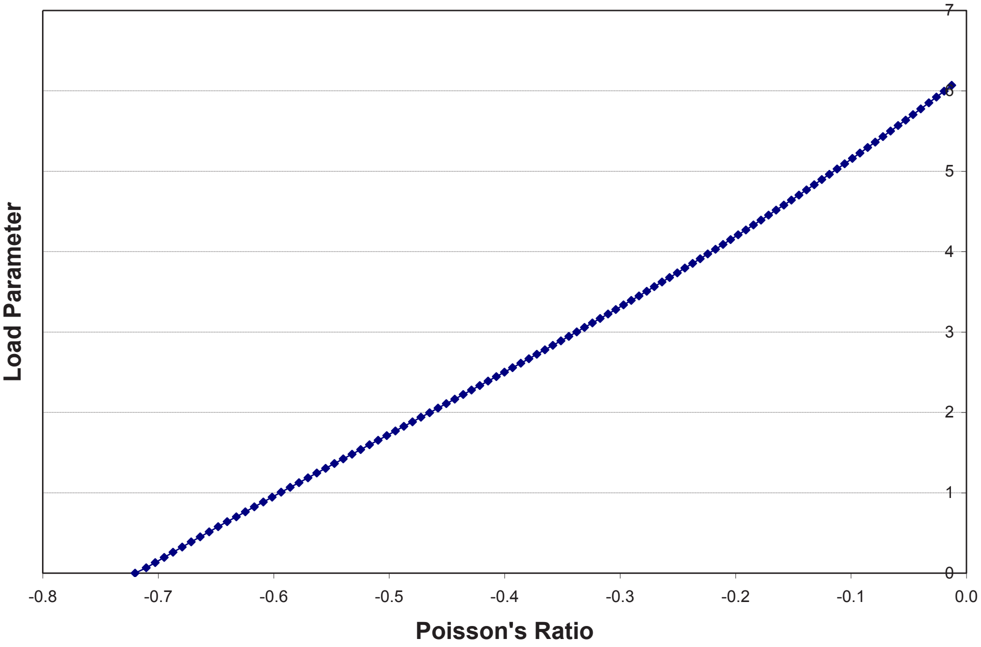

Figure 24: Variation of the effective Poison's ratio of the auxetic structure with the level of deformation.

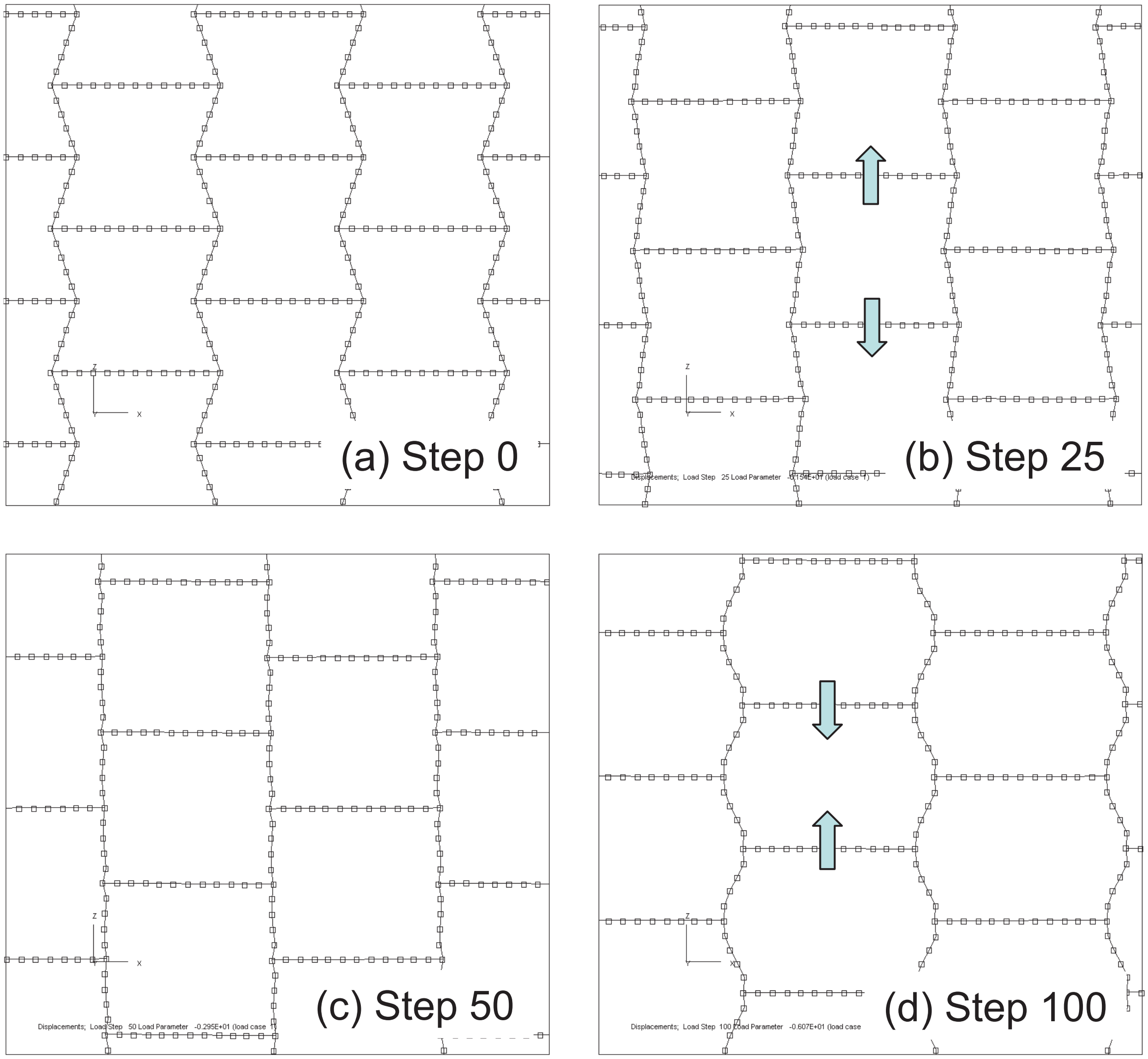

Figure 25: Typical deformed configurations of unit cells in horizontally loaded re-entrant honeycomb that explained deformation-dependent of Poisson's Ratio.

The deformed configuration of the re-entrant structure subjected to tension in the vertical direction is given in Figure 26. The load-vertical and horizontal displacement curves are shown in Figures 27 and 28, respectively. A very strong stress-hardening effect was observed in the horizontal direction. This was because after the originally angled ribs became vertical (as shown in Figure 27), no further horizontal contraction could possibly occur. Once again, this change in structural geometry due to large deformations resulted in a very significant variation in Poisson's ratio (Figure 29).

Under horizontal or vertical compression, the auxetic structure became unstable once the limits of elastic stability were reached. In this case, the structure might buckle either in a global failure mode, similar to collapse of a beam or a column, or in a local mode at the unit cell levels where the unit cells deformed like a mechanism. The elastic buckling load levels under both loading conditions were confirmed by linear buckling (eigenvalue) analyses.

As indicated by the load-displacement curves shown in Figures 31, 32, 35 and 36, in both load cases, the structure responded almost linearly at the early loading stage, where the displacement in the loading direction increased proportionally to the applied load and the structure contracted in the perpendicular direction. The initial values of the Poisson's ratios did match the results from linear elastic analyses as indicated in Figures 33 and 37. However, once the limit load levels were reached, significant geometric nonlinear effects started to develop and in this case, a rapid reduction of the Poisson's ratios was observed. The final collapse modes of the structure are shown in Figures 30 and 34 for horizontal and vertical loadings, respectively. It should be noted that the deformed shapes were generated using the actual magnitude of displacements (there was no amplification of the displacements, as is sometimes done when visualizing FE results). It is believed that the asymmetry of the collapsed structures is an artifact that arises from round-off errors.

These linear and nonlinear static analyses confirmed the correctness of the shell finite element models, such as the mesh layout, load definition and boundary conditions. In the meantime, it was also indicated that the auxeticity of re-entrant structures is strongly dependent upon the level of deformations. This is a consequence of the high sensitivity of the effective material properties to the geometric parameters, such as the re-entrant angle.

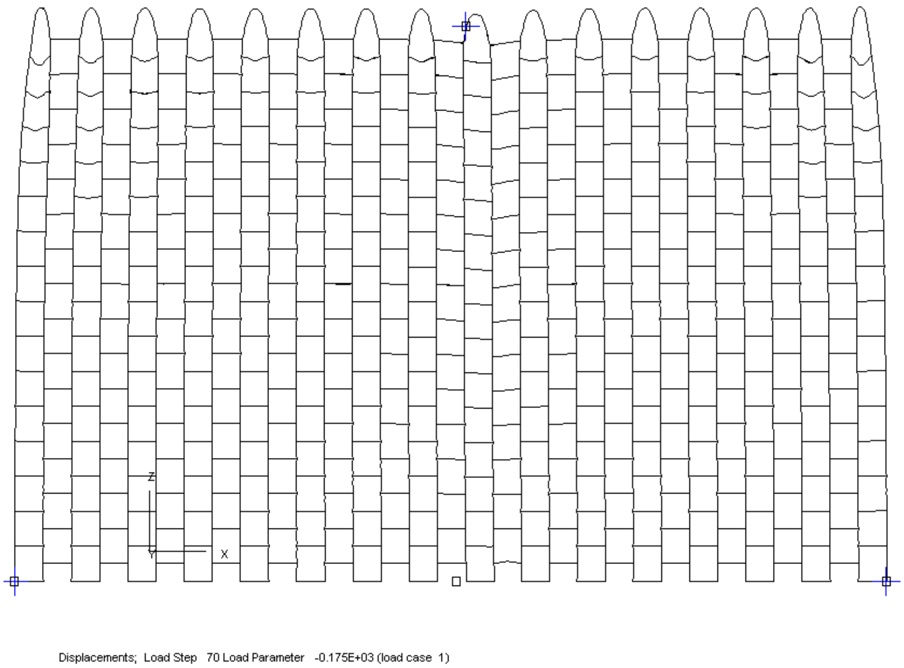

Figure 26: Final deformed configuration of an auxetic structure subjected to vertical tensile stresses.

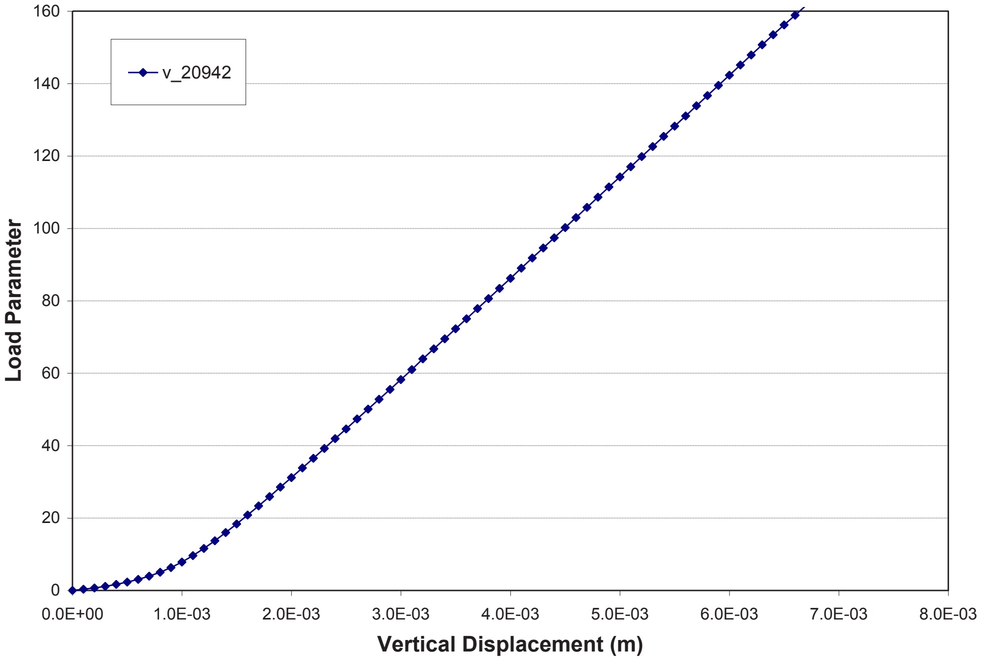

Figure 27: Load-vertical displacement curve of the node marked on the top edge.

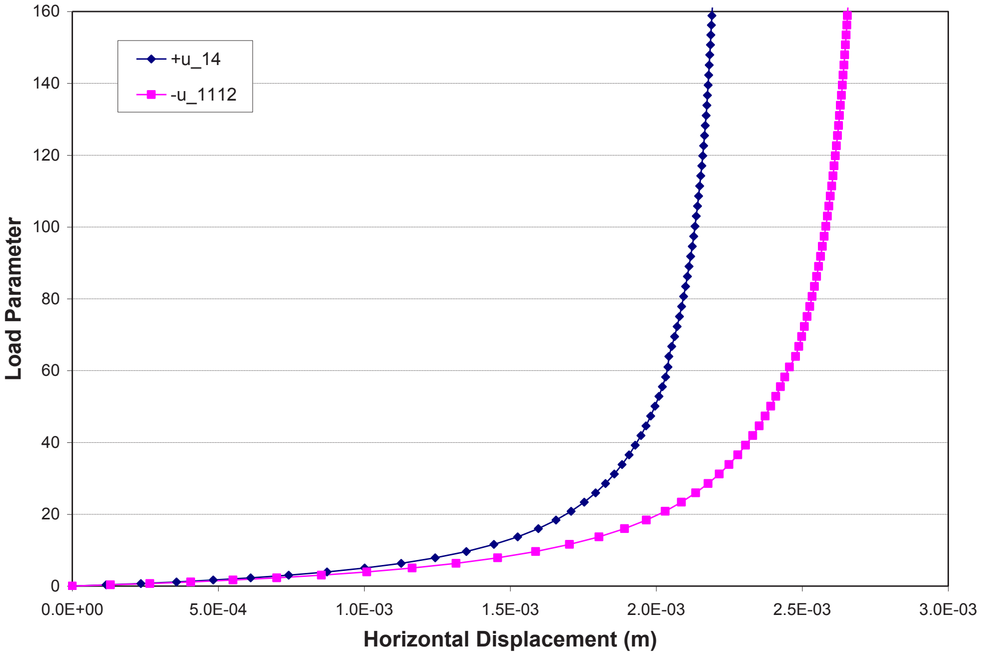

Figure 28: Load-horizontal displacement curves at the two nodes marked at the bottom of the right and left edges of the auxetic structure.

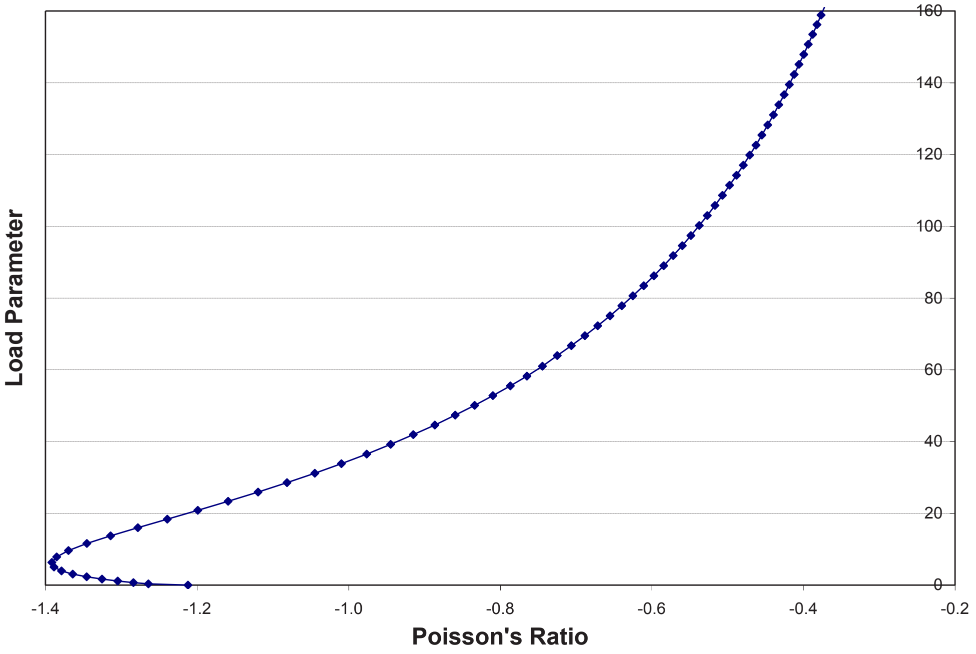

Figure 29: Variation of the effective Poison's ratio of the auxetic structure with the level of deformation.

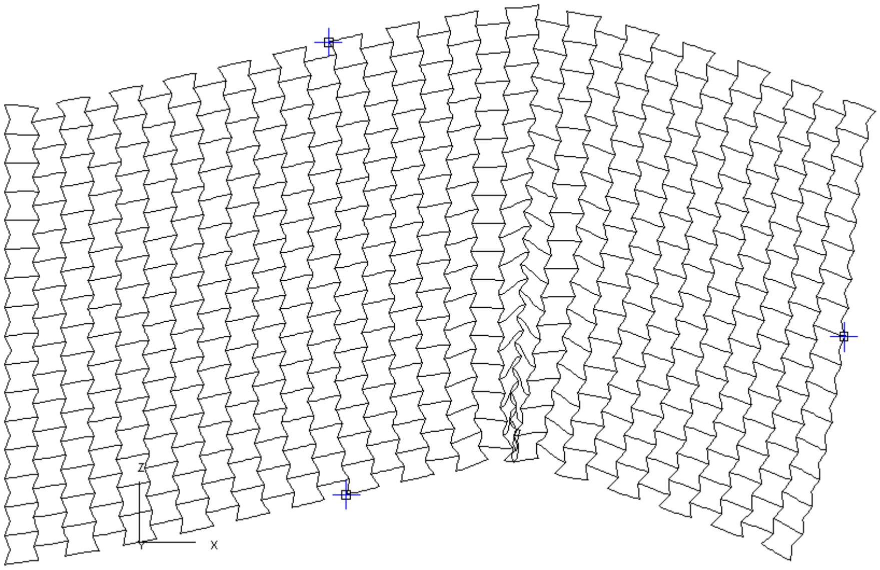

Displacements; Load Step 40 Load Parameter 0.461E+00 (load case 1)

Figure 30: Final deformed configuration of an auxetic structure subjected to horizontal compressive stresses.

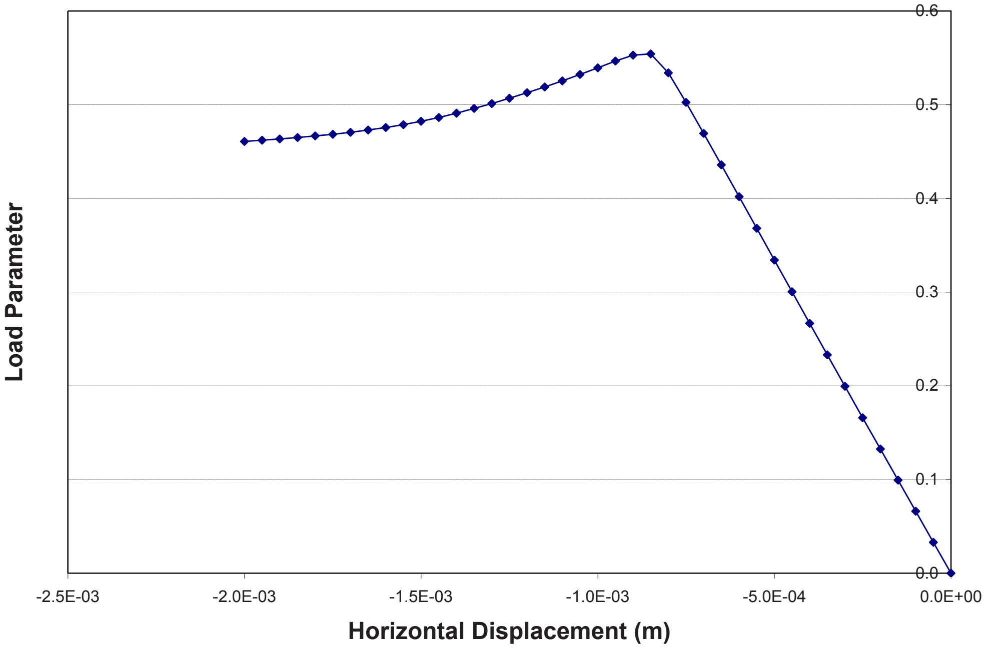

Figure 31: Load-horizontal displacement curve of the node marked on the right edge.

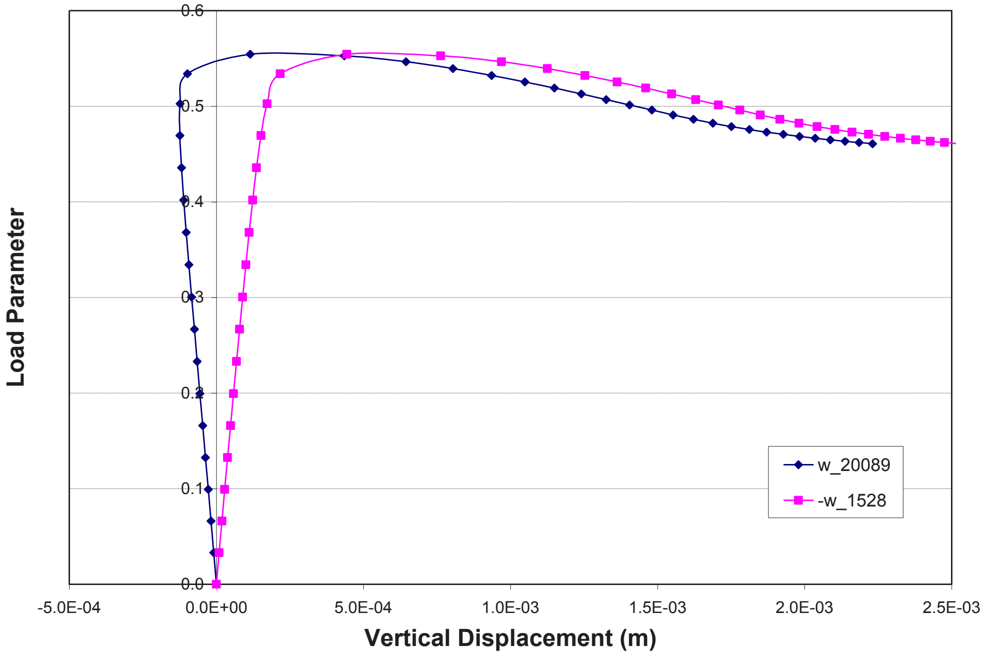

Figure 32: Load-vertical displacement curves at the two nodes marked on the top and bottom edges of the auxetic structure.

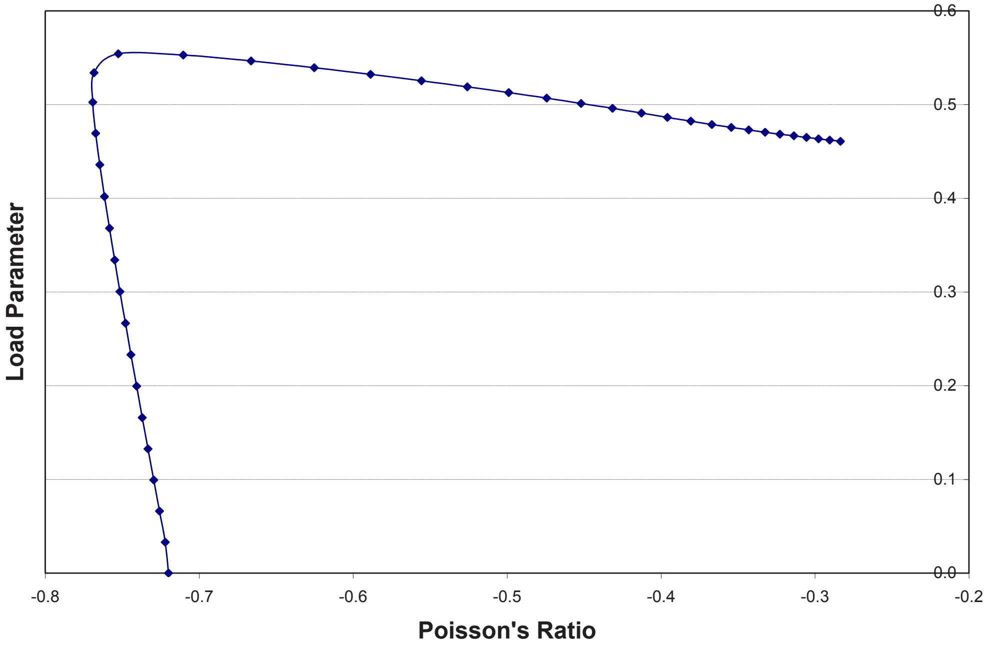

Figure 33: Variation of the effective Poison's ratio of the auxetic structure with the level of deformation.

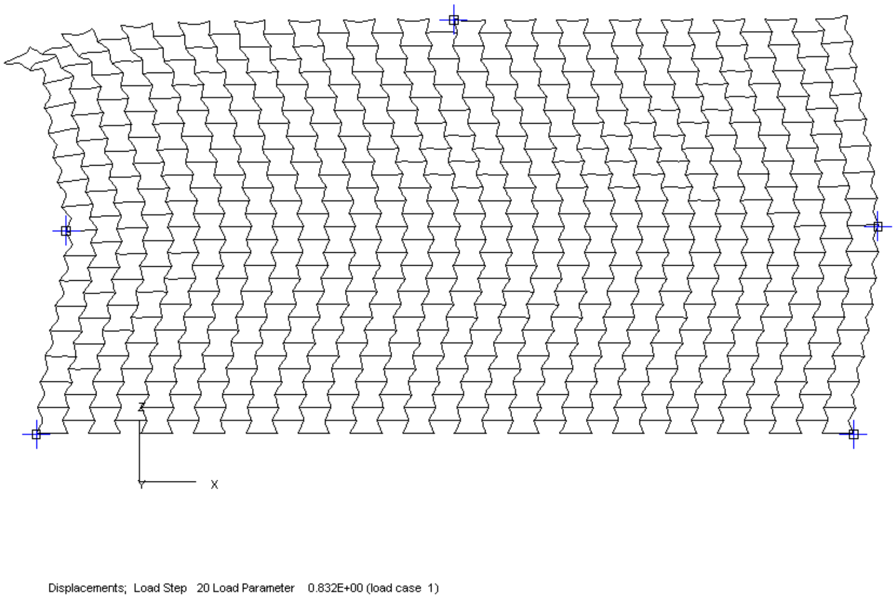

Figure 34: Final deformed configuration of an auxetic structure subjected to vertical compressive stresses.

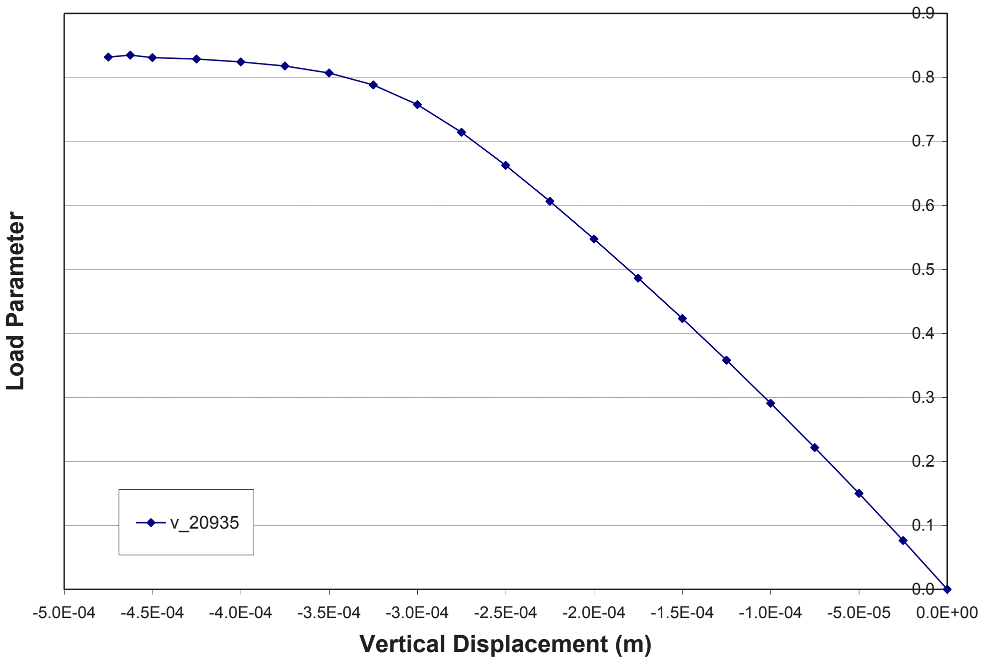

Figure 35: Load-vertical displacement curve of the node marked on the top edge.

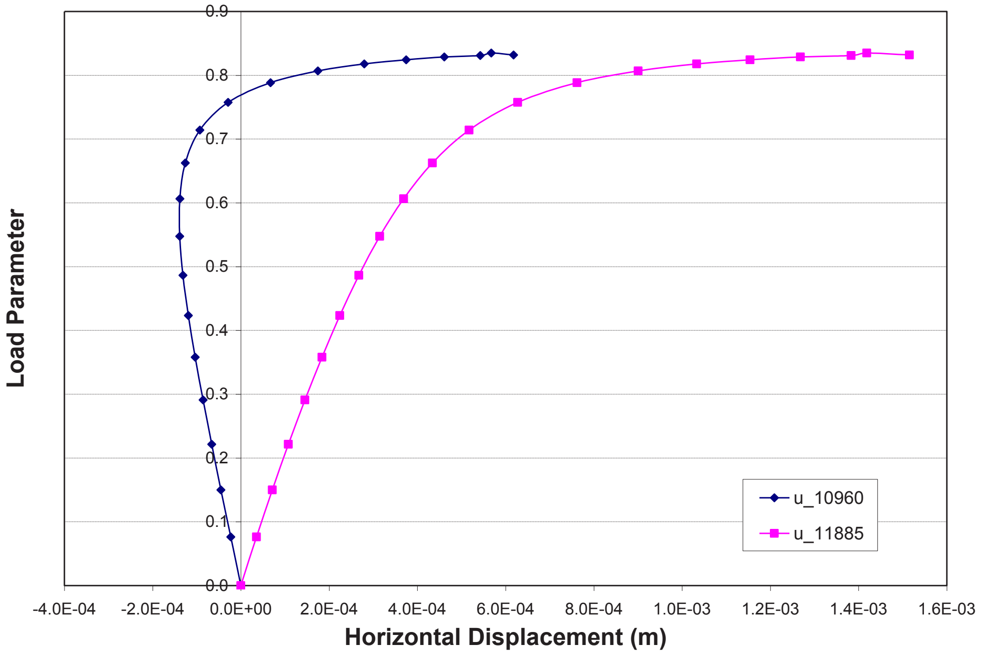

Figure 36: Load-horizontal displacement curves at the two nodes marked in the middle of the right and left edges.

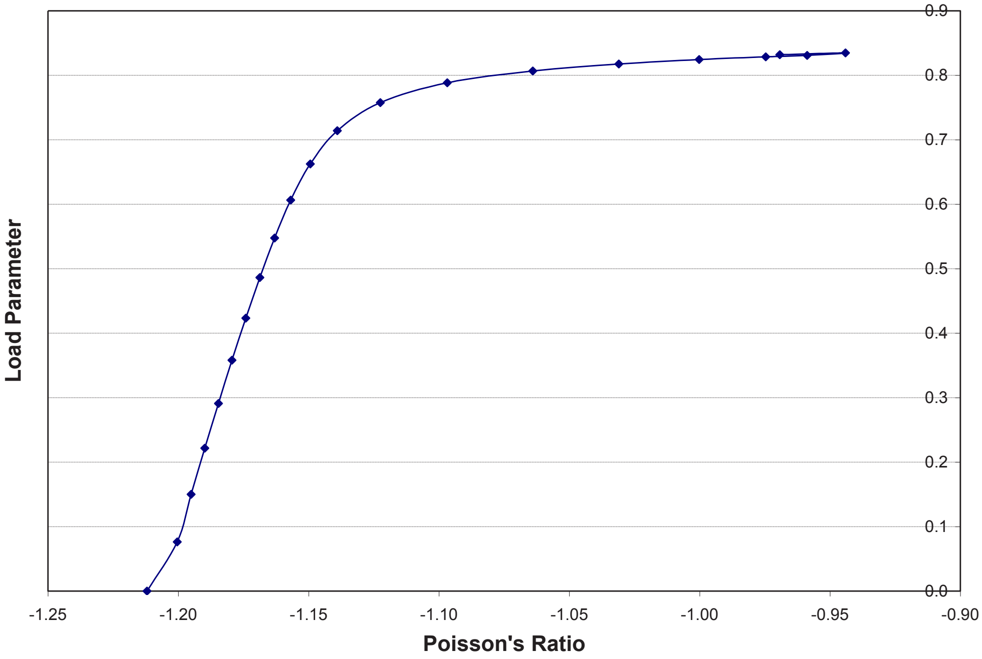

Figure 37: Variation of the effective Poison's ratio of the auxetic structure with the level of deformation.

3.4.2 Effect of extent of the finite element model

When generating finite element models for given honeycomb geometry using the method of model generation described earlier in this chapter, the unit cells were repeated in both horizontal and vertical directions. This method of model generation provided a convenient way to preserve certain features of the finite element models, such as the gross dimensions and the total mass, as that the results from a parametric study can be easily compared. However, the appropriate model size must still be determined. Wider models that included more columns of unit cells had the advantage of minimizing the edge effects and the instability, but required more computation time. In order to help identifying the proper model size, the influence of model width on the predicted impact properties of the auxetic materials was investigated.

The results from this study are given in Figures 38-41, where the predicted time histories of the reaction forces and internal energy absorbed by the auxetic material sample obtained using two different models are compared. Because both the force and internal energy were normalized against the mass of the structure, the results from different meshes are reasonably close to each other and revealed the same trends of variations with the re-entrant angles. These results indicated that for the purpose of the present study, the results were relatively insensitive to the model extent. However, to ensure structural stability, wider finite element models (up to 32 columns) were utilized in the actual parametric study.

3.4.3 Effect of material properties

As also discussed in the preceding section of this report, due to the unreliability of the viscoelastic material model for shell element, the nonlinear dynamic material behavior of the polymer had to be approximated by an elastic-plastic material model with strain rate-dependent hardening properties. This approximation required selection of a Young's modulus from the stress-strain curves provided by the Technical Authority. Because these curves did not contain distinct elastic ranges, the Young's modulus could be selected somewhat arbitrarily. To this end, two sets of elastic-plastic material properties were generated based on different values of Young's modulus, i.e., 84.7MPa and 166.7MPa, respectively, as described before in section 3.2.

Because the conversion of polymer material properties was not unique, it became interesting to evaluate the influence of these approximate material properties on numerical solutions. For this purpose, impact simulations for re-entrant honeycomb with $\theta=10^{o}$ were performed using both sets of approximate material properties and the results obtained using different material properties are compared in Figures 42-44. These results indicated that the use of a higher Young's modulus would reduce the arrival time of the first peak in the reaction force and increase the internal energy absorption. These are consistent with the increase of the elastic modulus. However, the general behaviors predicted by both sets of material properties are very similar. In these impact simulations, the impacter was modeled as a rigid body with a given mass and an initial velocity, rather than a rigid surface moving at a fixed speed as in the previous runs. The advantage of this modeling approach is that it permitted calculations of deceleration of the impact mass due to resistance by the auxetic structure, thus provided another indicator on their relative effectiveness as a protective layer. The impacter velocity time histories from different material parameters are very close to each other. Based on these results, the first set of material data were used throughout the parametric study.

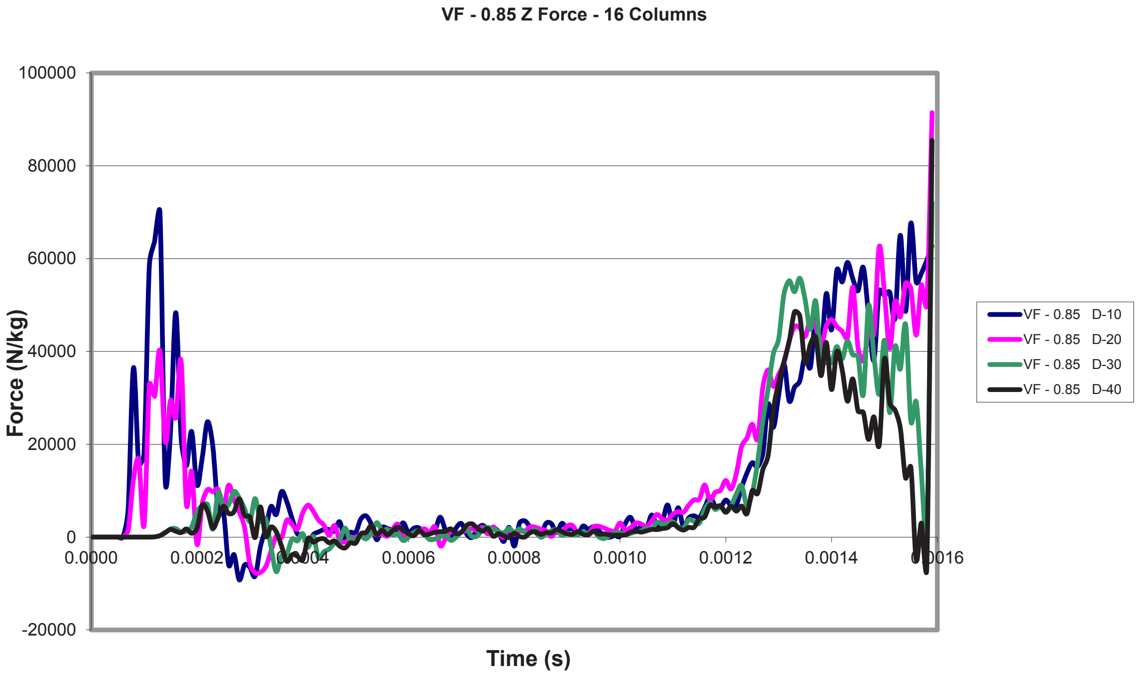

Figure 38: Normalized reaction force histories obtained using FE models of 16 columns of re-entrant unit cells with different angles.

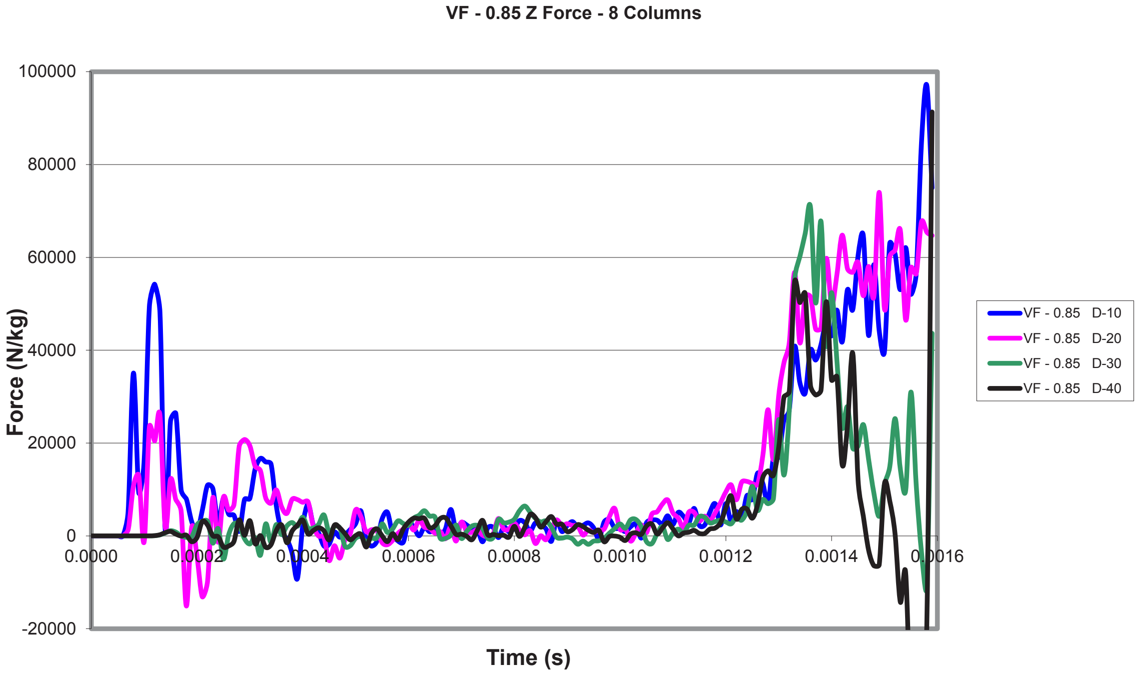

Figure 39: Normalized reaction force histories obtained using FE models of 8 columns of re-entrant unit cells with different angles.

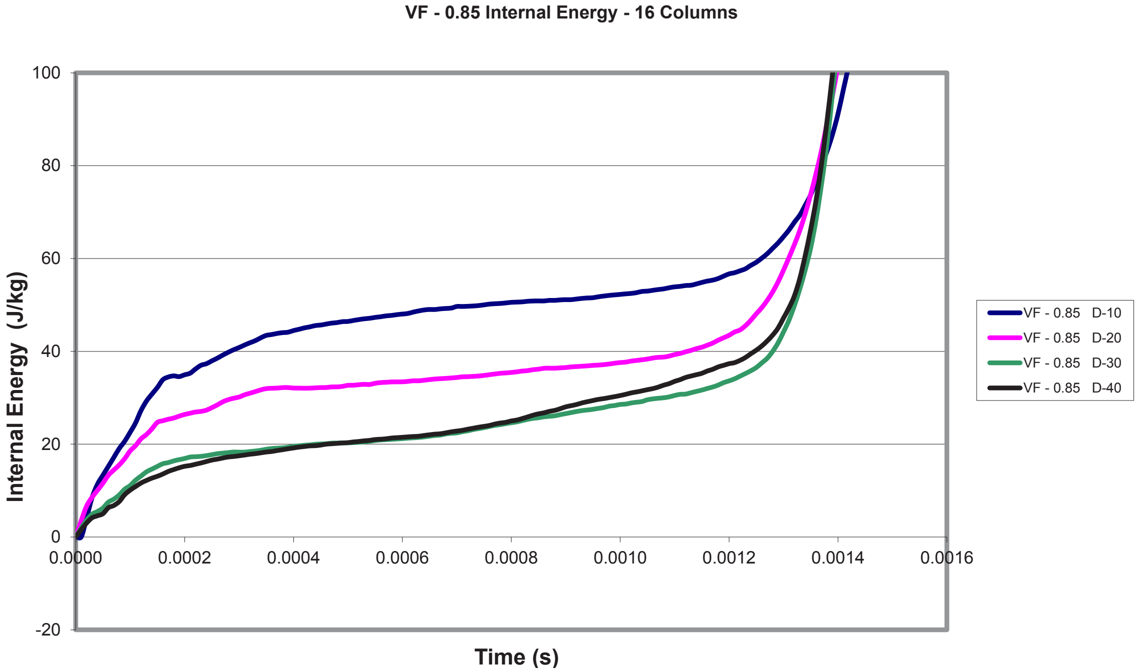

Figure 40: Normalized internal energy histories obtained using FE models of 16 columns of re-entrant unit cells with different angles.

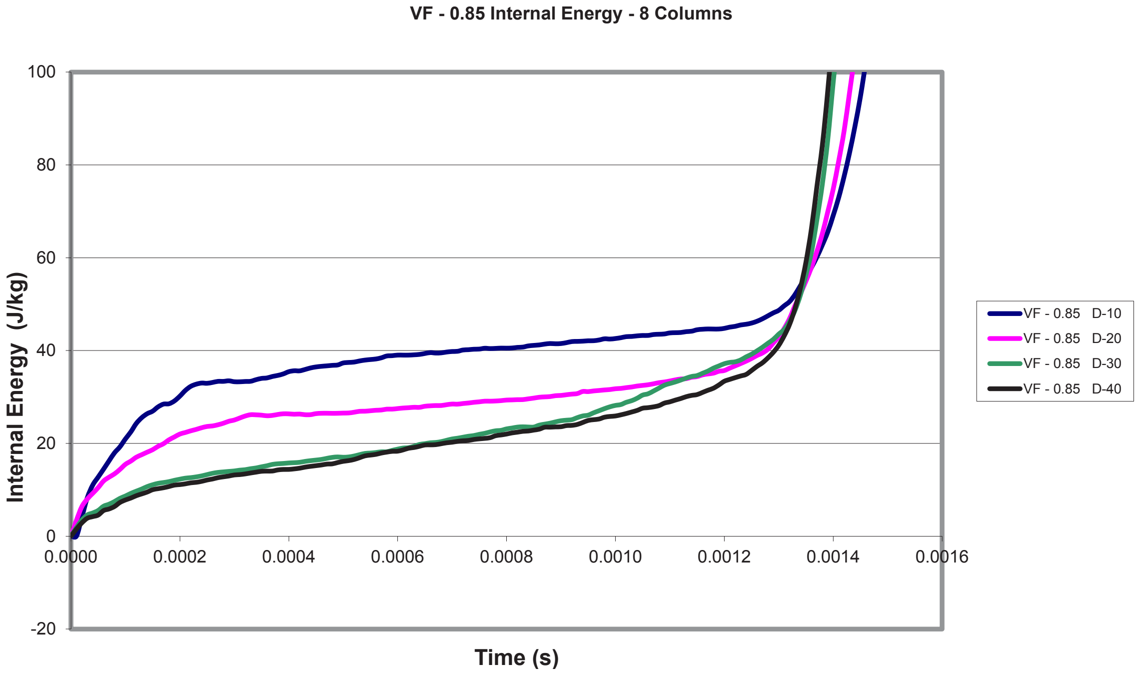

Figure 41: Normalized internal energy histories obtained using FE models of 8 columns of re-entrant unit cells with different angles.

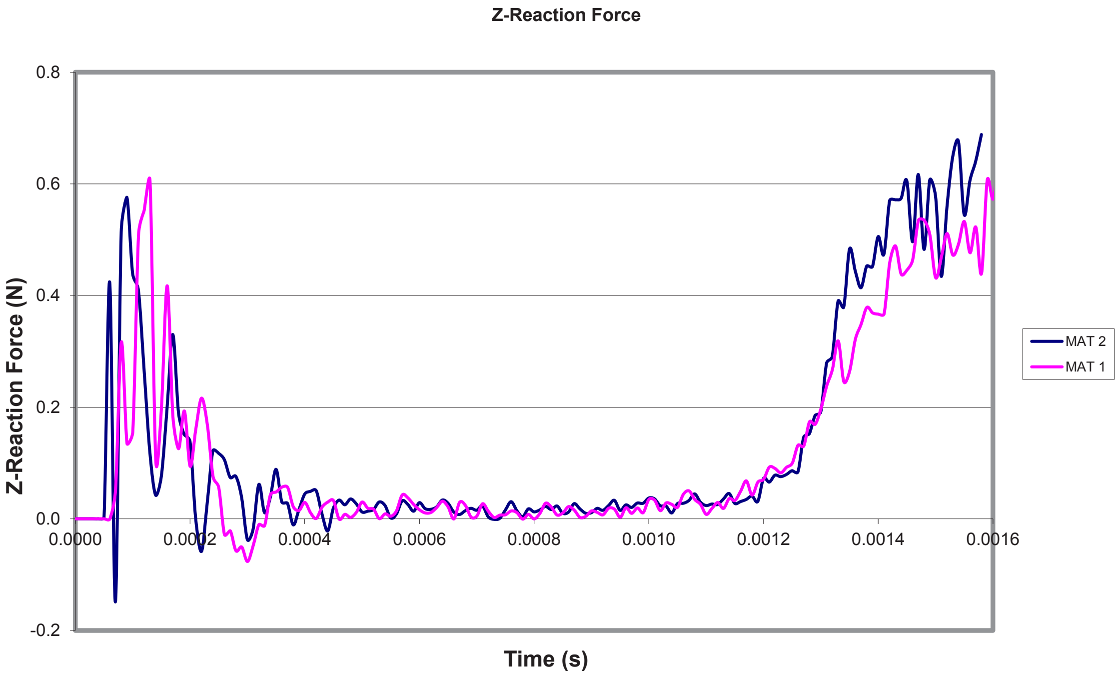

Figure 42: Reaction force histories obtained using different elastic-plastic material parameters that approximate the material behavior of polyurea.

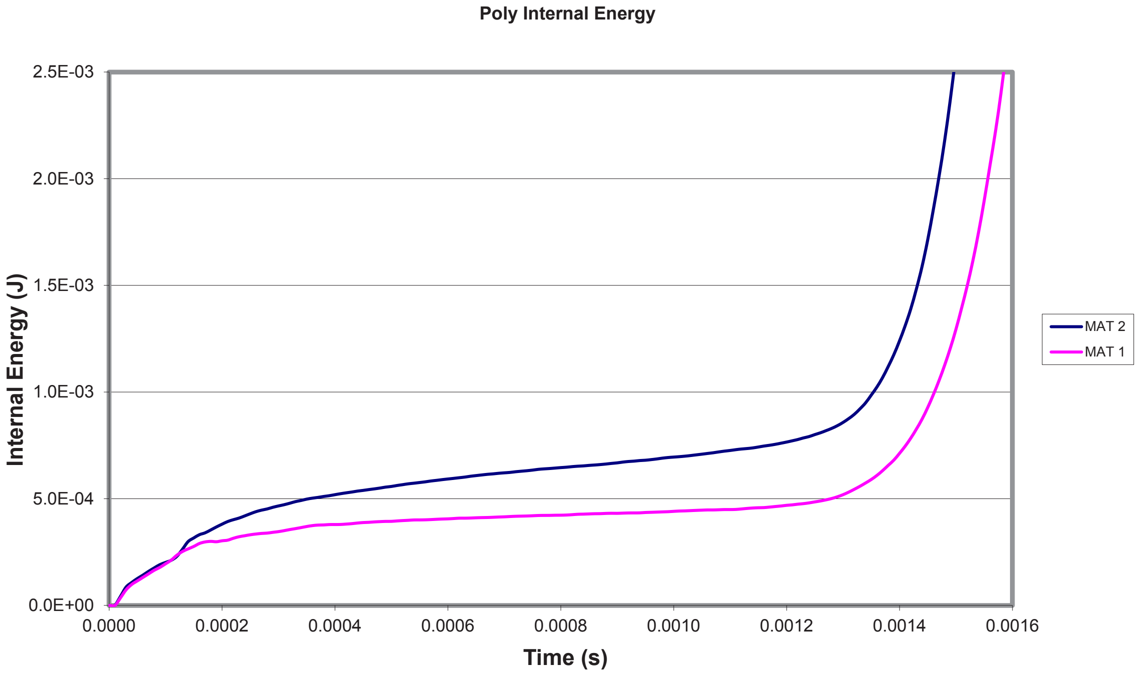

Figure 43: Internal energy histories obtained using different elastic-plastic material parameters that approximate the material behavior of polyurea.

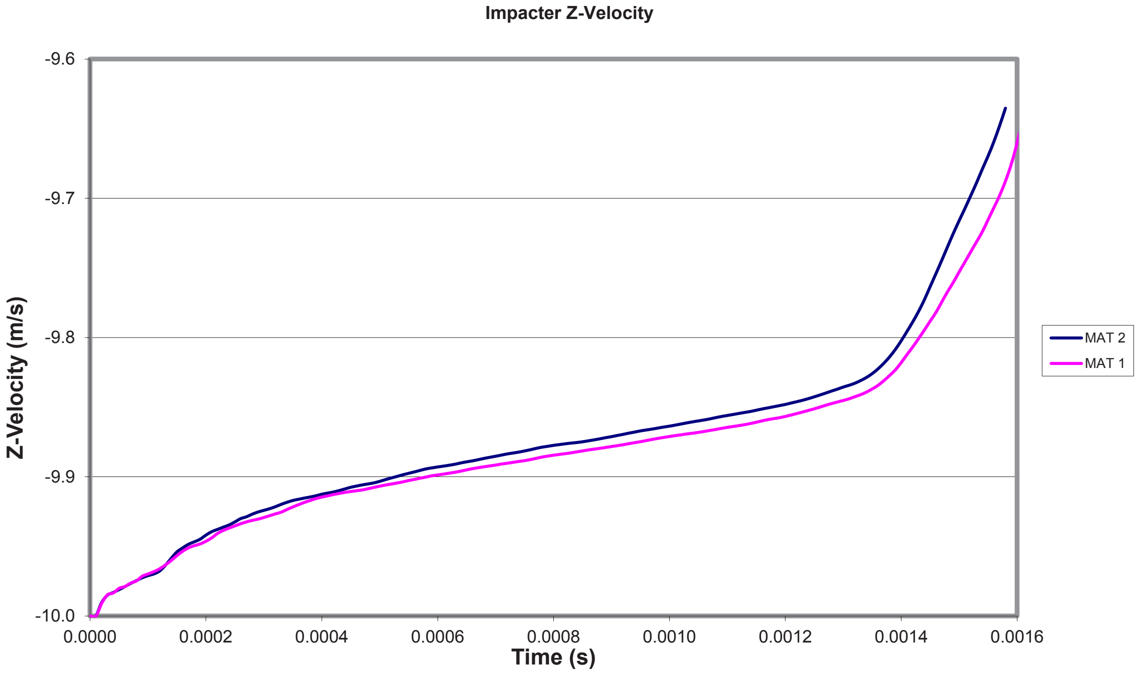

Figure 44: Velocity histories of the impacter obtained using different elastic-plastic material parameters that approximate the material behavior of polyurea.

3.4.4 Effect of impacter mass

As mentioned in the preceding section, the impact condition was modeled by an impacting mass at a given initial velocity. In this case, it becomes interesting to see how the predicted dynamic behavior is influenced by the ratio of the impacter mass and the mass of the auxetic structure, which is defined as the impact mass factor (IMF). Figures 45-47 showed results obtained for different vales of the impacter mass. For all these analyses, the same auxetic structure of a re-entrant honeycomb with θ=10^o and a void fraction of 0.847 has been utilized.

These results indicated that the impacter mass has very little influence on the impact force and the internal energy. The deceleration of the impacter was inversely proportional to its mass. This observation confirmed that the impact force is independent of the impacter mass. In all the later analyses, IMF=100 has been used.

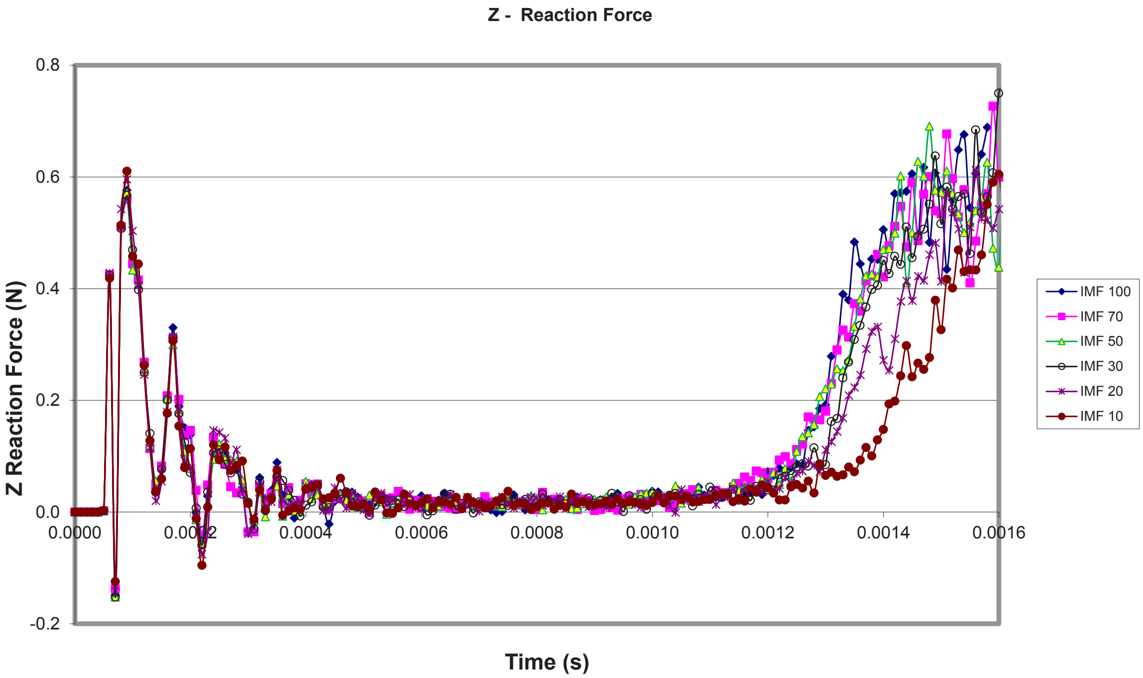

Figure 45: Reaction force histories obtained using different mass ratios of the impacter and the polyurea foam.

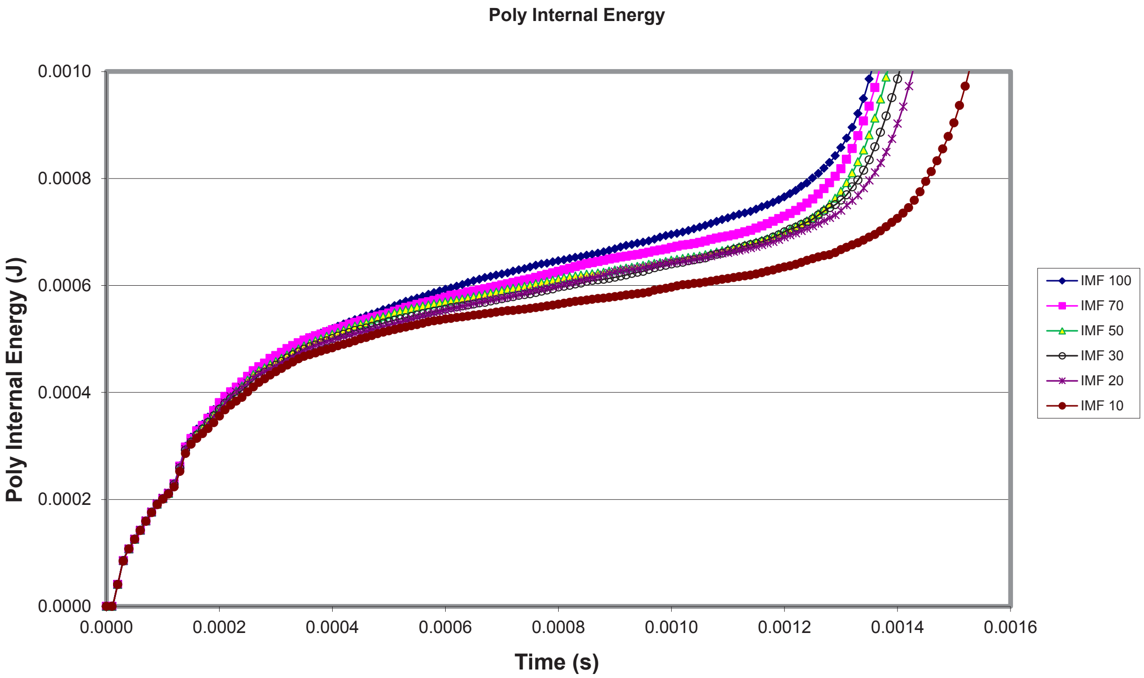

Figure 46: Internal energy histories obtained using different mass ratios of the impacter and the polyurea foam.

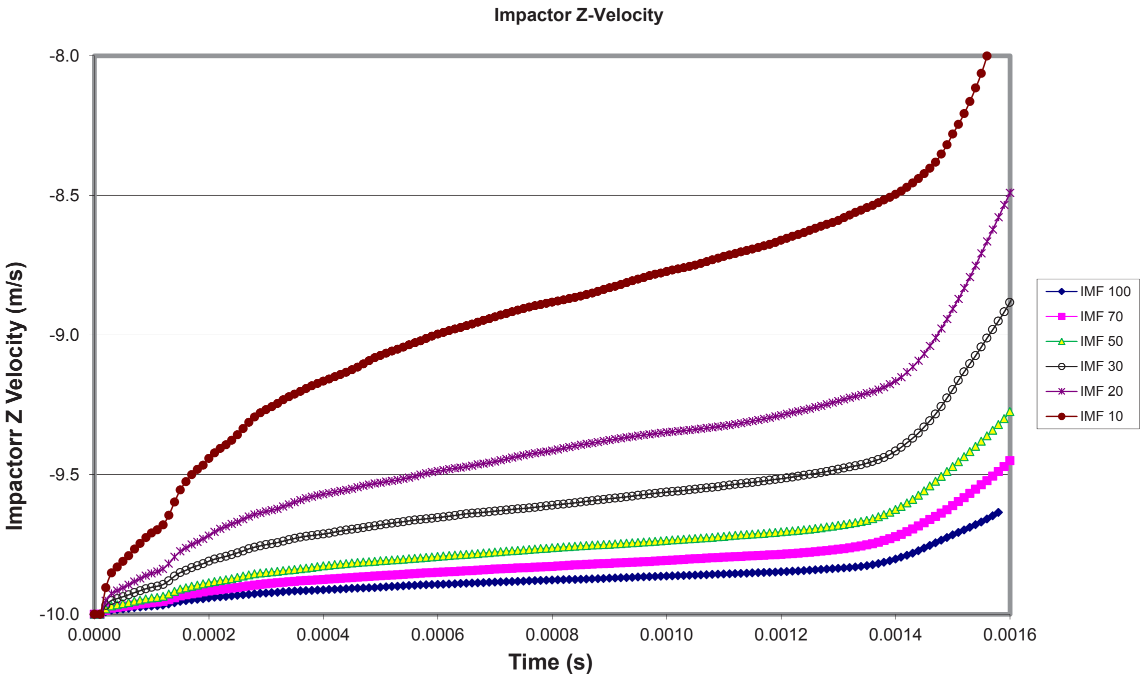

Figure 47: Velocity histories of impacter obtained using different mass ratio of the impacter and the polyurea foam.

4 Results of parametric study

4.1 Test cases for parametric study

Following the verification of the finite element models as described in the previous chapter, a parametric study was carried out to investigate the influences if various factors on the impact properties of auxetic materials. The factors that were considered in the parametric study included the re-entrant or conventional angle θ, the void fractions and the impacter orientation. The values taken for these factors in the present study are summarized in Table 5.

Table 5: Test matrix for parametric study.

Variables	Values	# of Cases
Re-entrant angle θ	-10, -20, -30, -40, -50	5
Conventional angle θ	+10, +20, +30, +40, +50	5
Void fraction	0.846, 0.70, 0.50	3
Impacter orientation	Vertical, Horizontal	2

The outer dimensions of the unit cell were fixed at $L=H=1.0$ mm from which the rib lengths and thickness are each test case were calculated using Equations (5) and (6). An array 16×32 unit cells were utilized in all finite element models, where the horizontal ($2h$) and diagonal (l) ribs were always represented by ten and five shell elements, respectively, as indicated in Figure 13n and one element was always utilized in the depth direction. The first set of material properties with E=84.7 MPa were employed in all impact simulations. It should be noted that the finite element models for all test cases have identical overall dimensions. However, the total masses were different for models with different void fractions.

The test matrix presented in Table 5 contained a total of 60 test cases. In addition, special test cases with $\theta=0^{o}$ were considered for all three values of void fractions and both impact directions. Finally, the cases for impact on solid polymer (void fraction of 0.0) were also considered.

4.2 Representative results of shell element

The shell element predicted deformation processes of a representative honeycomb structure with $\theta=40^{o}$ and void faction of 0.5 under vertical and horizontal impact loads are depicted in Figures 48 and 49, respectively. As indicated in Figure 49, in simulations of horizontal impact, the finite element model was rotated by 90^{o}, but the same boundary conditions were applied.

As mentioned in the preceding sections in this report, time histories of three variables would be extracted from the results of the present parametric study and used to evaluate the relative performance of the various conventional and re-entrant honeycombs as a protective layer on military structures. These variables included internal energy absorption, impact force and the reduction of impacter velocity. The last variable reflected the level of resistance of the auxetic material sample to the moving impacter. Because all of the finite element models utilized in the present parametric study had identical gross dimensions, models for different void fractions had different masses. To facilitate comparison of the results, all three variables mentioned above were normalized by the total mass of the auxetic structure. The normalized results are presented in Figures 50-73.

These results led to a number of interesting observations. First of all, the auxetic structures with smaller angles were more effective than structures with larger angles, as the former stored more internal energy and generated more resistance to the impacter for the same structural mass. Among the structures of same angle θ, the ones with lower void fractions were more effective. However, the performances of the conventional and re-entrant honeycomb structures were very similar and no obvious advantages were observed for the re-entrant honeycombs. These trends were observed for both vertical and horizontal impact cases. However, the differences were more pronounced under vertical impact.

However, at this point, some questions were raised on the treatment of the extremely complicated contact conditions in the interior of the structures under large deformations. As indicated in Figures 48 and 49, under the impact loads, the ribs in honeycomb structures underwent extremely large deformations and the interactions between these highly deformed ribs generated some very difficult contact situations. The doubt on the correctness of the numerical solutions was raised because the volume of the structure was found not to be correctly preserved and in some cases, the impacter and the bottom rigid surface were even in contact at the later stage of simulations. This was obviously non-physical and indicated that the contact conditions between the ribs were not treated properly.

A large number of contact algorithms are provided in LS-DYNA. In the present parametric study, option *CONTACT_SINGLE_SURFACE was utilized with SSTHK=1. This combination of contact solution control parameters is supposed to be able to automatically search for the contact surfaces between deformed ribs and the effect of shell thickness should be taken into account. After the above mentioned defects in the numerical solutions were discovered, attempts were made to use other contact options, such as *CONTACT_AUTOMATIC_SIGLE_SUREFACE. Unfortunately, this option resulted in numerical difficulties at early stage of the analyses.

4.3 Investigation of solid element

In order to develop a more reliable finite element model for impact simulations of honeycomb structures, a solid element model was created and tested for a selected auxetic structure with θ=40^{o} and void fraction of 0.5. A number of contact options and contact control parameters were tried and the sequence of deformation predicted using the AUTOMATIC_SINGLE_SURFACE option and control parameter SOFT=2 are reported in Figure 74. The model provided an improved treatment of the complicated contact problem. However, over-lapping elements and unrealistic deformations were still observed. The Martec project team is currently working with the technical support persons of LS-DYNA to resolve the problems.

The internal energy, impact force and impacter velocity predicted by the solid element models using various contact options are compared with the shell element solutions and the results for solid polymer in Figures 75-77. These results clearly indicated that the stiffness of the auxetic structure was seriously underestimated in the shell element solution.

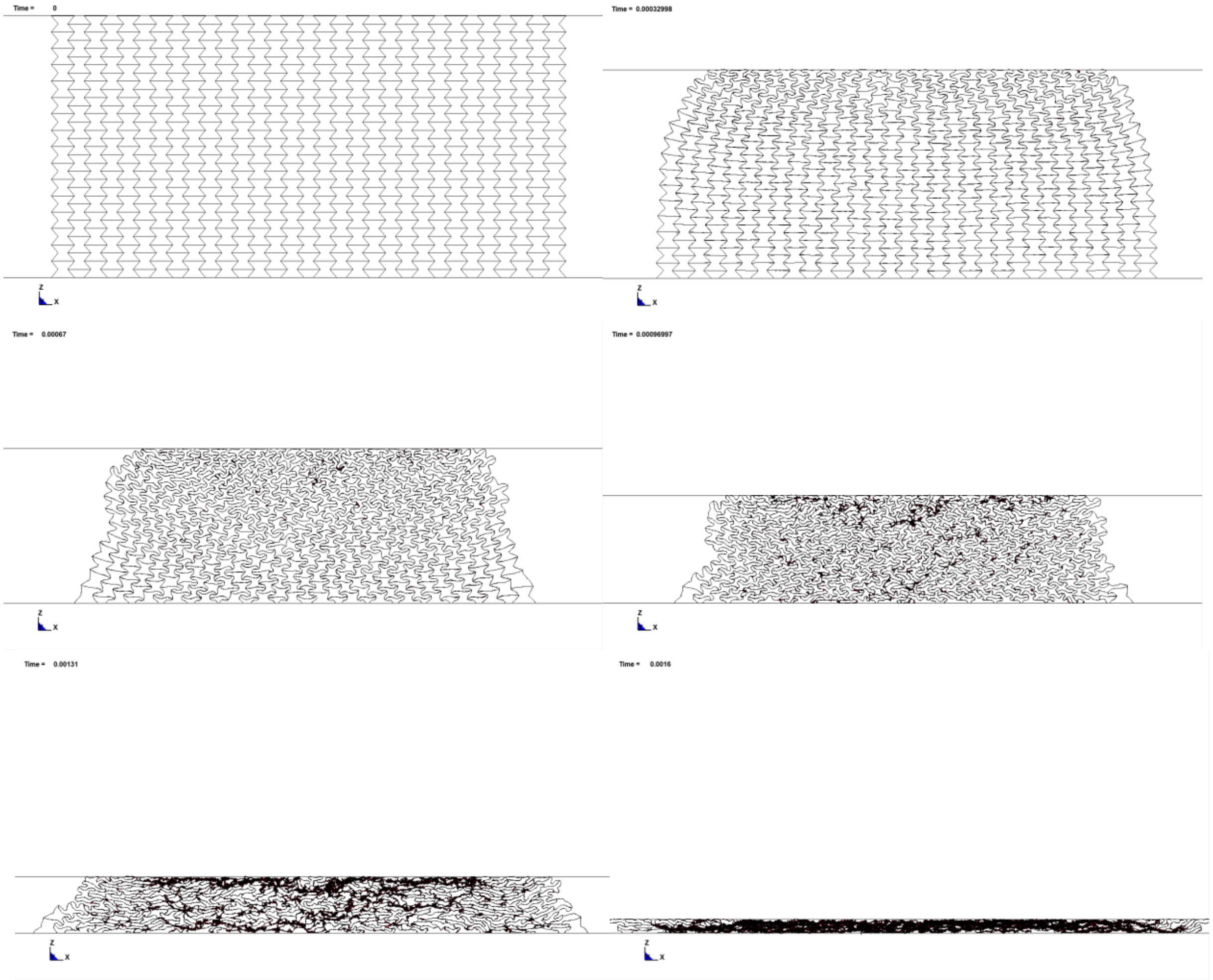

Figure 48: Shell element predicted deformation process for re-entrant honeycomb with $\theta=40^o$ and void fraction of 0.5 under vertical impact.

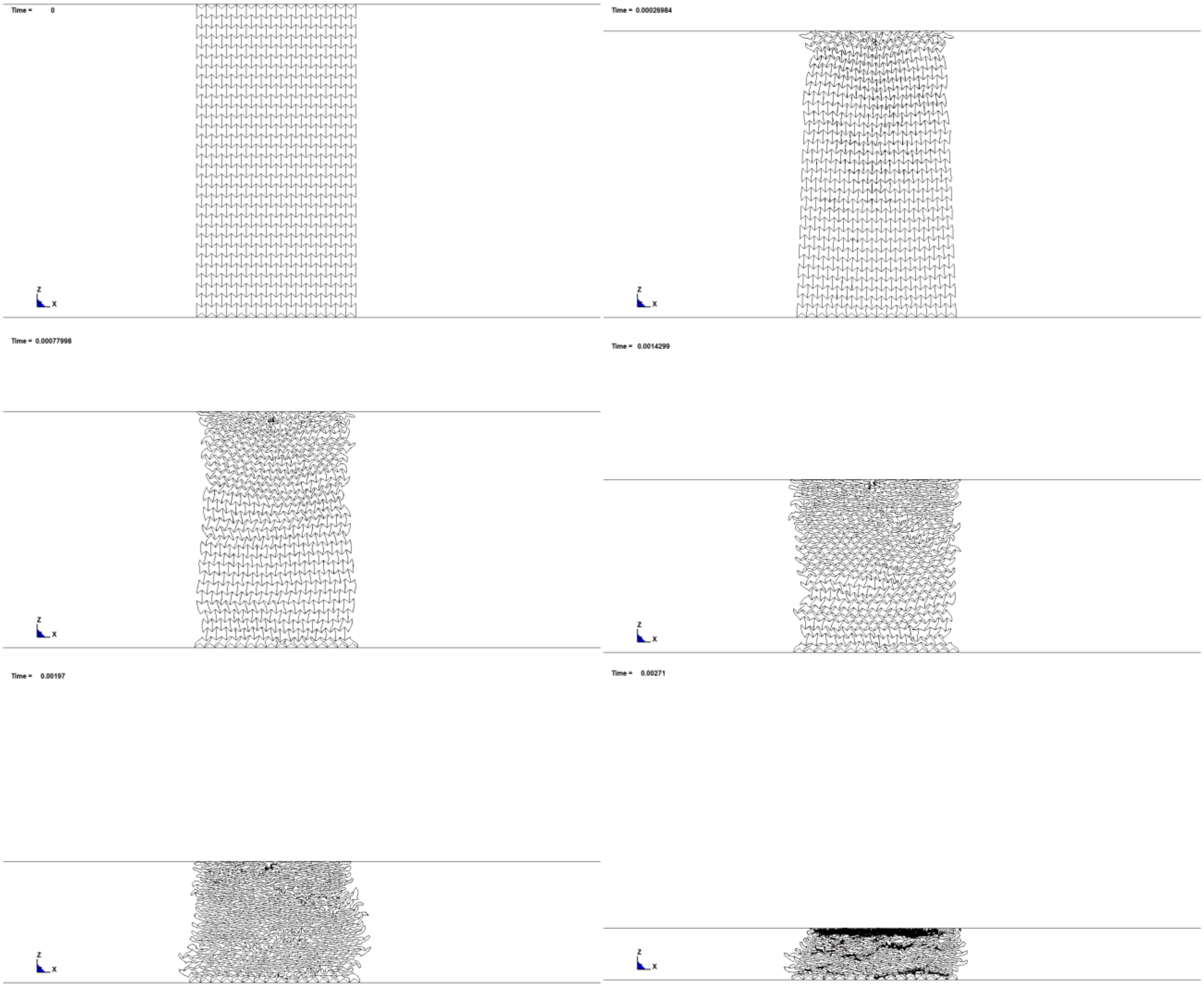

Figure 49: Shell element predicted deformation process for re-entrant honeycomb with θ=40^o and void fraction of 0.5 under horizontal impact.

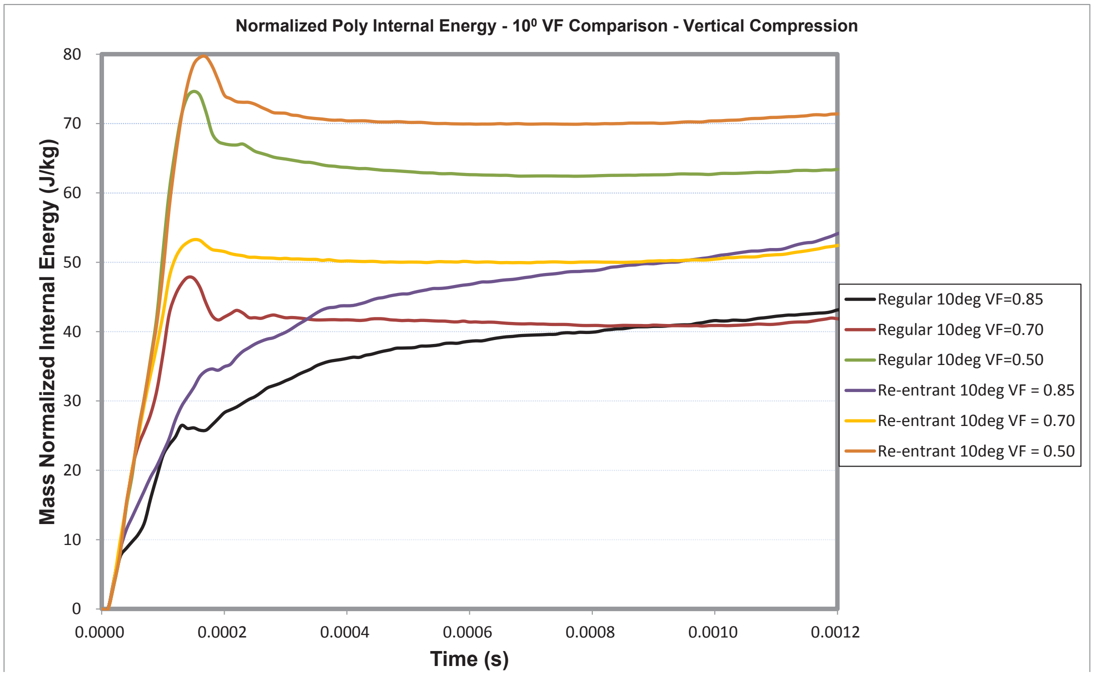

Figure 50: Normalized internal energy absorption for honeycomb structures with $\theta=10^o$ and various void fractions under vertical impact.

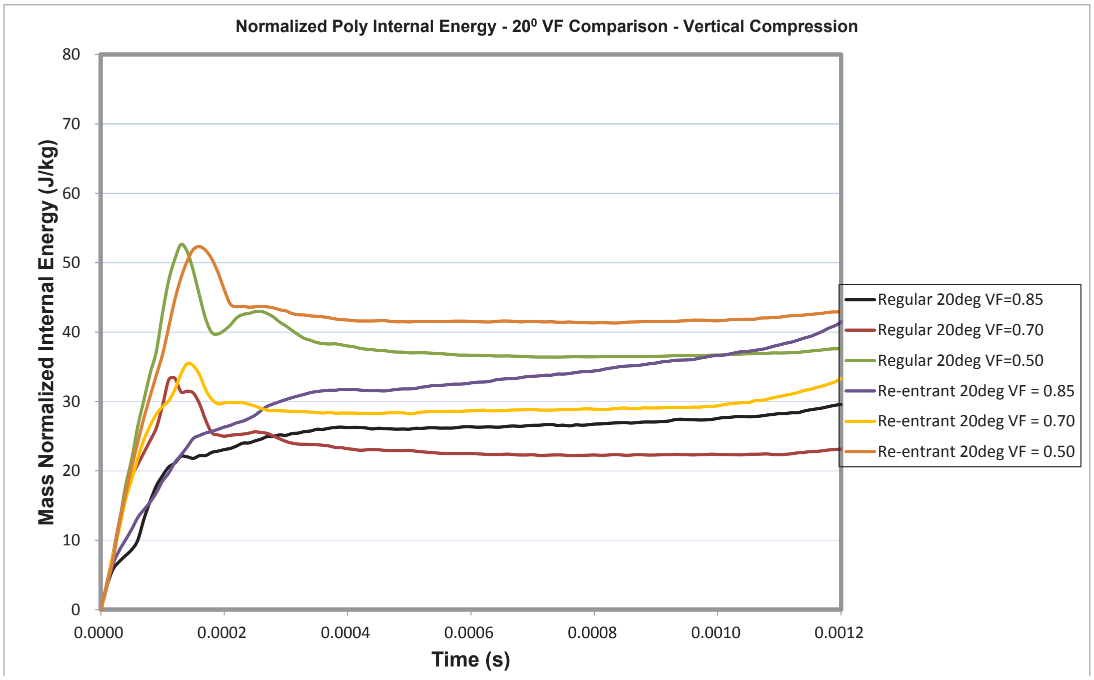

Figure 51: Normalized internal energy absorption for honeycomb structures with $\theta=20^o$ and various void fractions under vertical impact.

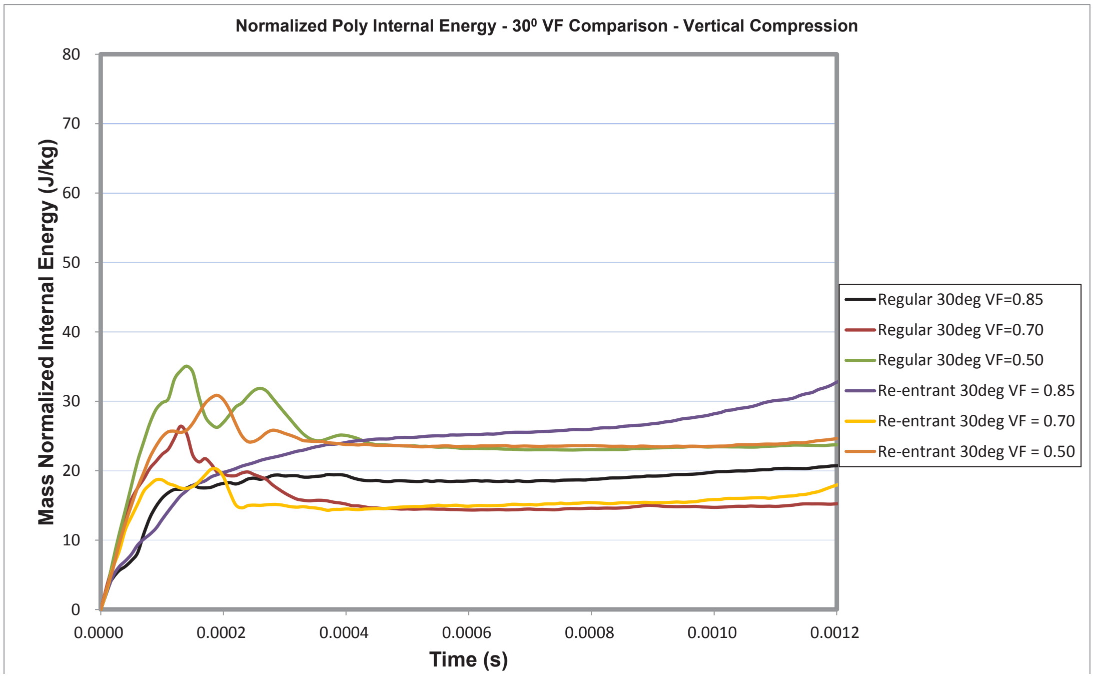

Figure 52: Normalized internal energy absorption for honeycomb structures with θ=30^o and various void fractions under vertical impact.

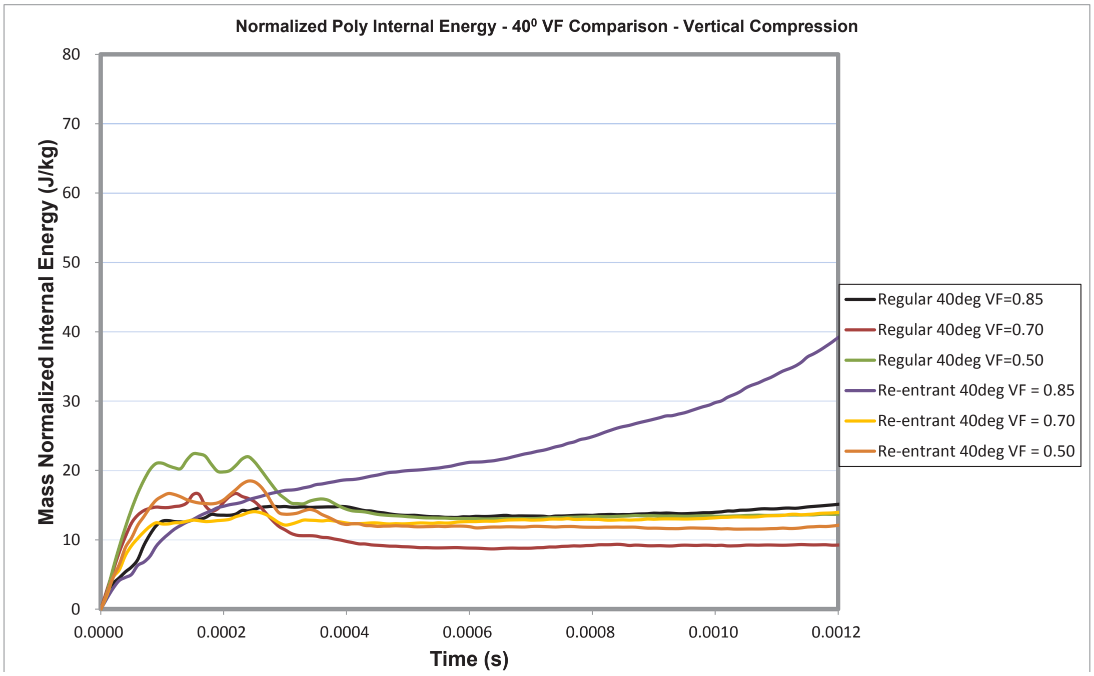

Figure 53: Normalized internal energy absorption for honeycomb structures with θ=40^o and various void fractions under vertical impact.

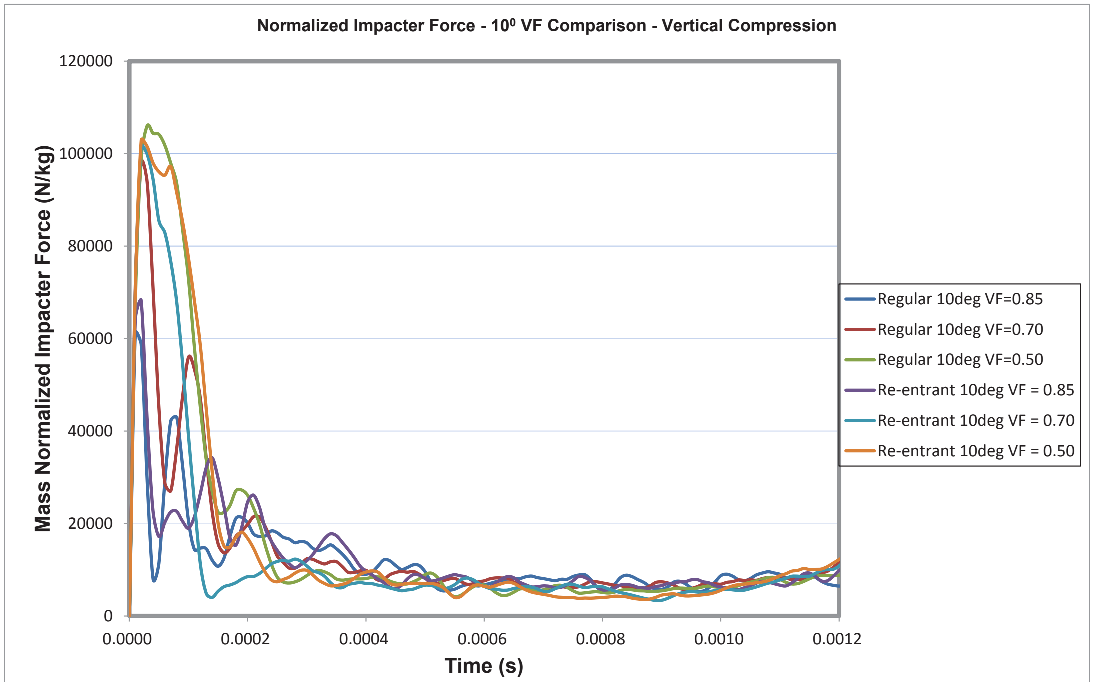

Figure 54: Normalized impact force for honeycomb structures with $\theta=10^o$ and various void fractions under vertical impact.

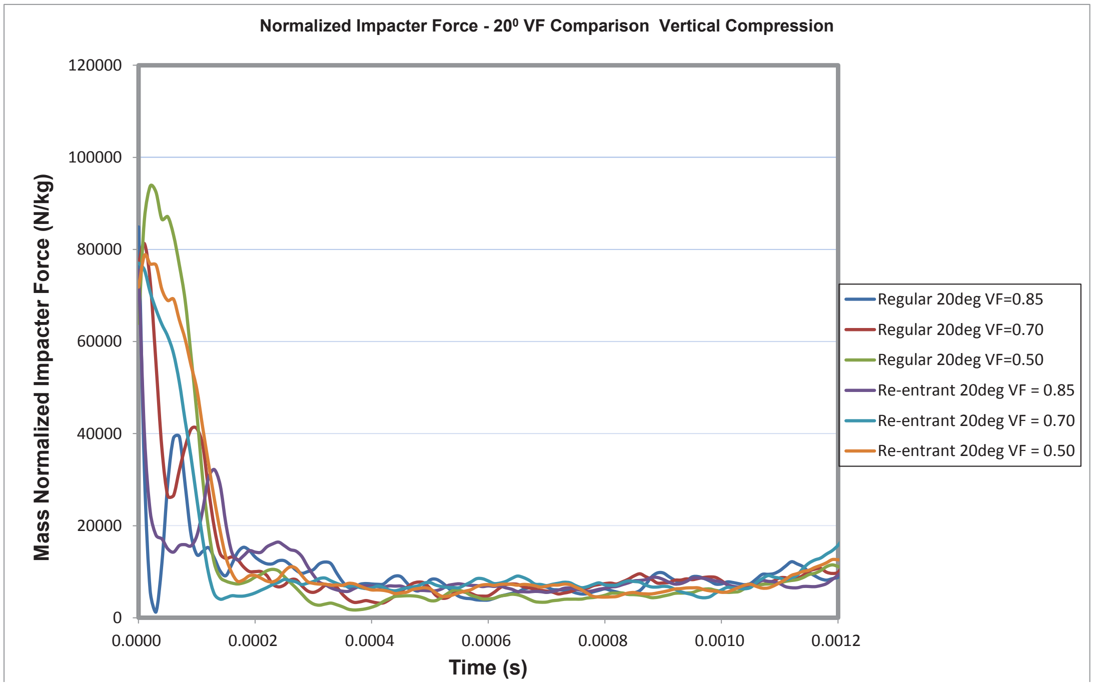

Figure 55: Normalized impact force for honeycomb structures with $\theta=20^o$ and various void fractions under vertical impact.

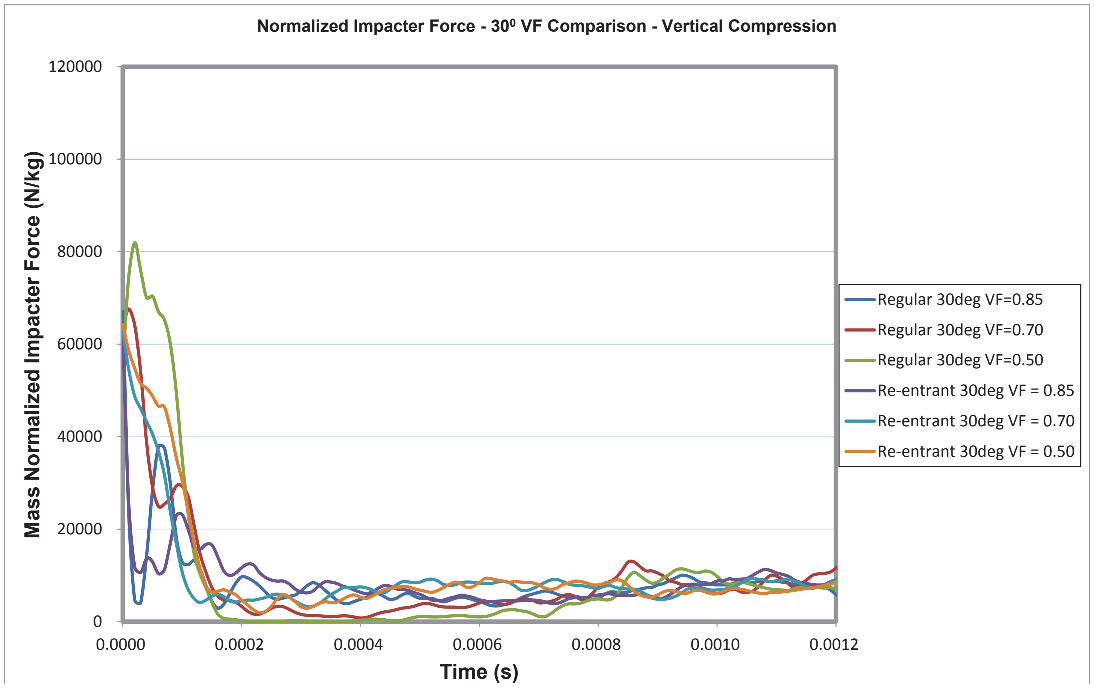

Figure 56: Normalized impact force for honeycomb structures with $\theta=30^o$ and various void fractions under vertical impact.

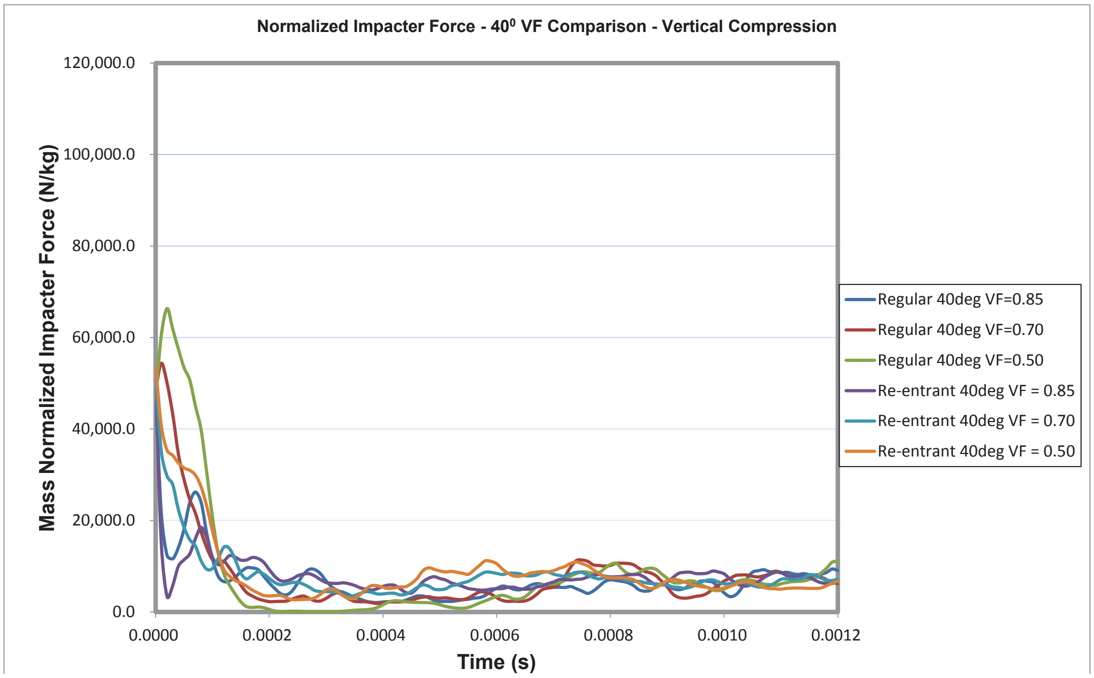

Figure 57: Normalized impact force for honeycomb structures with $\theta=40^o$ and various void fractions under vertical impact.

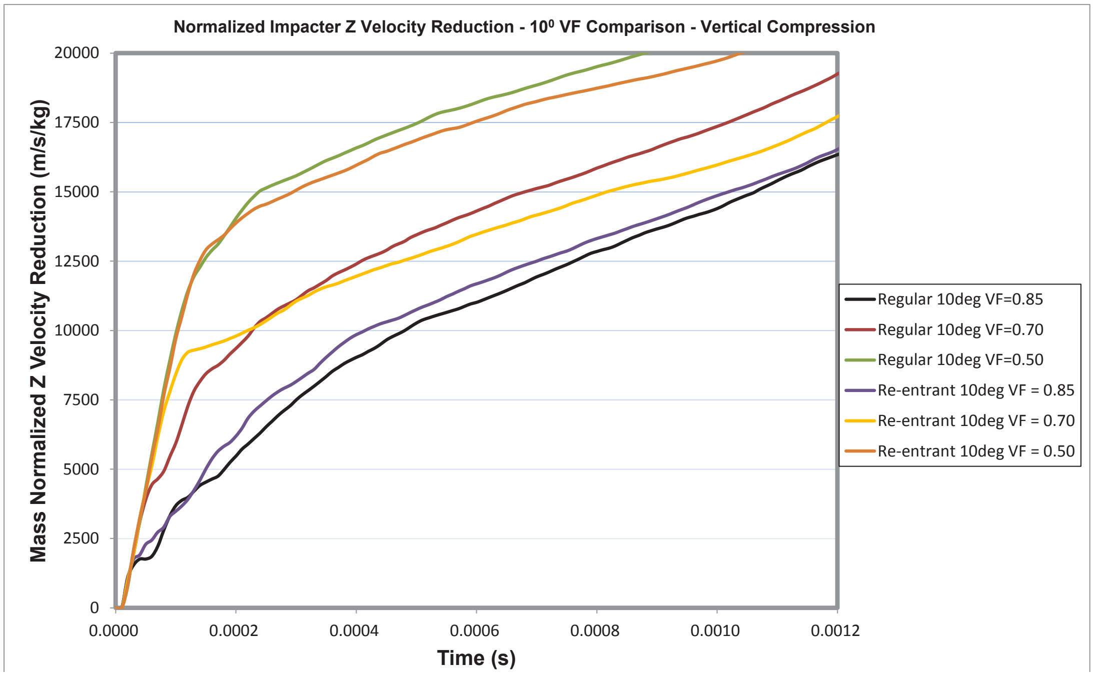

Figure 58: Normalized reduction of impacter velocity for honeycomb structures with $\theta=10^o$ and various void fractions under vertical impact.

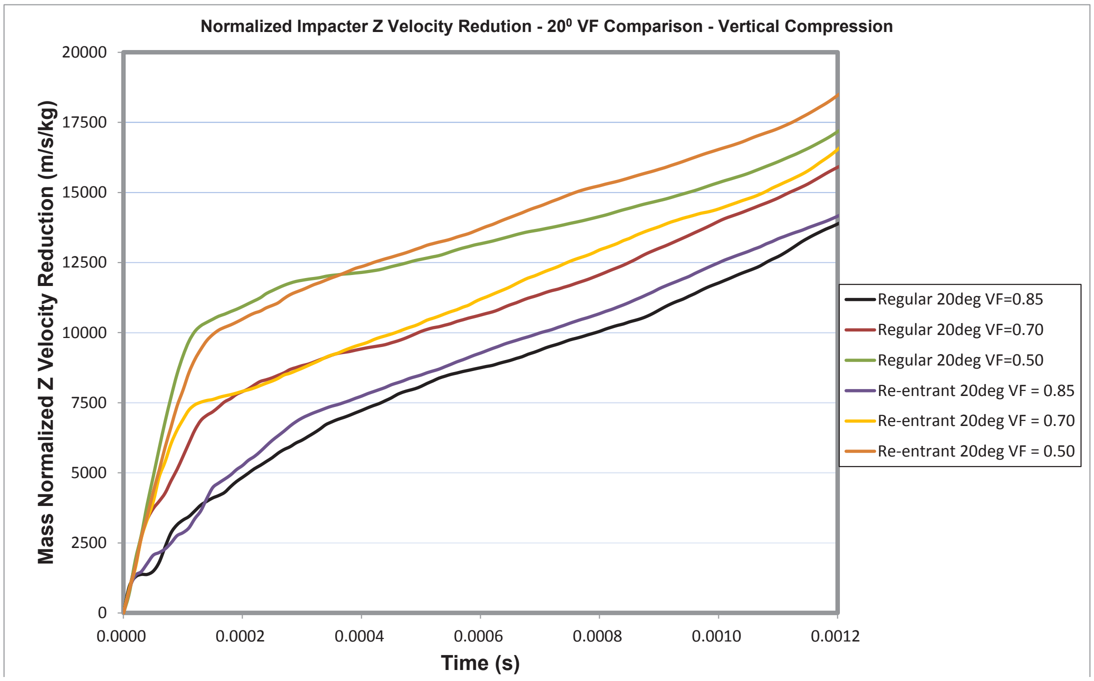

Figure 59: Normalized reduction of impacter velocity for honeycomb structures with $\theta=20^o$ and various void fractions under vertical impact.

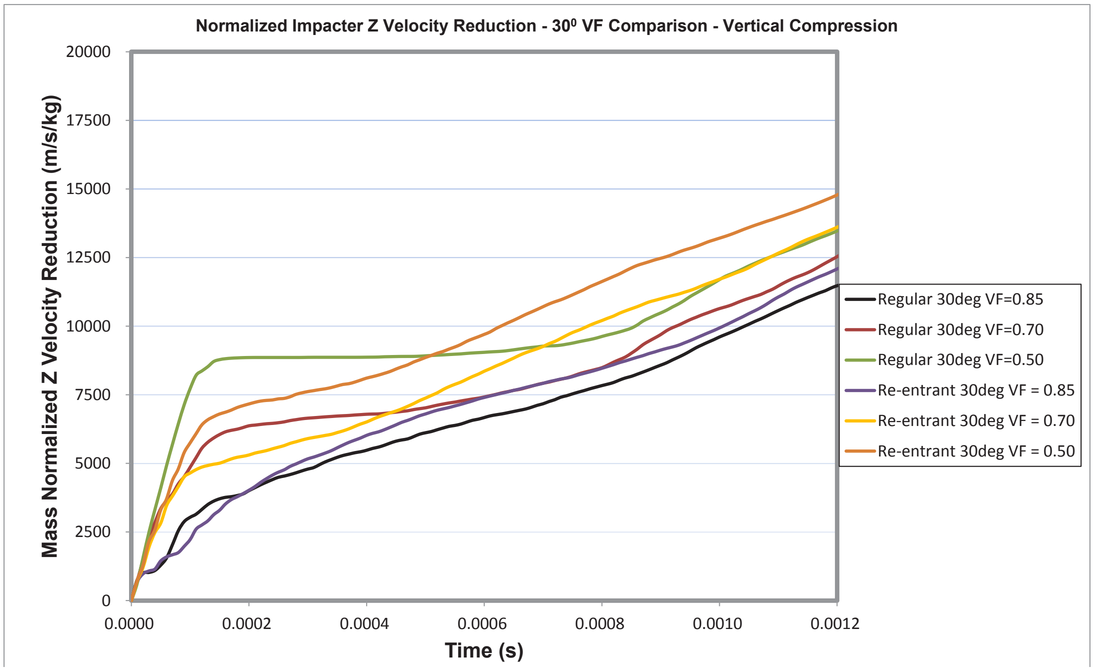

Figure 60: Normalized reduction of impacter velocity for honeycomb structures with $\theta=30^o$ and various void fractions under vertical impact.

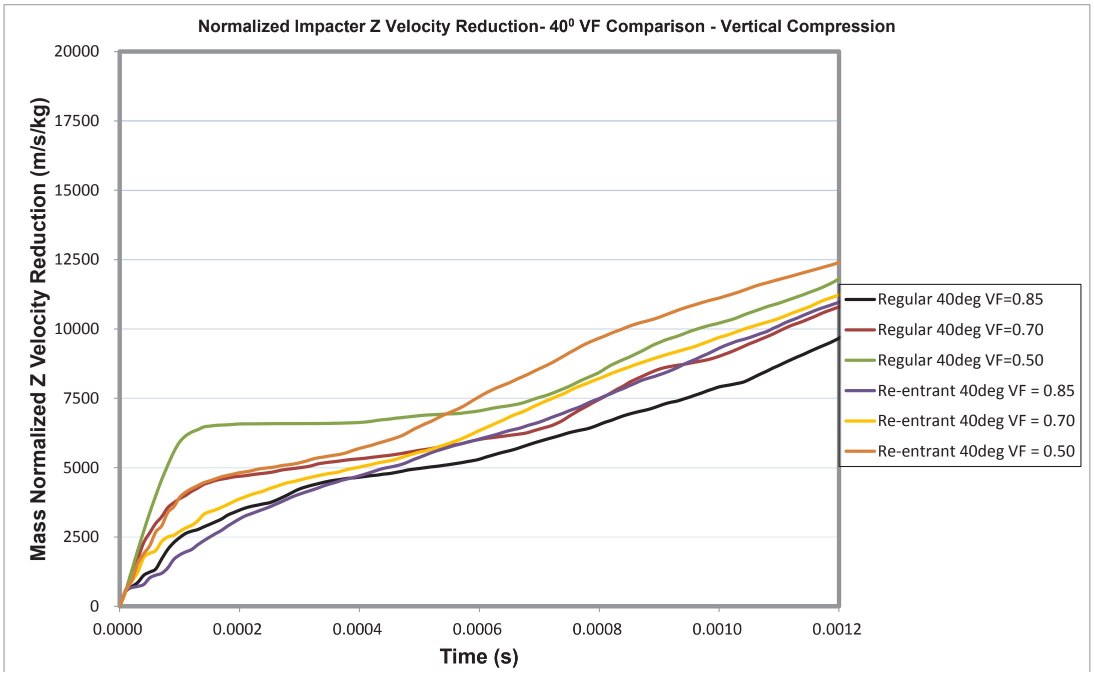

Figure 61: Normalized reduction of impacter velocity for honeycomb structures with $\theta=40^o$ and various void fractions under vertical impact.

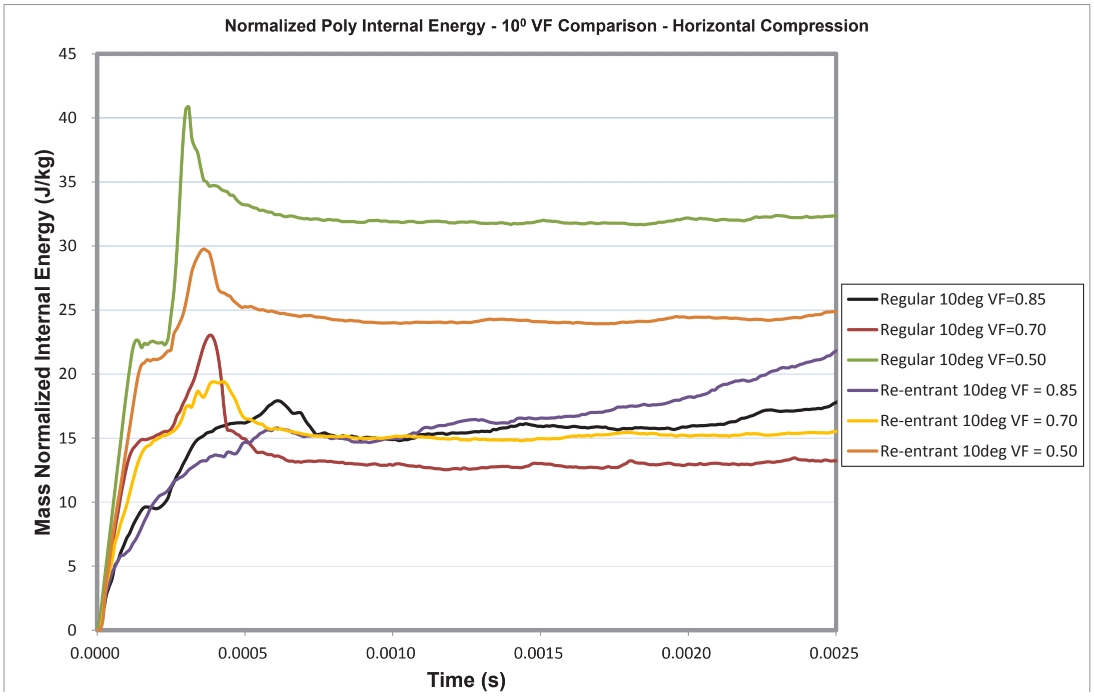

Figure 62: Normalized internal energy absorption for honeycomb structures with $\theta=10^o$ and various void fractions under horizontal impact.

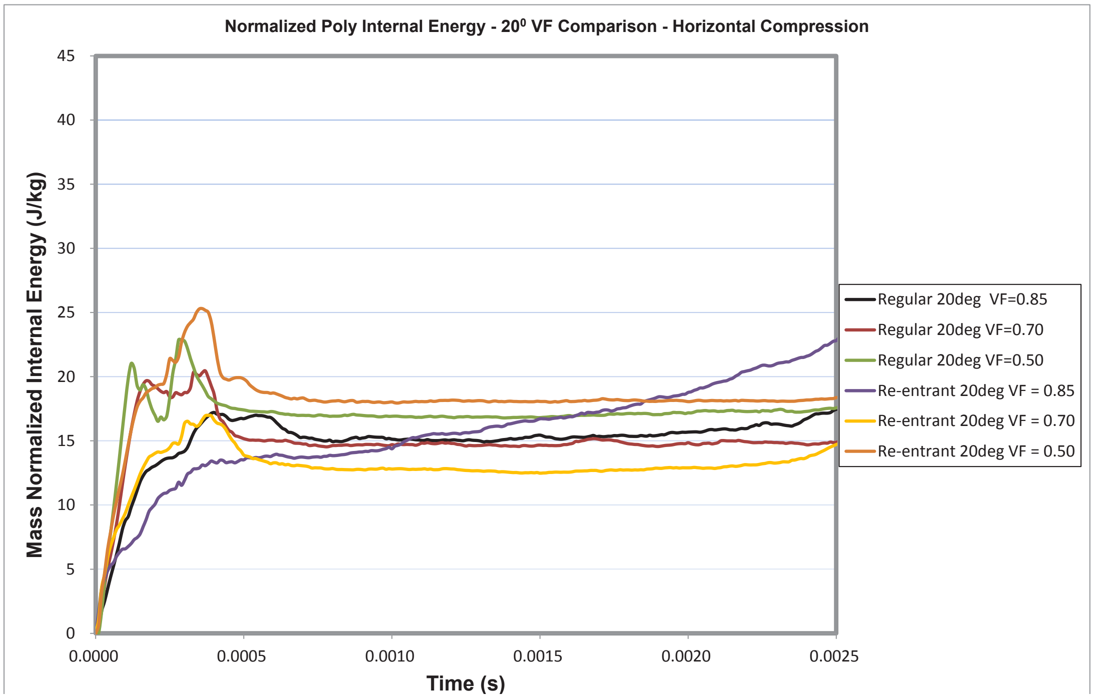

Figure 63: Normalized internal energy absorption for honeycomb structures with $\theta=20^o$ and various void fractions under horizontal impact.

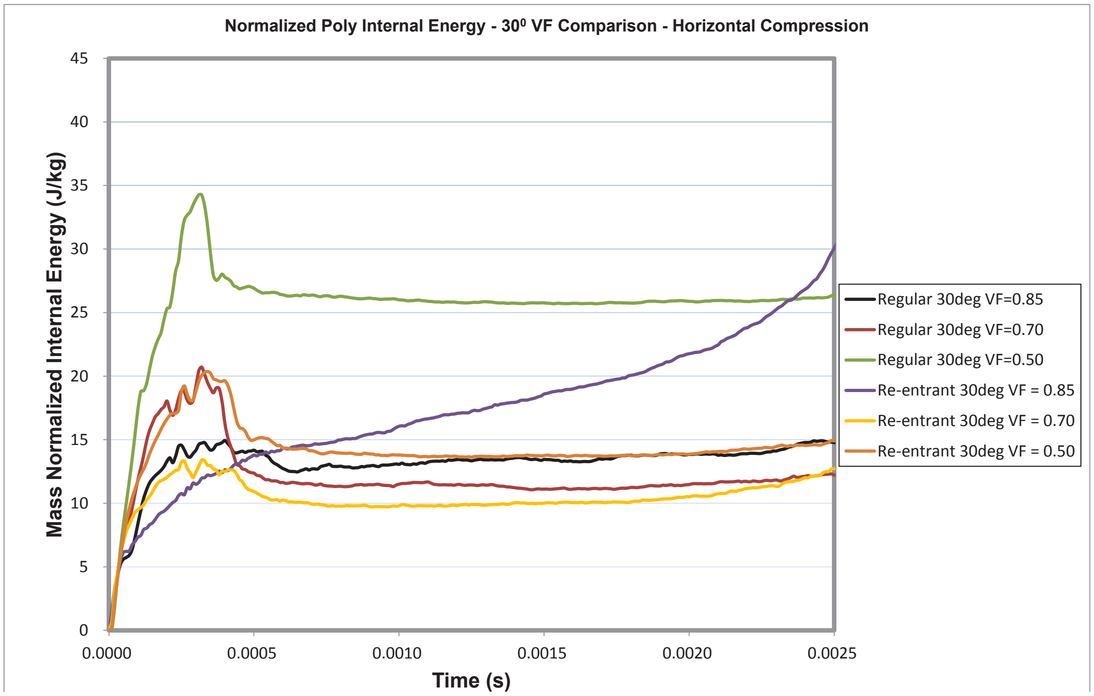

Figure 64: Normalized internal energy absorption for honeycomb structures with $\theta=30^o$ and various void fractions under horizontal impact.

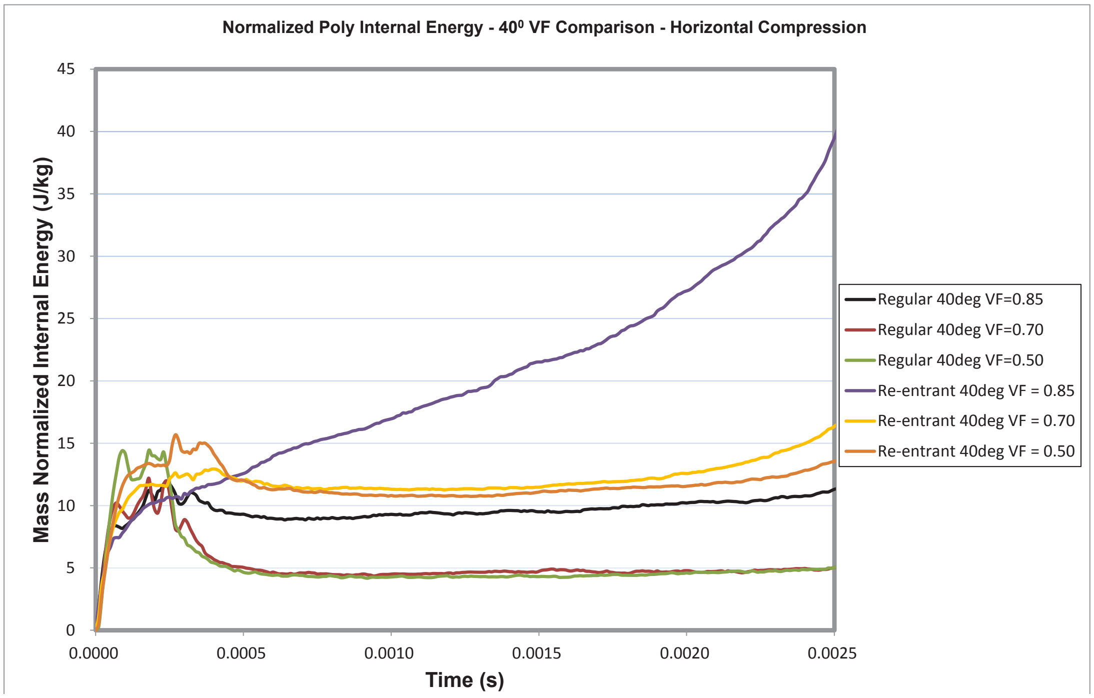

Figure 65: Normalized internal energy absorption for honeycomb structures with $\theta=40^o$ and various void fractions under horizontal impact.

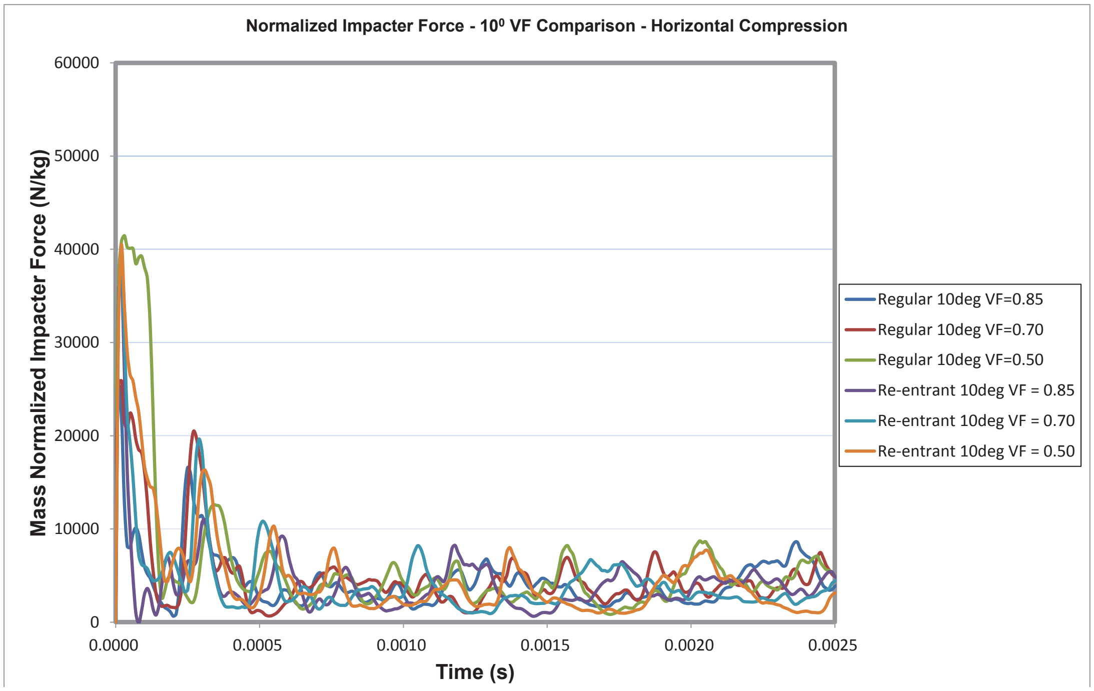

Figure 66: Normalized impact force for honeycomb structures with θ=10^o and various void fractions under horizontal impact.

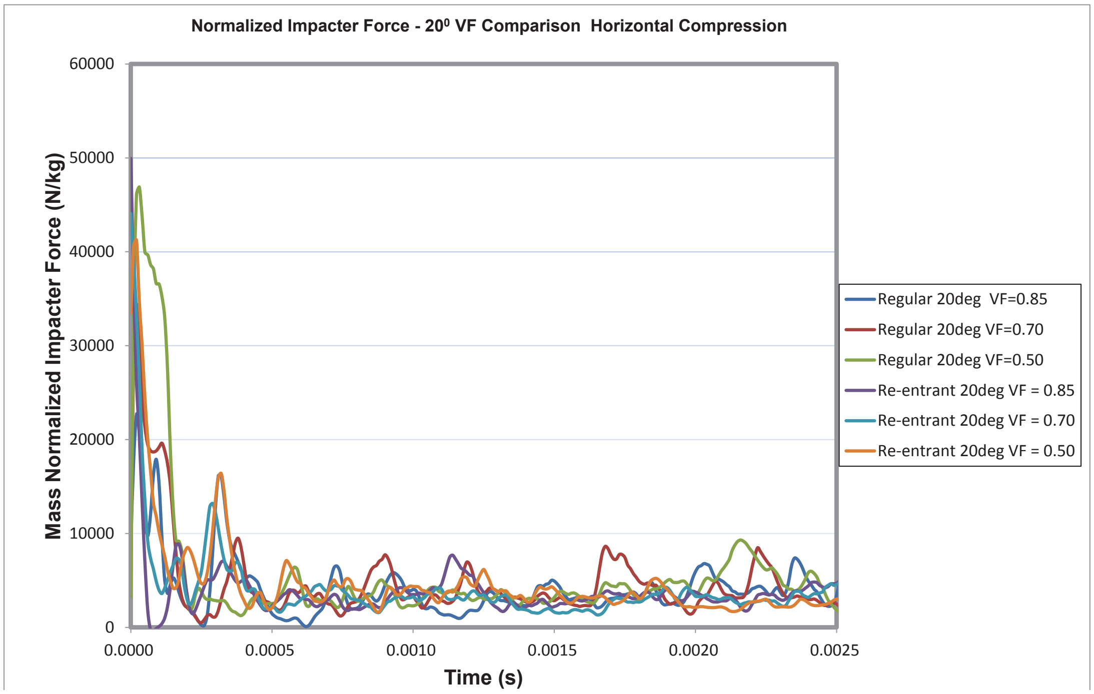

Figure 67: Normalized impact force for honeycomb structures with θ=20^o and various void fractions under horizontal impact.

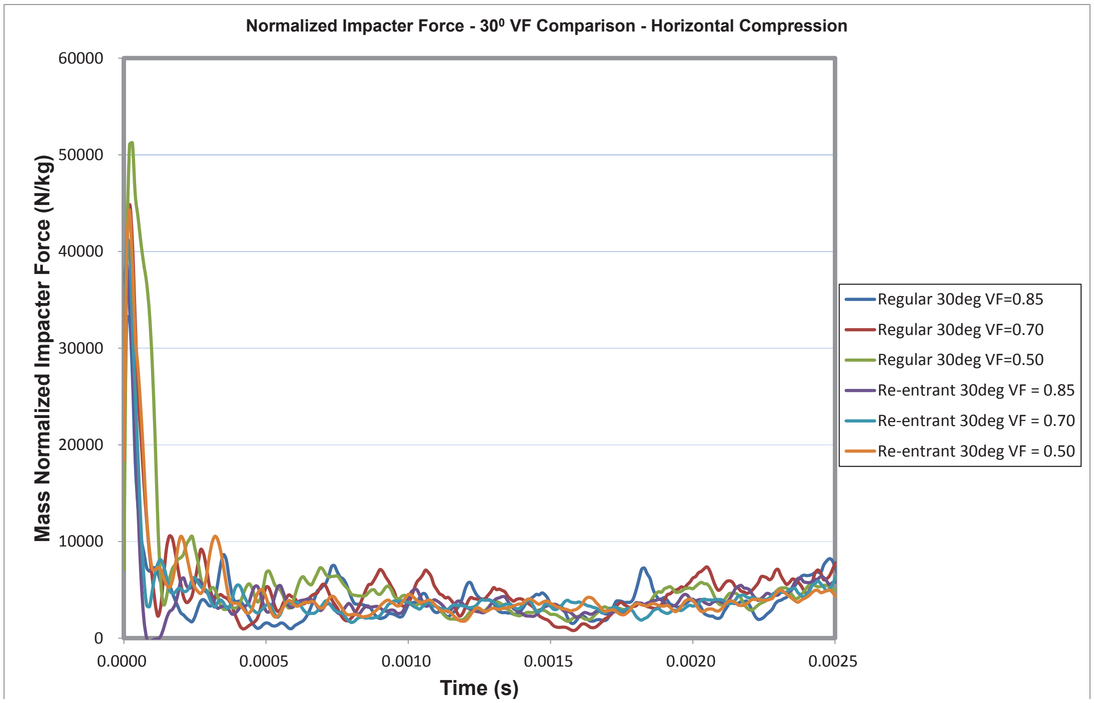

Figure 68: Normalized impact force for honeycomb structures with $\theta=30^o$ and various void fractions under horizontal impact.

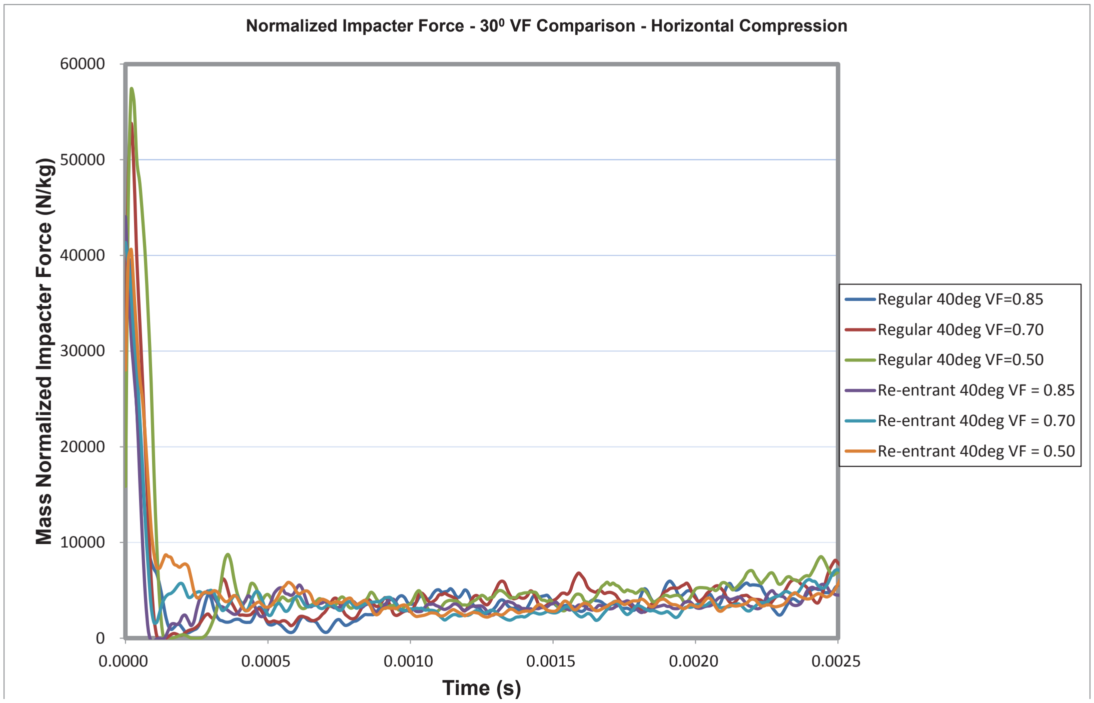

Figure 69: Normalized impact force for honeycomb structures with $\theta=40^o$ and various void fractions under horizontal impact.

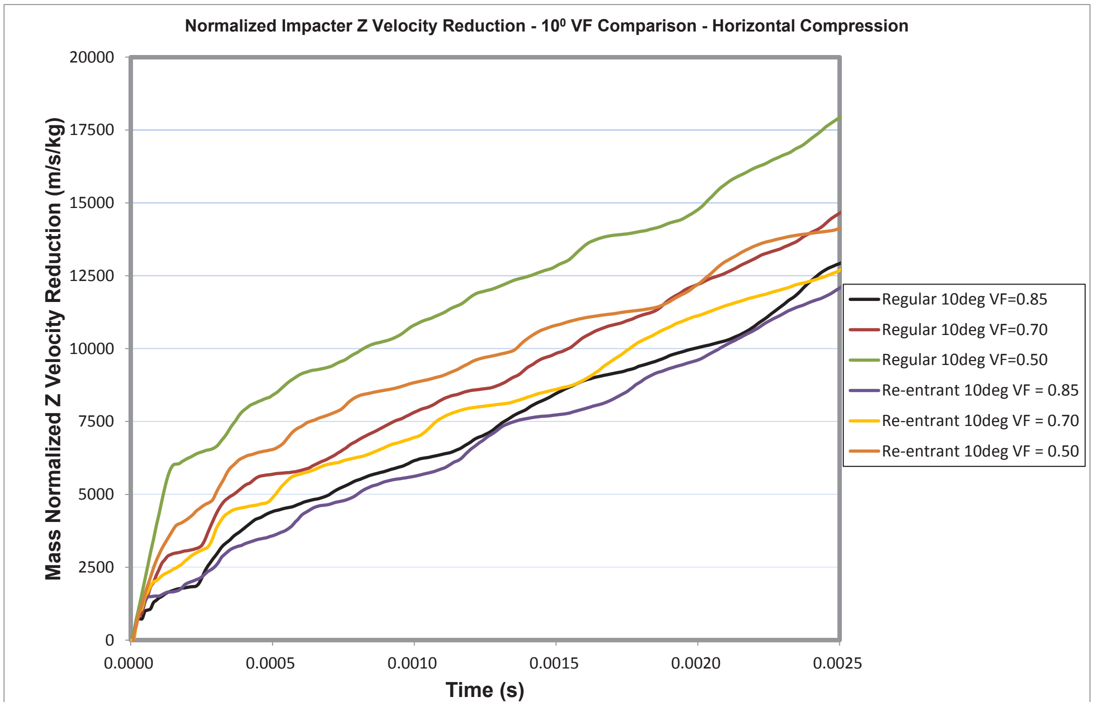

Figure 70: Normalized reduction of impacter velocity for honeycomb structures with $\theta=10^o$ and various void fractions under horizontal impact.

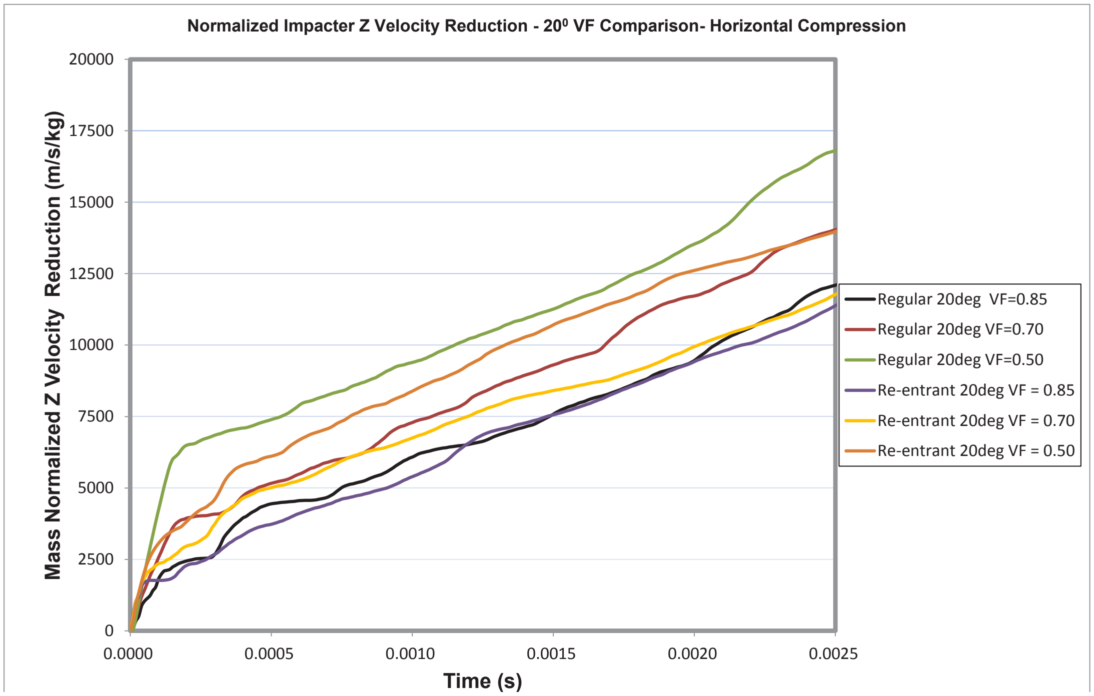

Figure 71: Normalized reduction of impacter velocity for honeycomb structures with $\theta=20^o$ and various void fractions under horizontal impact.

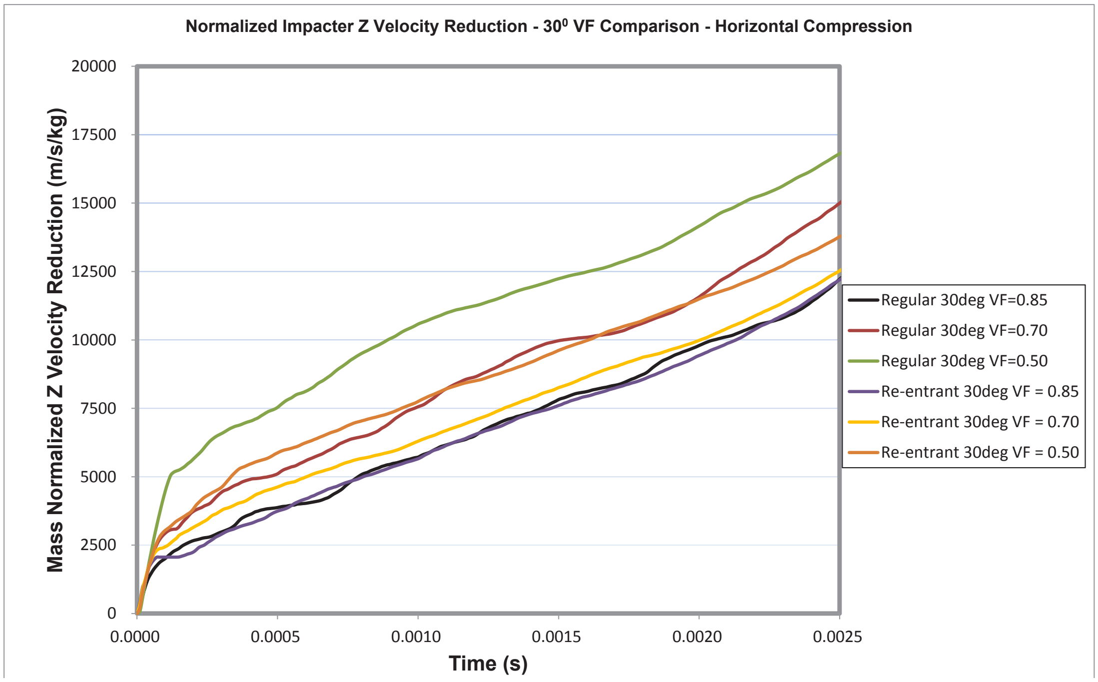

Figure 72: Normalized reduction of impacter velocity for honeycomb structures with $\theta=30^o$ and various void fractions under horizontal impact.

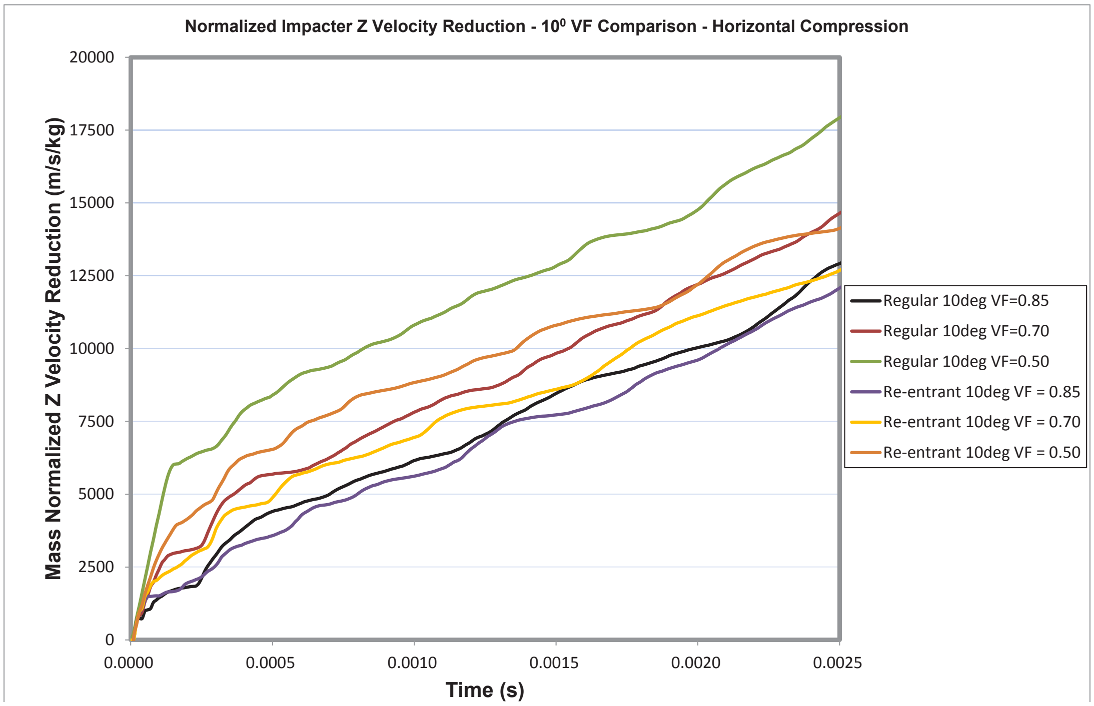

Figure 73: Normalized reduction of impacter velocity for honeycomb structures with $\theta=40^o$ and various void fractions under horizontal impact.

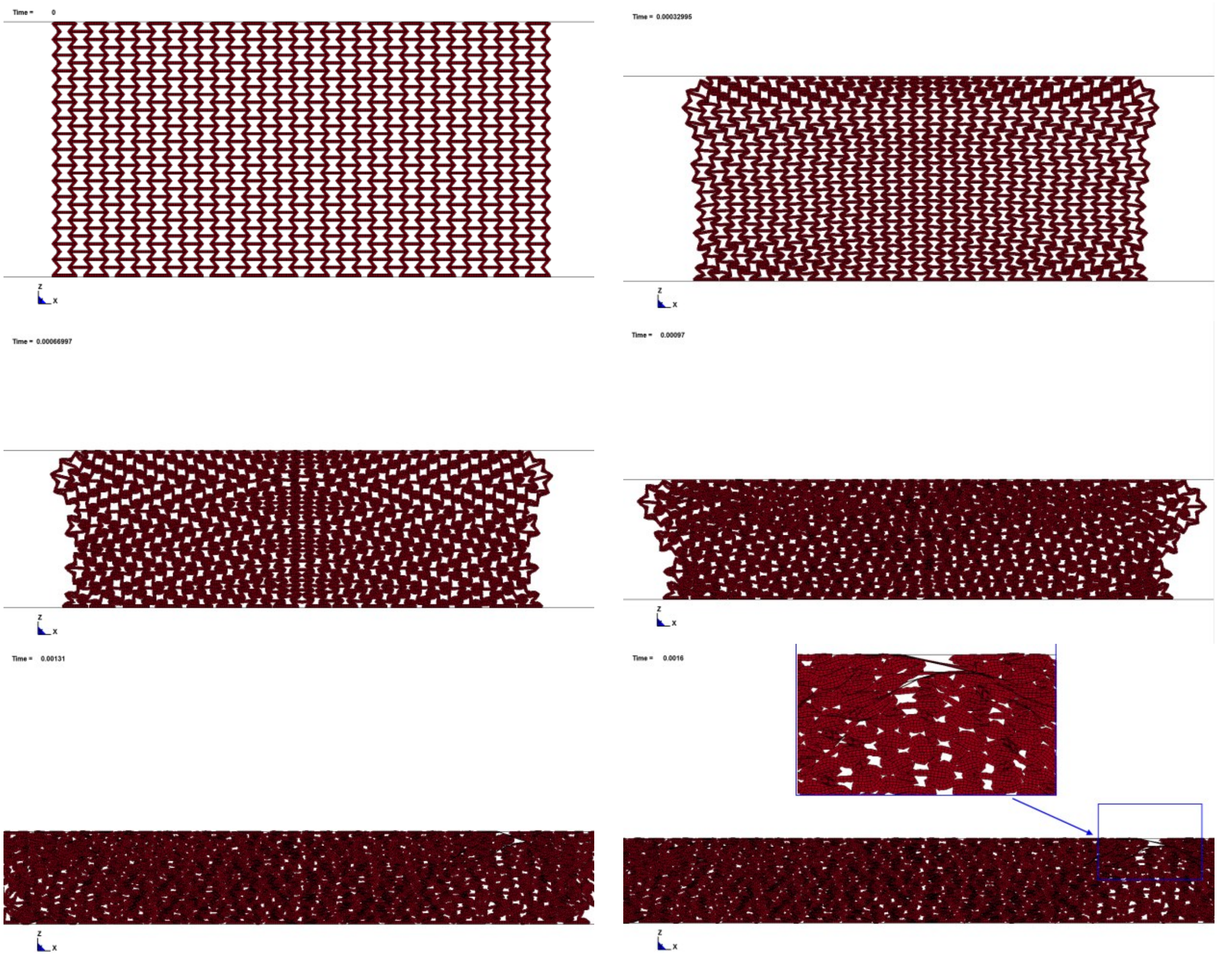

Figure 74: Solid element predicted deformation process for re-entrant honeycomb with $\theta=40^o$ and void fraction of 0.5 under vertical impact.

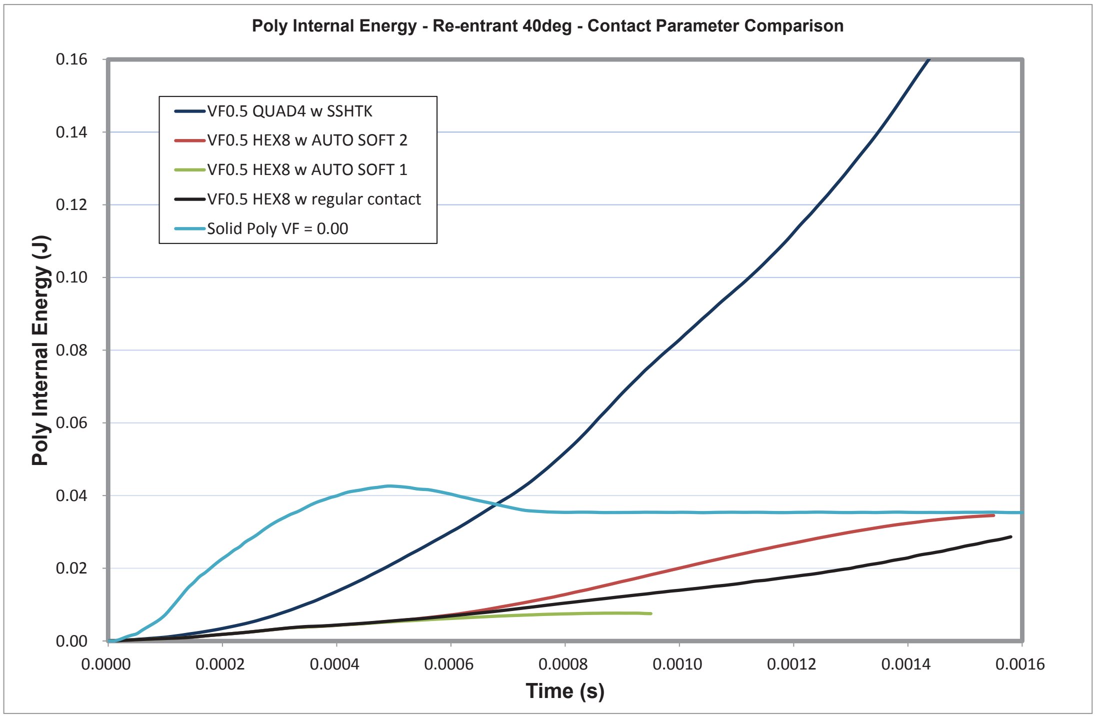

Figure 75: Internal energy absorption for honeycomb structure with $\theta=40^o$ and void fraction of 0.5 under vertical impact predicted using different elements and contact options.

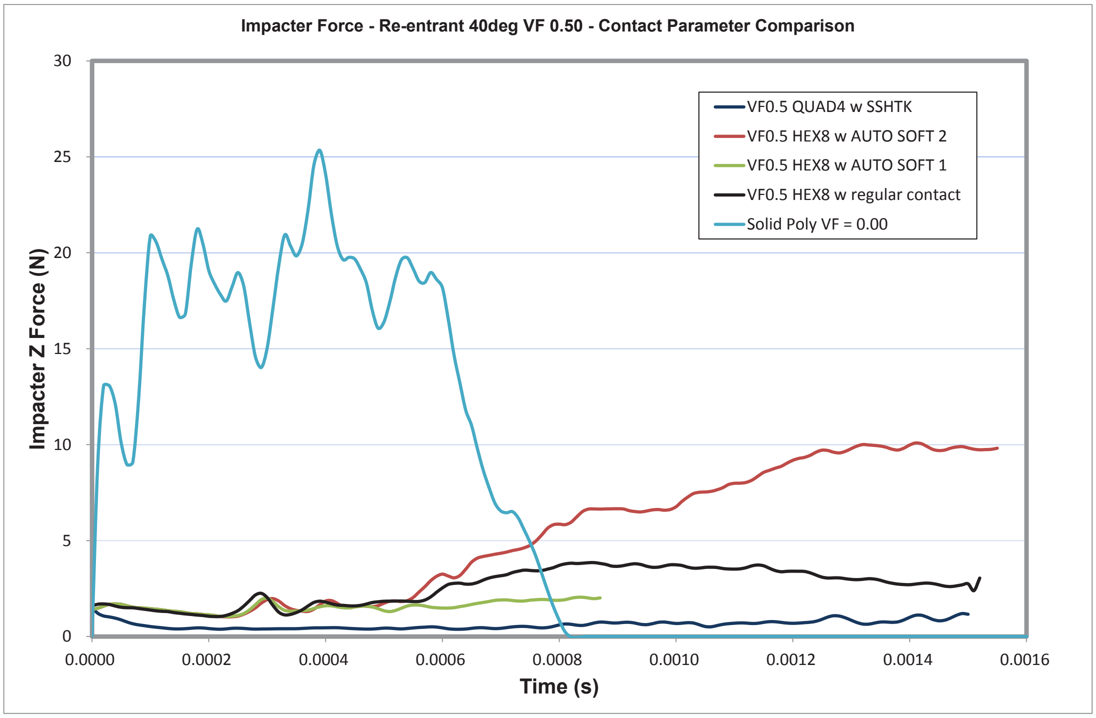

Figure 76: Impact force for honeycomb structure with $\theta=40^o$ and void fraction of 0.5 under vertical impact predicted using different elements and contact options.

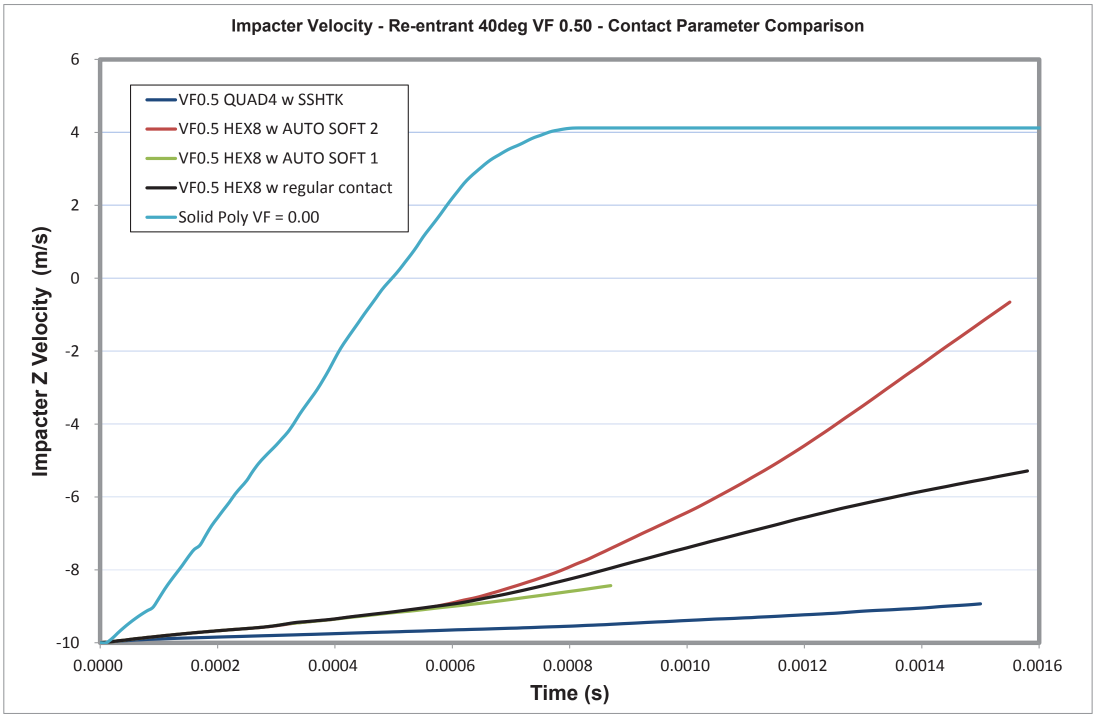

Figure 77: Reduction of impacter velocity for honeycomb structure with $\theta=40^o$ and void fraction of 0.5 under vertical impact predicted using different elements and contact options.

5 Conclusions

In this report, we have described a recent numerical investigation on impact properties of auxetic materials. Auxetic materials are special materials that have negative Poisson's ratios. This class of materials have received a great deal of attention recently and have been demonstrated to exhibit some unique characteristics that provide advantages over conventional engineering materials for certain applications. The objective of the present study is to investigate the impact properties of the auxetic polymer materials and determine the influence of the geometric parameters associated with the auxetic materials on their protective performance against impact loadings.

The present study was based on an idealized numerical model that included auxetic material samples between a rigid surface and a rigid impacter mass moving at an initial velocity. Among the physical variables involved in impact problems, the internal energy absorption, impact force and velocity reduction of the impacter mass were identified as the key indicators for protective performance of the auxetic polymer foam. LS-DYNA was used for the impact simulations. The finite element model was first constructed using the shell element, inspired by a previous study on the similar problems. Prior to the dynamic analyses, the finite element models were verified using linear and nonlinear static analyses and the numerically predicted equivalent material properties were compared with the analytical solutions with close agreement. The nonlinear results were reasonable and indicated that the Poisson's ratios of the auxetic materials are sensitive to the level of deformations due to the variation of the auxetic geometry.

Following verification of the finite element models, a test matrix was constructed for the present parametric study, in which more than sixty test cases were proposed, covering a wide range of honeycomb geometry, void fraction and impact directions. The results seemed to suggest that the materials having smaller angle θ and lower void fractions are more effective as a protecting layer and these effects are more significant under vertical impact. However, because some defects have been discovered in the shell element solutions related to the treatment of the highly complicated contact conditions between the deformed ribs, the above observations became questionable.

An investigation has been initiated to perform impact simulations using the solid elements which provided a more reliable treatment of contact conditions. This investigation will continue into the next phase of the contract.

This page intentionally left blank.

References

[1] Evans, K.E. and Alderson, A. (2000), Auxetic materials: fundamental materials and structures from lateral thinking, Advanced Materials, 12 (9): 617-628.

[2] Yang, W., Li, Z.-M., Shi, W., Xie, B.-H. and Yang, M.-B. (2004), Review on auxetic materials, Journal of Materials Science, 39 (10): 3269-3279.

[3] Alderson, A. and Alderson, K. (2007), Auxetic materials, Proceedings of the Institution of Mechanical Engineers, Part G: Journal of Aerospace Engineering, 221 (4): 565-575.

[4] Liu, Y. and Hu, H. (2010), A review on auxetic structures and polymeric materials, Scientific Research and Essays, 5 (10): 1052-1063.

[5] Prawoto, Y. (2012), Seeing auxetic materials from the mechanics point of view: A structural review on the negative Poisson's ratio, Computational Materials Science, 58: 140-153

[6] Choi, J.B. and Lakers, R.S. (1995), Analysis of elastic modulus of conventional foams and of re-entrant foam materials with a negative Poisson's ratio, International Journal of Mechanical Science, 37 (1): 51-59.

[7] Grima, J.N., Gatt, R., Ravirala, N., Alderson, A. and Evens, K.E. (2006), Negative Poisson's ratios in cellular foam materials, Materials Science and Engineering A, 423: 214-218.

[8] Shufrin, I., Pasternak, E. and Dyskin, A.V. (2012), Planar isotropic structures with negative Poisson's ratio, International Journal of Solids and Structures, 49: 2239-2253.

[9] Pasternak, E. and Dyskin, A.V. (2012), Materials and structures with macroscopic negative Poisson's ratio, International Journal of Engineering Science, 52: 103-114.

[10] Scarpa, F., Yates, J., Ciffo, L. and Patsias, S. (2002), Dynamic crushing of auxetic open-cell polyurethane foam, Proceedings of the Institution of Mechanical Engineers, Part C: Journal of Mechanical Engineering Science, 216 (12): 1153-1156.

[11] Scarpa, F., Cannas, A. and Yates, J. (2005), Static and high constant strain rate loading on auxetic and conventional PU foam, Journal of Advanced Materials, 37 (3): 11-14.

[12] Scarpa, F., Ciffo, L. and Yates, J. (2004), Dynamic properties of high structural integrity auxetic open cell foam, Smart Materials and Structures, 13: 49.

[13] Scarpa, F., Pastorino, P., Garelli, A., Patsias, S. and Ruzzene, M. (2005), Auxetic compliant flexible PU foams: static and dynamic properties, Physica Status Solid (b), 242 (3): 681-694.

[14] Gibson, L.J., Ashby, M.F., Schajer, G.S. and Robertson, C.I. (1982), The mechanics of two-dimensional cellular materials, Proceedings of the Royal Society of London, A382: 25.

[15] Masters, I. and Evans, K. (1996), Models for the elastic deformation of honeycombs, Composite Structures, 35 (4): 403-422.

[16] Henderson, B., Whitty, J., Myler, P. and Chirwa, C. (2007), Crash performance of cellular foams with reduced relative density part 1: rib thickness variation, International Journal of Crashworthiness, 12 (6): 677-688.

[17] Henderson, B., Whitty, J., Myler, P. and Chirwa, C. (2007), Crash performance of cellular foams with reduced relative density part 2: rib deletion, International Journal of Crashworthiness, 12 (6): 689-698.

[18] Dos Reis, F. and Ganghoffer, J.F. (2012), Equivalent material properties of auxetic lattices from discrete homogenization, Computational Materials Science, 51: 314-321.

[19] Wan, H., Ohtaki, H., Kotosaka, S. and Hu, G. (2004), A study of negative Poisson's ratios in auxetic honeycombs based on a large deflection model, European Journal of Mechanics A/Solids, 23: 95-106.

[20] Prall, D. and Lakes, R. (1997), Properties of a Chiral Honeycomb with a Poisson's Ratio of -1, International Journal of Mechanical Sciences, 39 (3): 305-314.

[21] Evans, K.E., Nkansah, M.A. and Hutchinson, I.J. (1994), Auxetic foam: modelling negative Poisson's ratio, Acta metal. mater., 42 (4): 1289-1294.

[22] Dirrenberger, J., Forest, S., Jeulin, D. and Colin, C. (2011), Homogenization of periodic auxetic materials, Procedia Engineering, 10: 1851-1856.

[23] Dirrenberger, J., Forest, S. and Jeulin, D. (2012), Elastoplasticity of auxetic materials, Computational Material Science, in press.

[24] Horrigan, E.J., Smith, C.W., Scarpa, F.L., Gaspar, N., Javadi, A.A., Berger, M.A. and Evans, K.E. (2009), Simulated optimization of disordered structures with negative Poisson's ratios, Mechanics of Materials, 41: 919-927.

[25] Strek, T., Maruszewski, B., Narojczyk, J.W. and Wojciechowski, K.W. (2008), Finite element analysis of auxetic plate deformation, Journal of Non-crystalline Solids, 354: 4475-4480.

[26] Argatov, I.I., Guinovart-Diaz, R. and Sabina, F.J. (2012), On local indentation and impact compliance of isotropic auxetic materials from the continuum mechanics viewpoint, International Journal of Engineering Science, 54: 42-57.

[27] Wang, Y.C. and Lakers, R. (2002), Analytical parametric analysis of contact problem of human buttocks and negative Poisson's ratio foam cushions, International Journal of Solids and Structures, 39: 4825-4838.

[28] Yang, S., Qi, C., Guo, D.M. and Wang, D. (2012), Energy absorption of re-entrant honeycombs with negative Poisson's ratio, Applied Mechanics and Materials, 148: 992-995.

[29] Jiang, L., Pearson, D. and Dunbar, T. (2010), Modelling of Explosion resistant Coating – Phase 2, Martec Technical Report TR-10-11, Martec Limited, Halifax.

DOCUMENT CONTROL DATA

(Security classification of title, body of abstract and indexing annotation must be entered when the overall document is classified)

1. ORIGINATOR (The name and address of the organization preparing the document. Organizations for whom the document was prepared, e.g., Centre sponsoring a contractor's report, or tasking agency, are entered in section 8.)

Martec Limited
400-1800 Brunswick Street
Halifax, Nova Scotia
B3J 3J8 Canada

2. SECURITY CLASSIFICATION (Overall security classification of the document including special warning terms if applicable.)

UNCLASSIFIED
(NON-CONTROLLED GOODS)
DMC A
REVIEW: GCDC APRIL 2011

3. TITLE (The complete document title as indicated on the title page. Its classification should be indicated by the appropriate abbreviation (S, C or U) in parentheses after the title.)

Modeling of Impact Properties of Auxetic Materials: Phase 1

4. AUTHORS (last name, followed by initials – ranks, titles, etc. not to be used)

Jiang, Lei; Pearson, Dustin; MacKay, Ken

5. DATE OF PUBLICATION (Month and year of publication of document.)

August 2013

6a. NO. OF PAGES (Total containing information, including Annexes, Appendices, etc.)

82

6b. NO. OF REFS (Total cited in document.)

29

7. DESCRIPTIVE NOTES (The category of the document, e.g., technical report, technical note or memorandum. If appropriate, enter the type of report, e.g., interim, progress, summary, annual or final. Give the inclusive dates when a specific reporting period is covered.)

Contract Report

8. SPONSORING ACTIVITY (The name of the department project office or laboratory sponsoring the research and development – include address.)

Defence R&D Canada – Atlantic
9 Grove Street
P.O. Box 1012
Dartmouth, Nova Scotia B2Y 3Z7

9a. PROJECT OR GRANT NO. (If appropriate, the applicable research and development project or grant number under which the document was written. Please specify whether project or grant.)

02rz01

9b. CONTRACT NO. (If appropriate, the applicable number under which the document was written.)

W7707-135609/001/HAL

10a. ORIGINATOR'S DOCUMENT NUMBER (The official document number by which the document is identified by the originating activity. This number must be unique to this document.)

TR-13-36

10b. OTHER DOCUMENT NO(s). (Any other numbers which may be assigned this document either by the originator or by the sponsor.)

DRDC Atlantic CR 2013-103

11. DOCUMENT AVAILABILITY (Any limitations on further dissemination of the document, other than those imposed by security classification.)

Unlimited

12. DOCUMENT ANNOUNCEMENT (Any limitation to the bibliographic announcement of this document. This will normally correspond to the Document Availability (11). However, where further distribution (beyond the audience specified in (11) is possible, a wider announcement audience may be selected.))

Unlimited

13. ABSTRACT (A brief and factual summary of the document. It may also appear elsewhere in the body of the document itself. It is highly desirable that the abstract of classified documents be unclassified. Each paragraph of the abstract shall begin with an indication of the security classification of the information in the paragraph (unless the document itself is unclassified) represented as (S), (C), (R), or (U). It is not necessary to include here abstracts in both official languages unless the text is bilingual.)

The report describes a recent investigation on the impact properties of auxetic materials which are special materials with a negative Poisson's ratio. These materials have been demonstrated to have some unique characteristics and may provide advantages over the conventional engineering materials in certain applications. The objective of the present study was to gain a better understanding of the behaviour of the auxetic materials subjected to impact loads and to determine the influence of the various geometric parameters associated with the material on its performance as protective layer of military structures through a parametric study. A simplified model was utilized, which included conventional and re-entrant honeycomb foam structures resting on a rigid surface and impacted by a rigid mass. The time histories of the internal energy absorption, the impact force and the velocity reduction of the impacter were predicted and used to compare the relative performance of the honeycombs with different geometries. The numerical analyses were first carried out based on shell elements in LS-DYNA and the finite element models were verified for linear and nonlinear static analyses. However, the numerical results of impact simulations indicated some issues with the treatment of the internal contacts between the deformed ribs. Further analyses are underway at the present time to use solid elements which can deal with the contact conditions more reliably.

14. KEYWORDS, DESCRIPTORS or IDENTIFIERS (Technically meaningful terms or short phrases that characterize a document and could be helpful in cataloguing the document. They should be selected so that no security classification is required. Identifiers, such as equipment model designation, trade name, military project code name, geographic location may also be included. If possible keywords should be selected from a published thesaurus, e.g., Thesaurus of Engineering and Scientific Terms (TEST) and that thesaurus identified. If it is not possible to select indexing terms which are Unclassified, the classification of each should be indicated as with the title.)

Auxetic; impact; modelling

Defence R&D Canada

Canada's leader in defence
and National Security
Science and Technology

R & D pour la défense Canada

Chef de file au Canada en matière
de science et de technologie pour
la défense et la sécurité nationale

DEFENCE DÉFENSE

www.drdc-rddc.gc.ca